

MULTICHANNEL PHONOCARDIOGRAPHY SYSTEM FOR CARDIAC DIAGNOSIS

Thesis

submitted in partial fulfillment of the requirements for the degree of
Doctor of Philosophy in Electronics and Communication Engineering

by

MADHU BABU ANUMUKONDA

201250890

madhubabu.a@research.iiit.ac.in



International Institute of Information Technology, Hyderabad

(Deemed to be University)

Hyderabad - 500 032, INDIA

November 2023.

Copyright © Madhu Babu Anumukonda, 2023
All Rights Reserved

International Institute of Information Technology
Hyderabad, India

CERTIFICATE

It is certified that the work contained in this thesis, titled “*MULTICHANNEL PHONOCARDIOGRAPHY SYSTEM FOR CARDIAC DIAGNOSIS*” by Madhu Babu Anumukonda, has been carried out under my supervision and is not submitted elsewhere for a degree.

Date

Advisor: Dr. Shubhajit Roy Chowdhury

" MULTICHANNEL PHONOCARDIOGRAPHY SYSTEM FOR CARDIAC DIAGNOSIS "

ABSTRACT

The current research aims to develop a multichannel phonocardiography system to improve the efficiency in detecting low-frequency cardiac auscultation and diagnosis of heart failures. In particular, the research work has been carried out with respect to two aspects. Firstly, a hardware prototype of a MEMS-based multichannel phonocardiography system has been developed, along with the placement of microphones and methods for heart sound localization to enhance signal quality. Secondly, proposed the signal processing algorithm for heart sound segmentation to identify the low-frequency components and neural network-based data analytic technique for feature extraction and implemented the proposed algorithms on SoC-FPGA to differentiate the normal and abnormal heart sound components.

Cardiac auscultation is one of the non-invasive methods to diagnose heart abnormalities. Along with four significant heart sounds (S1, S2, S3, and S4), other murmur sounds are generated due to pathological conditions. These anomalies help in proper diagnosis and prevent the possibility of heart failure. MEMS are becoming the most popular due to their size and free ambient noises and are vital in developing noninvasive diagnostic instruments. In addition, The development of cardiac auscultation devices advantages significantly from using MEMS microphones. This research has developed the MEMS-based phonocardiography instrument to capture and analyze the heart sound S3, S4, and murmur components at cardiac auscultation points. The main contribution of this thesis is developing the mathematical model for source localization algorithms to derive microphone positions with a high signal-to-noise ratio (SNR). The proposed cross-correlation method improves the system's sensitivity in detecting low-frequency cardiac sound components (S1, S2, S3, S4 and stenosis, regurgitation murmurs). The segmentation approach combining wavelet and Shannon energy was implemented on Field Programmable Gate Arrays (FPGAs) to categorize the heart sound components. The proposed segmentation algorithm revealed an excellent sensitivity of 99.17 percent and a detection error rate of 1.5 percent.

Accurate measurements of the cardiac components were obtained using a combination of traditional statistical approaches and neural network based algorithms from multiple signals received simultaneously from several PCG systems. The proposed multichannel phonocardiography system analysis the cardiac sound components using artificial neural networks (ANN). The Inverse delayed (ID) function model of a neuron is used to compute synaptic weights after being simulated in MATLAB. The proposed ANN model was implemented in a Field Programmable Gate Array (FPGA). An SoC FPGA (ZYNQ SoC) performs most of the required data processing, eliminating the need for robust and expensive computer systems. Using regression analysis, a statistical model was developed to identify abnormal heart sounds from the captured signals. The receiver operating characteristic (ROC) curve has been used to evaluate the performances of the proposed model. The ANN system examined both abnormal and normal samples, and experimental results revealed a good sensitivity of 99.1% and an accuracy of 0.9.

The research concluded that signal acquisition from multiple sensors and source localization methods produces a high-quality signal suitable for analyzing low-frequency cardiac sounds (S1, S2, S3, S4, stenosis, regurgitation murmurs). In addition, the proposed ANN classification method, based on the inverse delayed (ID) function model of neuron, can resolve combinatorial optimization problems. The negative resistance of the ID model can destabilize a neural network's stable equilibrium points, reducing the possibility of unknown values in suboptimal synaptic weight solutions obtained using an ANN based on a traditional neuron model. Furthermore, the repeatability and reproducibility measurements are used for the performance analysis.

TABLE OF CONTENTS

CHAPTER 1. INTRODUCTION.....	15
1.1 CARDIAC AUSCULTATION AND PATHOLOGY.....	16
1.2 COMMON PROBLEMS AND CHALLENGES IN PHONOCARDIOGRAPHY SYSTEMS.....	19
1.3 RESEARCH OBJECTIVES AND SCOPE.....	21
1.4 CONTRIBUTIONS OF THIS THESIS.....	22
1.5 ORGANIZATION OF THIS THESIS.....	23
CHAPTER 2. RESEARCH BACKGROUND AND REVIEW OF LITERATURE	28
2.1 INTRODUCTION	28
2.2 EVALUATION OF PHONOCARDIOGRAPHY SYSTEM	28
2.3 LITERATURE REVIEW ON PHONOCARDIOGRAPHY SENSORS	29
2.4 CARDIAC SOUND SENSOR PLACEMENTS AND DETECTION	31
2.5 CARDIAC SOUND SIGNAL PROCESSING METHODS FOR CLASSIFICATION AND ANALYSIS ..	33
CHAPTER 3. DEVELOPMENT OF MEMS MICROPHONE BASED MULTI-CHANNEL PHONOCARDIOGRAPHY SYSTEM.....	37
3.1 INTRODUCTION	37
3.2 MATERIALS AND METHODS	39
3.2.1 <i>High-Performance Multichannel phonocardiography system Design</i>	39
3.2.2 <i>Heart sound localization and microphone placement</i>	42
3.2.3 <i>Cross-Correlation methods for TDOA calculation</i>	47
3.2.4 <i>Feature sets for cardiac sound assessment</i>	50
3.2.5 <i>Performance Evaluation</i>	51
3.3 EXPERIMENTAL RESULTS	52
3.4 SUMMARY.....	55
CHAPTER 4. CLASSIFICATION OF ABNORMAL AND NORMAL CARDIAC SOUNDS USING WAVELET DECOMPOSITION AND SHANNON ENERGY.....	58
4.1 INTRODUCTION	58
4.2 THEORETICAL FRAMEWORK	59
4.2.1 <i>Daubechies Wavelet Transform:</i>	59
4.2.2 <i>Shannon energy</i>	61
4.3 MATERIALS AND METHODS	62
4.3.1 <i>Algorithm for Heart sound data analysis</i>	62
4.3.2 <i>Performance Evaluation</i>	65
4.4 EXPERIMENTAL RESULTS	65
4.4.1 <i>Study 1: Normal cardiac sounds S1 and S2</i>	66
4.4.2 <i>Study 2: Aortic stenosis cardiac sounds</i>	67
4.4.3 <i>Study 3: Mitral stenosis cardiac sounds</i>	68
4.4.4 <i>Study 4: Mitral Regurgitation heart sounds</i>	69
4.4.5 <i>Study 5: S3 and S4 gallop cardiac sounds</i>	70
4.5 SUMMARY.....	72
CHAPTER 5. EXTRACTION CARDIAC SOUND COMPONENTS BASED ON INVERSE NEURON DELAYED NEURON MODEL	74

5.1	INTRODUCTION	74
5.2	MATERIALS AND METHODS	75
5.2.1	<i>Inverse delayed function model of neuron</i>	75
5.2.2	<i>Prediction model using ID function model of neuron</i>	77
5.2.3	<i>Realization of inverse activation function</i>	78
5.3	EXPERIMENTAL RESULTS	82
5.4	SUMMARY	87
CHAPTER 6. CONCLUSION.....		89
6.1	SUMMARY OF THE PRESENT WORK	89
6.2	CONCLUSION.....	90
6.3	SCOPE OF FUTURE WORK	91
CHAPTER 7. APPENDIX A- PROCESSING BOARD SCHEMATICS.....		94
BIBLIOGRAPHY		113

LIST OF FIGURES

Figure 1-1: The top 10 causes of death from WHO [2016].	15
Figure 1-2 Heart Sensing Valves	17
Figure 1-3: Cardiac systole-diastole cycle	17
Figure 1-4: Heart Sound Spectrum	19
Figure 3-1: Phonocardiography System Block Diagram	39
Figure 3-2: MEMS microphone Frequency response	40
Figure 3-3a: Cardiac sound detection jacket with four sensors	41
Figure 3-4b: High speed data processing unit with LCD Display	41
Figure 3-5: Microphone Placement for Heart sound source Localisation	42
Figure 3-6: PCG sensors placement for the experiment	46
Figure 3-7: PCG Sensor Printed Circuit Board (10x10mm)	46
Figure 3-8: Signal capture from four channels	52
Figure 3-9: Signal after correlation	53
Figure 3-10: Error vs. Frequency with different S/N values	54
Figure 3-11: S/N vs. Frequency before and after correlation	54
Figure 3-12: Microphone co-ordinates placement Deviation index	55
Figure 4-1: The members of the Daubechies wavelet family [db1 to db10]	60
Figure 4-2: Multilevel decomposition of wavelet analysis	61
Figure 4-3: Algorithm for high-performance phonocardiography system	62
Figure 4-4: 7-level wavelet decomposition	63
Figure 4-5: Extraction of normal and abnormal heart sounds	64
Figure 4-6: Decomposition detail of S1 and S2	67
Figure 4-7: Shannon Energy peaks of S1 and S2	67
Figure 4-8: Decomposition detail of Aortic stenosis	68
Figure 4-9: Shannon Energy peaks of Aortic stenosis	68
Figure 4-10: Decomposition detail of Mitral stenosis	68
Figure 4-11: Shannon Energy envelope of Mitral stenosis	69
Figure 4-12: Decomposition detail of Mitral regurgitation	69
Figure 4-13: Shannon Energy peak of Mitral regurgitation	70

Figure 4-14: Decomposition detail of third heart sound(S3)	70
Figure 4-15: Shannon Energy envelope of Third heart sound (S3)	71
Figure 4-16: Decomposition detail of Fourth heart sound(S4)	71
Figure 4-17: Shannon Energy envelope of Fourth heart sound (S4)	71
Figure 5-1: ANN using ID function neuron model.....	78
Figure 5-2: Transfer function.....	79
Figure 5-3: Real-time experimental setup with proposed hardware	80
Figure 5-4: Flow diagram for extraction of Cardiac Sound components	80
Figure 5-5: Neuron Model	81
Figure 5-6: System Generator Implementation of ANN Model	82
Figure 5-7: RTL Schematic – Neuron Model	83
Figure 5-8: Physical layout for the proposed system.....	83
Figure 5-9: Resource utilization of the proposed system.....	83
Figure 5-10: Regression analysis of neural network based on ID Function model of neuron	84
Figure 5-11: Training state analysis of neural network based on ID Function model of neuron	85
Figure 5-12: Performance analysis of neural network based on ID Function model of neuron	85
Figure 5-13. ROC Curve Analysis of Heart Sound components with the inverse delayed function of Neuron Model (a) First and Second Heart sound (b) Third and Fourth Heart sound (c) Aortic Stenosis (d) Mitral Stenosis (e) Mitral Regurgitation	87

LIST OF TABLES

Table 3-1: Cardiac sounds Feature sets	50
Table 3-2: Repeatability and Reproducibility Results	53
Table 4-1. Performance Evaluation of phonocardiography system.....	66
Table 4-2. Comparison of Performance Evaluation of other states of art algorithms	66
Table 5-1. Accuracy of the proposed system for different cardiac components in heart sounds	86
Table 5-2. Comparison of Performance Evaluation of ID model with other states of art algorithms	86

Dedicated to Almighty

ACKNOWLEDGEMENTS

I would like to thank my advisor Dr. Shubhajit Roy Chowdhury, for all his support and timely suggestions throughout my research and thesis work.

I thank my advisor for showing continuous belief in me even though I was employed in the semiconductor industry performing a full-time job in parallel. His timely advice with kindness, meticulous scrutiny, and scientific approach has helped me accomplish this research.

I profusely thank all the staff of CVEST and the administration staff, specifically Kishore. Y, Prathima, and Pushpalatha. B for their kind help and cooperation throughout my Ph.D. journey.

It is my privilege to thank my parents, in-laws, my wife, and my two daughters for their constant motivation and support throughout my research.

I owe a deep gratitude to all of my teachers, mentors, friends, colleagues, and specifically Prasad Raju LV S R, without whose support I may not have been able to conduct this research.

Chapter 1. Introduction

Worldwide, Heart diseases are the primary cause of human death. Heart disease and stroke are the world's biggest killers, accounting for a combined 15.2 million deaths out of 56 million deaths in 2016. These diseases have remained the leading cause of death globally in the last 15 years [1]. Early detection of heart failure and its related symptoms helps properly diagnose heart diseases and reduces the death rate. In the modern technological revolution, many diagnosis methods like phonocardiogram (PCG), electrocardiogram (ECG), Echocardiogram (Echo), Cardiac Magnetic Imaging (CMRI), and Computed Tomography (CT) heart scan are available to detect early heart failure.

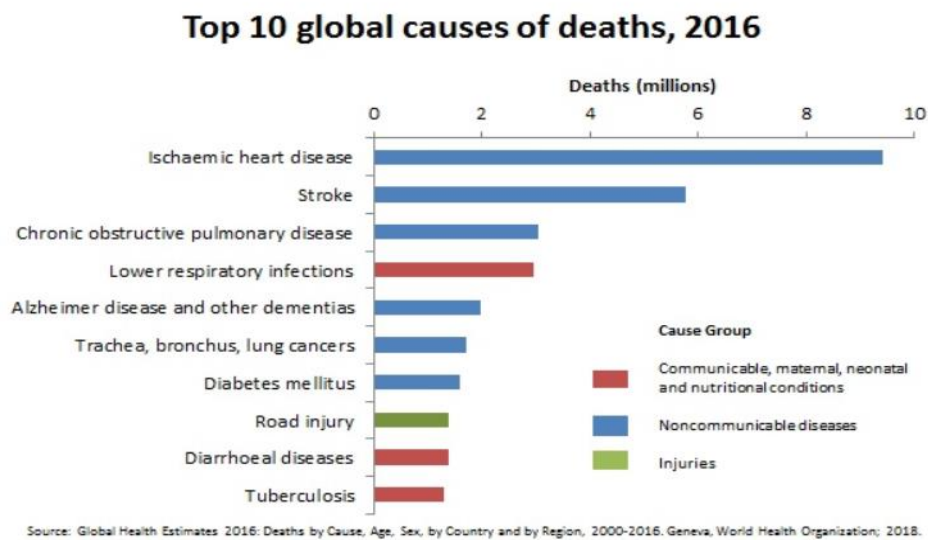


Figure 1-1: The top 10 causes of death from WHO [2016].

However, most of these methods have drawbacks, like using ECG, which has challenges detecting the heart valve's structural abnormalities. Sound-based methods detect cardiac abnormalities by heart murmurs. Echo, CMRI, and CT scans provide accurate results, but these are expensive and not economically affordable for many people [2].

phonocardiography is a noninvasive method for detecting significant heart sounds and murmurs. The stethoscope was the primary phonocardiography instrument that played a significant role in detecting cardiac auscultation, but this had its limitations in terms of clinical expertise to analyze the low-frequency amplitudes such as third, fourth heart sound components (S3 & S4) systolic, diastolic murmurs [2] formed during heart failures. However, these can be overcome by using advanced signal processing techniques for Heart sound detection and

prediction by data analysis techniques like Artificial Intelligence (AI) based machine learning(ML), deep learning(DL) methods for providing inferences, and accurate parameter derivation. These methods motivate us to work on the multichannel phonocardiography system using multiple advanced sensors to detect cardiac auscultation based on source localization. Analysis of the heart sound using advanced signal processing techniques and computational data analytics software for the classification, recognition, and modeling simulations.

1.1 Cardiac Auscultation and Pathology

Heart sounds are produced by the heart valve's contraction and expansion as blood traverses into the heart and throughout the body. Using a stethoscope, the doctor listens to the heart's sound during a heart examination and analyses each sound component's characteristics during the cardiac cycle. Systolic and diastolic phases make up each heart cycle. Four primary heart valves, known as the auscultation sites, are where the heart sounds are recorded. Each auscultation site's examination of the heart sound reveals the heart's functionality and identifies any irregularities to identify the sickness. The Mitral area (fifth intercostal space, mid clavicular line), Tricuspid area (mid-left sternal border), pulmonic area (left second intercostal space), and Aortic area (right second intercostal space) [3-9] are the four heart sound areas in Figure 1-2. These locations, each of which corresponds to a different heart valve, are as follows:

Mitral valve: Blood flows from the left atrium (the upper-left chamber) to the left ventricle (the lower-left chamber) and is controlled by the mitral valve.

Aortic valve: The aortic valve controls the lower-left chamber of the heart (the left ventricle)'s blood flow into the aorta. The main blood vessel that carries blood throughout the body is the aorta.

Tricuspid valve: Blood flows to the right ventricle (lowermost chamber) from the heart's right atrium (uppermost chamber) and is controlled by the tricuspid valve.

Pulmonary valve: Blood flows between the pulmonary artery and the heart's right ventricle (the lower-right chamber) and is controlled by the pulmonary valve.

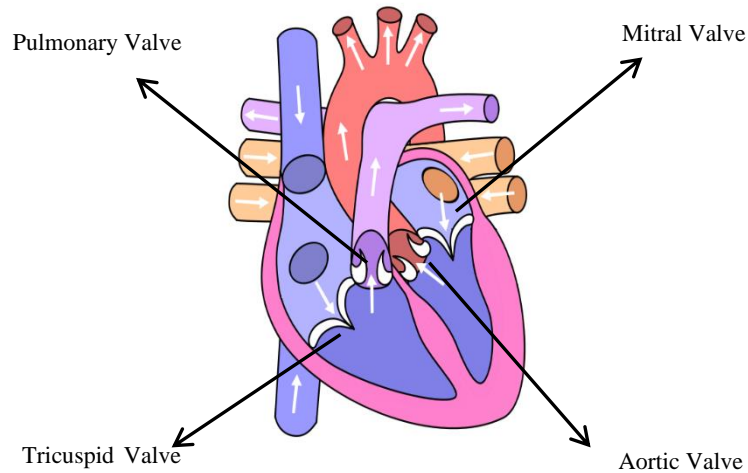


Figure 1-2 Heart Sensing Valves

[10-17] These four valves help the heart pump blood throughout the body. The four main heart sounds are produced as the heart valves open and close during blood pumping. The aortic and pulmonary valves open, and the tricuspid and mitral valves close during the systole cycle, resulting in the first cardiac sound, S1. S1 is best heard as "dub" at the top of the heart. The pulmonary and aortic valves close during diastole while the tricuspid and mitral valves expand, resulting in the second heart sound, S2. At the heart's center, S2 is best heard as "lub." S3, the third heart sound, is produced during the rapid filling phase of the pre-diastole cycle when blood flow strikes the ventricular wall. The low-pitched S3 sound is best discernible at the peak and is best described as "lub-dub-sum." When blood flow strikes the wall of the ventricular chamber during the atrial systole phase in the pre-systolic cycle, the fourth heart sound, S4, is generated. S4 has a low-pitched heart sound best described as "da-lub-dub" at its apex. Figure 1-3 depicts the S1, S2, S3, and S4 heart sounds during the cardiac systole-diastole cycle.

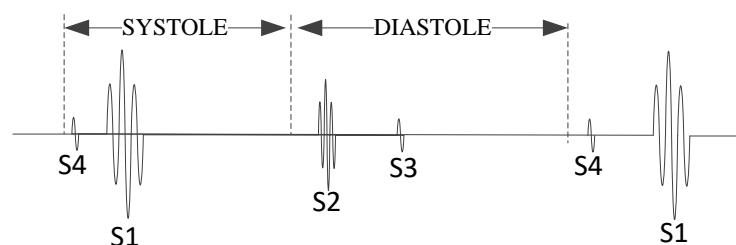


Figure 1-3: Cardiac systole-diastole cycle

The two main pathological disorders are stenosis and regurgitation, both of which are caused due to blood flow via the heart valves. Blood flowing backward due to an incorrect heart valve closure is known as regurgitation. Blood flow through constrictive heart valves is referred to as heart stenosis. Limited blood flows from the heart to the body's organs are brought on by heart valve stenosis and regurgitation. As a result, the heart needs to function harder to circulate the blood, which leads to heart failure.

The return of blood into the left atrium is known as mitral regurgitation (MR). The return of blood from an inflated valve in the aorta into the left ventricle is known as aortic regurgitation (AR). The return of blood that flows from the right ventricle to the right atrium is referred to as tricuspid regurgitation (TR). The passage of blood that flows from the pulmonary arteries to the right ventricle is known as pulmonary regurgitation (PR).

The narrowing of the mitral valve, known as mitral stenosis (MS), causes blood to pool in the left atrium rather than flow into the left ventricle. The narrowing of the aortic valve is the cause of aortic stenosis (AS). This controls the blood flow into the aorta from the left ventricle. The tricuspid valve narrowing is what causes tricuspid stenosis (TS). This controls the blood flow into the right ventricle from the right atrium. Narrowing of the pulmonary valve and control of blood flow from the right ventricle into the pulmonary arteries cause pulmonary stenosis (PS). Issues with the tricuspid and pulmonary valves are infrequent compared to the mitral and aortic valves. The current research focuses on identifying and evaluating Mitral and Aortic abnormalities.

The third cardiac sound(S3) is frequently heard in normal children and adolescents, although it can also be reported in the low-frequency channel in adults (but not heard). It's a low-pitched (low-frequency) sound with a weak pitch. S3 disappears due to aging, caused by increased cardiac mass-dampening vibrations. However, a rapid filling rate or alterations in the anatomical characteristics of the ventricle might create an amplified third sound. If S3 appears beyond 40 years, it is considered abnormal. A pathological S3 is found in mitral regurgitation, aortic stenosis, and ischemic heart disease.

The fourth cardiac sound (S4) coincides with the atrial contraction, and thus the originated increased blood flow through the mitral valve with consequences as mentioned for the third

sound. It is seldom heard in ordinary cases, sometimes in older people, but is registered more often in the low-frequency channel. The sound level increases in cases of augmented ventricular filling or reduced ventricular distensibility. A pathological S4 is found in mitral regurgitation, aortic stenosis, hypertensive cardiovascular disease, and ischemic heart disease.

Cardiac sounds are audible at very low frequencies, the lowest range of human hearing. Figure 1-4 illustrates the frequency ranges that make up the heart sound spectrum, which ranges from 20 Hz to 1 kHz. S1 and S2 heart sounds range from 40 to 150 Hz in this spectrum, whereas S3 and S4 gallops range from 20 to 70 Hz, stenosis murmurs range from 25 to 80 Hz, ejection noises range from 110 to 500 Hz, and regurgitation murmurs range from 110 to 900 Hz.

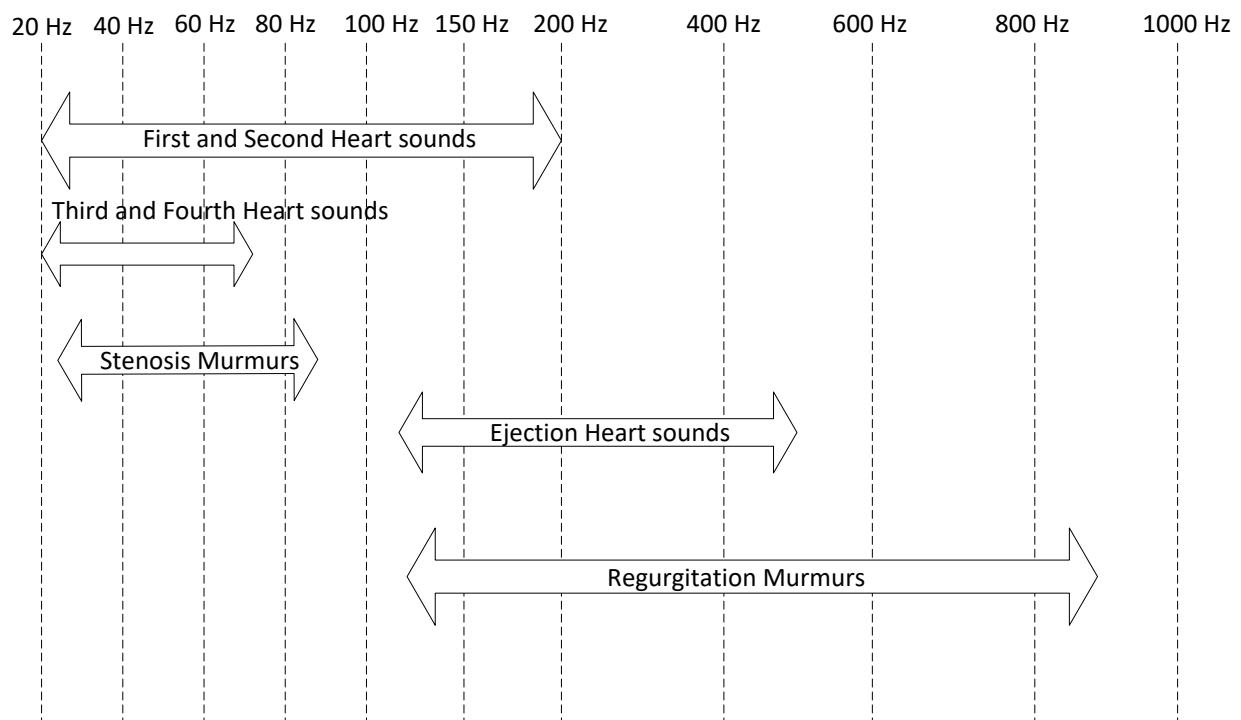


Figure 1-4: Heart Sound Spectrum

1.2 Common Problems and Challenges in Phonocardiography Systems

The reasons for real-world issues are frequently unknown and have minimal information. This is because of the complexity of the systems and the noninvasive approaches scientists and engineers use to investigate them. Signal and image processing techniques used

to analyze such systems tend to be blind. Earlier, training signal-based techniques were used extensively for such analyses. But often, these training signals are not practicable to be availed by the analyzer or become a burden on the system itself.

Phonocardiography signals are examined for pathological patterns, relative intensities, intensity variations, timing, and duration of events. More objective evaluation can be performed, ranging from simple, accurate phenomena to advanced waveform analysis and comparing recorded results with available reference data. The importance of auscultation can be explained by the technique's simplicity and by the ear's strong abilities concerning pattern recognition in acoustic phenomena [18]. When comparing abnormal and normal heart sounds to diagnose pathological disorders, the medical professional must have a high level of clinical skill [5]. For obtaining equivalent information with phonocardiography, a single recording fails to be sufficient: A set of the frequency-filtered signals, each of them emphasizing gradually higher frequency components (by using high pass or band-pass filters), is needed. In this way, visual inspection of sound phenomena in different frequency ranges, adapted by a compensating amplification for the intensity falloff of heart sounds toward higher frequencies, is made possible, thus rendering the method equivalent to hearing performance: pattern recognition abilities and increasing sensitivity toward higher frequencies within the above mentioned frequency range.

Also, hidden elements like background noise, respiration noise, muscle tremors, stomach rumbling, nonoptimal recording sites, and weak sounds (obese patients) are captured during heart sound recording. The presence of artifacts and noises can visually mask weak heart sounds. So, getting high-quality heart sound recordings with a high signal-to-noise ratio is challenging. Based on auscultation in PCG, one discriminates between heart sounds and murmurs. It has already been indicated that the source types and the acoustic impressions they provoke are different. From the standpoint of signal analysis, heart sounds correspond better with transients originating from a sudden impact, whereas murmurs, except for the musical types, have a random character. If one considers a set of subsequent heart cycles, one may find that heart sounds are more coherent than murmurs. For example, averaging of sounds of subsequent heart cycles to an appropriate time reference gives a meaningful result. Still, the same fails for murmurs due to their random character.

As the spectral performance of phonocardiography may exceed the possibilities of human hearing, inaudible low frequency phenomena can be recorded; They are also indicated as "(inaudible) sounds." Acoustic phenomena originating from the heart are classified into heart

sounds and murmurs [19][20]. Although the distinction between them is not strict, one can state that heart sounds have a more transient, musical character and a short duration (Fig. 1). In contrast, most murmurs have a predominantly noisy character and generally (but not always) exist for a longer duration (e.g., a "blowing" murmur, a "rumbling" murmur). It is also believed that the genesis of both types is different. Heart sounds are indicated as resonant phenomena of cardiac structures and blood due to one or more sudden events in the cardio hemic system (such as valve closure), and most heart murmurs are said to originate from blood flow turbulence [21][22][23]. Many aspects of the problem of the genesis of these phenomena are still being discussed, including the relative importance of the valves and the cardio hemic system in the generation of heart sounds (valvular theory versus cardio hemic theory).

In addition, the pathological condition of the heart may not always be identifiable in the raw time-domain PCG signal—failure to present information on the frequency of heart sounds and their components. Also, the difference between different frequencies of various sounds lacks information on the energy variations in various sounds. The auscultation technique, which uses a single acoustic sensor, may not provide accurate analysis in detecting low-volume signals due to the generation source in the cardiac cycle. This will be addressed in the current study by recording cardiac auscultations with a multichannel acoustic sensor and analyzing the signal through segmentation, feature extraction, and classification.

1.3 Research Objectives and Scope

The current medical systems on the market, specifically the electronic non-invasive phonocardiography system and related point of care (POC) medical systems, may not be embedded with multichannel or multimodal computations for effective low-frequency cardiac signal detection or continuous non-invasive patient monitoring. Additionally, the challenges involved in the detection and processing of low-frequency cardiac signals from an adult (or from single or multiple fetuses of a pregnant patient) or the detection and analysis of low-frequency respiratory and gastric bio-signals and their effects on cardiac include the need for a high sensitivity phonocardiogram sensor with robust characteristics, the placement of sensors, the localization of heart sounds, and the requirement for multichannel signal detection.

The current research mitigates the above problems and evaluates the heart sound detection system to determine the structural abnormalities of heart failure using a multichannel phonocardiogram system. This system helps to improve the efficiency of detecting low-

frequency, low-amplitude cardiac sounds like S3, S4, and heart murmurs to diagnose heart failures. This will be achieved by following objectives:

- ❖ **Development of Multi-channel phonocardiography Instrument:** To capture the multi-channel heart sounds using a MEMS microphone-sensor and computational platform to implement the algorithms to analyze the heart sounds in real-time.
- ❖ **Placement of Microphones:** Derivation of sensor placement on the chest to get the good signal quality using the time difference of arrival (TDOA) method and cross-correlation techniques with the help of the heart sound source localization mathematical model.
- ❖ **Algorithm for heart sound classification:** Propose and implement the algorithm to classify the low-frequency heart sound components S3, S4, and murmurs.
- ❖ **ANN-based Feature extraction:** Develop and implement the algorithm using the Inverse delayed model of a neuron based on input feature sets of heart sounds and find the abnormal heart sound components.

The designed PhonoCardioGraphy system enhances the capability to provide inferences in predicting a cardiac-related illness by processing the multi-signal input data and performing data analytics on the data collected from these various sensors for pathological Completeness. Apart from cardiac health, providing this developed multichannel MEMS-based PhonoCardioGraphy system research platform and its analysis technique to be explored for applicability to determine the health of the respiratory system and gastric signals analysis and or determining the health of single or multi-fetus by monitoring non-invasively.

1.4 Contributions of this Thesis

This research project aims to develop a portable phonocardiography hardware system to detect low-frequency heart sounds S3, S4, and murmurs using multiple sensors. The proposed system addresses the present problems and challenges of the phonocardiography system (mentioned in Section 1.2) and improves the efficiency with the below major contributions:

- Designed and built an experimental hardware device for multi-channel data acquisition and real-time algorithm computations. (**Chapter 3**)
- The proposed source localization methods and accurate microphone positioning improved the cardiac signal quality (SNR). (**Chapter 3**)

- Improved the real-time classification of the low-frequency S3, S4, and abnormal heart sounds by implementing advanced signal processing in FPGAs. (**Chapter 4**)
- Artificial Intelligence (AI) based on the Inverse delayed model of a neuron was used to extract the features of the cardiac sounds. (**Chapter 5**)

1.5 Organization of this thesis

This thesis is organized into six chapters

Chapter 1: This chapter provides the introduction to the problem statement and the necessity of a phonocardiography system to detect human cardiac diseases. Explains the preliminaries of cardiac auscultation areas (Mitral valve, Aortic valve, Tricuspid valve, and Pulmonary valve) and generation of S1, S2, S3, S4, and heart mummer-like regurgitation, stenosis. Detailed about the pathology related to cardiac sounds and its evolution over the years. Also, the common issues and challenges of phonocardiography, such as capturing heart sounds, complex pathological patterns, relative intensities and intensity variation, timing and short duration of events, fast variation with time, and transient nature, have been presented. Research objectives and scope the current research provide the methods to mitigate the above problems by developing the MEMS-based multi-channel phonocardiography system and major contribution of this thesis in the area of phonocardiography and finally outlines the thesis organization by chapter wise.

Chapter 2: This chapter introduces the research background and literature study on the evaluation of phonocardiography systems, a review of phonocardiography sensors, cardiac sound sensors placement, and cardiac signal processing methods for classification and analysis. Literature on phonocardiography sensors explored the different sensors used for auscultation over the years, drawbacks, advantages to detecting the low frequency cardiac sound components, and consideration of the MEMS microphones for developing multi-channel phonocardiography systems. Cardiac sound sensor placement and detection provides the literature study on multi-channel cardiac sound recordings advantages and shortfalls of placement for proper auscultations. Research background on different heart sound localization techniques like time difference of arrival (TDOA), Generalized Cross Correlation, Multi-Channel Cross correlation (MCCC), Cross Power Spectrum Phase (CSP), Generalized Cross Correlation using Phase Transform (GCC-PHAT), Multiple Signal Classification (MUSIC),

Estimation of Signal Parameters through Rotational Invariant Technique (ESPRIT, and root-MUSIC. Finally, this chapter covers the cardiac signal processing methods for classification. In the literature, many signal processing procedures for cardiac sound segmentation, classification, and feature extraction for identifying anomalies have been proposed. The literature study on different algorithms like Fourier Transforms (FT), Short-Time Fourier transforms (STFT), Wigner-Ville distribution (WVD), Wavelet transforms, Artificial Neural Networks (ANN), Multi Layer Perceptron- Back propagation (MLP-BP), k-nearest neighbor (kNN) and Convolutional Neural Network (CNN). Several studies are investigating various ways to develop a tool that may offer consistent and dependable results in a simple and cost-effective manner.

Chapter 3: This chapter introduction provides an overview of the phonocardiography system, MEMS sensors, heart source localization, and microphone placement. The material and Methods section covers the High-performance Multi-channel phonocardiography system design, Heart sound localization and microphone placement, cross-correlation methods for TDOA calculation, Feature sets for cardiac sound assessment, and Performance evaluation metrics. High-performance multi-channel phonocardiography system design explains the design details of the Cardiac sound detection unit, High speed processing unit, and Graphic Display unit. Heart sound localization and microphone placement provide the mathematical model for finding the sensor placements based on Time Delay of Arrival (TDOA). Cross-correlation methods for TDOA calculation provide the cross-correlation (CC) details, Generalized Cross Correlation (GCC) details, Multi Chanel Cross-Correlation Coefficients approach, and Phase Transform (PHAT) weighing function. The feature set for cardiac assessment provides the twelve features that are identified for signal extrication. Performance Evaluation covers the metric required for statistical assessments of the proposed system. The Repeatability, Reproducibility, and error in coordinate positions concerning SNR are used for performance criteria. The experimental results section demonstrates the final output of the signal derived from the four channels after applying the proposed correlation analysis to reduce the noise level, statistical assessment metrics values of Standard deviation, Repeatability coefficient, variance coefficient, signal-to-noise ratio versus coordinate errors percentage, and deviation index for the error coordinates. Finally, the Summary section summarizes the multichannel phonocardiography hardware development, source localization methods, and results.

Chapter 4: This chapter's introduction covers a few signal processing methods for heart sound segmentation. The Theoretical Framework section explains the theory behind the Daubechies wavelet transform and Shannon energy details. Daubechies wavelets are well set for the analysis of non-stationary heart sound signals. The Daubechies wavelets are ideal for analyzing non-stationary heart sounds. Furthermore, Daubechies wavelets are perfect for providing the smallest support for many vanishing moments. In the current suggested algorithm, the Daubechies wavelet db9 is used for the breakdown of the heart sound signal. The Shannon energy can emphasize low and medium heart sound levels more than the traditional square energy operation. As a result, the heart sound signal following Shannon energy processing has no significant amplitude changes, allowing to use of a single thresholding technique in the heart sound peak detection algorithm. The Materials and methods section provides the algorithm for heart sound data analysis. The wavelet decomposition module processed the normalized cardiac sound output for decoding the sub-bands. The 9th-order Daubechies (db) wavelet Level 7 was used for the wavelet decomposition. After decomposition, process the data through Shannon entropy and moving average filtering for the intensity peak detection. Performance Evaluation provides the metrics for statistical assessments of the proposed system. The sensitivity, specificity, positive predictive rate, and detection error rate are used for performance metrics. The experimental Results section demonstrates five evaluations. In the present study, the results of normal heart sound S1 and S2, study 2 presents the results of Aortic stenosis heart sounds, Study 3 presents the Mitral stenosis heart sounds, Study 4 presents the results of Mitral Regurgitation heart sounds, and Study 5 presents the results of S3 and S4 gallop heart sounds. Finally, the summary section summarizes the proposed algorithm and final results compared with other state-of-the-art algorithms.

Chapter 5: This chapter's introduction covers the overview of Artificial Neural Networks (ANN) and the inverse delayed function model of neuron. The Materials and Methods section covers the inverse delayed neuron function model of neuron, the prediction model using the ID function model of neuron, and the realization of the activation function of the ID function model of the neuron. The inverse delayed model function of the neuron section details the theoretical derivation of the model and its features to use in cardiac sound assessment. The prediction model using the ID function model of neuron shows a neural network algorithm

with an input layer using six inputs, a second layer constructed on 12 hidden neurons, and an output layer that consists of five output neurons. The realization of the activation function covers the implementation of the tan sigmoidal function. Hardware implementation of the proposed algorithm covers the Xilinx system generator model of neuron function and the total ANN model. Performance Evaluation provides the metrics for statistical assessments of the proposed system. The sensitivity, specificity, positive predictive rate, and detection error rate are used for performance metrics. Experimental results show the RTL schematic of the neuron model and implemented resource utilization of the device, training state analysis of neuron network based on ID function model of a neuron, Mean square error of different 11 epochs and selection of best valid epoch, regression analysis of ID function model of a neuron. The performance assessment of the proposed neuron model provides the sensitivity, specificity, and accuracy of extraction of normal and abnormal cardiac components. Receiver Operating Characteristics (ROC) curve results for the accuracy evaluation. Finally, the summary section summarizes the proposed algorithm and final results compared with other state-of-the-art algorithms.

Chapter 6: This chapter covers the summary of the present work, the final conclusion, and the scope of future work. Summary of the present work brief the problem statement and development of multi-channel phonocardiography, proposed source localization methods for sensor placement and system performance assessment results, proposed segmentation algorithm details, proposed ANN model using ID function model of neuron and normal and abnormal sounds classification results. The conclusion section briefs this thesis work's research activities and major contributions. Finally, the scope of future work provides possibilities for further activities of present research continuation, limitations of the present thesis work, and enhancements to improve the system.

Chapter 2. Research Background and Review of Literature

2.1 Introduction

The human heart consists of multiple anatomical structures, each producing distinct sounds. However, these sounds are often mixed and attenuated as they propagate through the chest wall. Additionally, environmental noise, patient-specific factors, and signal artifacts complicate localizing specific sound sources within the heart. During the initial stages of modern medicine, heart sound analysis is one of the major non-invasive methods to diagnose humans for illnesses [23][24]. The stethoscope was the primary phonocardiography instrument that played a major role in detecting heart auscultation, but this had its limitations regarding clinical expertise to analyze heart sounds [26]. In the digital era, phonocardiography has advanced Heart sound signal processing techniques for detecting, representing, analyzing, recognizing, and simulating heart sounds.

In recent years, Micro-Electrical-Mechanical Systems (MEMS) have become popular as it is inexpensive and play a vital role in medical research, especially in diagnostic devices [27]. The phonocardiography signals are primarily detected by the acoustic sensor in MEMS microphones, which are used to measure the heart sound's acoustics. The classification of the heart sound signal into its individual components and extracting features for the pathophysiological data make up the analysis of heart sound signals [28]. The present work aims at developing a high-performance phonocardiography system to help medical professionals capture and analyze heart sounds at the bedside.

2.2 Evaluation of phonocardiography system

The stethoscope has been the main tool used in phonocardiography to detect heart sounds and diagnose heart diseases from ancient times to the present digital era. Hyacinth Laennec (1816) was the first to listen to the sounds of the heart, not only directly with his ear to the chest, but he also invented the stethoscope and provided the basis of contemporary auscultation. As physiological knowledge increased through the following decades, faulty interpretations of heart sounds were progressively eliminated. The first transduction of heart sounds was made by Hurthle (1895), who connected a microphone to a frog nerve-muscle preparation. Einthoven (1907) was the first to record phonocardiograms with a carbon

microphone and a string galvanometer [18]. The evolution of PCG is strongly coupled with auscultatory findings, and clinicians predominantly drove the development [28]. A result of this situation is that a large variety of apparatus has been designed, mainly according to a medical researcher's specific needs or scientific interests [29]. During the 1960s, the necessity for standardization was strongly felt. Standardization committees made valuable proposals [7–9], but the impact on clinical phonocardiograph apparatus design was limited. During the 1970s and the 1980s, fundamental research on the physical aspects of recording, genesis, and transmission of heart sounds was performed [10–12]. Together with clinical investigations, understanding the heart sound phenomena improved considerably. At the same time, ultrasonic methods for heart investigation became available and gradually improved. Doppler and echocardiography provided closer information about heart action in a heart valve, wall movement, and blood velocity. Moreover, obtaining high-quality heart sound recordings with a high signal-to-noise ratio is problematic.

The review is carried out on the following topics to study the available methods in the present literature on multichannel phonocardiography systems.

- Literature study on phonocardiography sensors
- Cardiac sound sensor placements and detection
- Cardiac sound signal processing methods for classification and analysis

2.3 Literature review on phonocardiography sensors

The electronic stethoscope's advantages over traditional stethoscopes for cardiac sound detection include speed of usage, low cost, and familiarity with health care professionals. A digital stethoscope explicitly designed for cardiac diagnosis is thus appropriate for use in hospitals with limited equipment budgets. There are a number of difficulties implied by the stethoscope's portability [30]. The stethoscope's portability constrains the possible recording duration because it requires the healthcare professional to go outside the patient's comfort area. The presence of traction surges in recordings is a second issue with the handheld stethoscope. Since it's impossible to keep the stethoscope stationary, friction between the diaphragm and the skin causes noise in captured cardiac data. The creation of portable digital auscultation equipment for personal cardiac-sound evaluation has recently drawn more study attention due to the quick growth of semiconductors and precise manufacturing technologies [31].

In phonocardiography systems, acoustic sensors detect and record heart sounds. The most popular devices are microphones, including piezoelectric and acceleration sensors (accelerometers). The acoustic sensors based on condenser (electrostatic) microphones are used widely but need complex circuitry to measure the heart sounds. An alternative option for condenser microphones is “an electret microphone”. In this case, the immobile armature is a plate of polarized serum. Such a microphone does not require an external power supply since an electrostatic charge is formed during production [18]. This microphone has high sensitivity, but noise levels are more than 100Hz [32-33]. Piezoelectric microphones are a bit less popular in phonography. They are characterized by a simple structure instead of excellent frequency characteristics in the sphere of low frequencies; however, it is they are due and moisture. The drawbacks of piezoelectric sensors are a need for hard and high-quality contact with the patient’s skin (it is achieved utilizing suitable dielectric mediums, especially sticky lubricants, and gels) and low mechanical durability. The latter is conditional because thin ceramic films are used in sensitive acoustic sensors, 100 mm thick or less [34]. The size of the cardiac-sound sensors is increased by these cavities, making portable cardiac-sound detection devices impractical [35-36]. According to theoretical research by Wang et al. [37], auditory correlates of coronary turbulence will be at relatively high frequencies, exceeding 200 Hz and as high as 1 kHz, due to the tiny channel size. These frequencies have not been specifically targeted for detection by modern phonocardiography technologies since they are substantially higher than the components of valve sounds, and the majority of murmurs are detected using regular auscultation or phonocardiography.

The cardiac sound murmurs are low audible signals and challenging to capture with standard acoustic transducers. The acoustic transducer needs to be highly sensitive and have a high signal-to-noise ratio. Air-linked microphones and accelerometers are the two main sensor types that are frequently employed to record heartbeats. In the air-coupled configuration, a microphone is placed in a coupler mold, and the coupler mold's edges rest against the chest wall. The relative motion of the skin contained within the coupler mold determines how much of the recorded signal is proportionate [38]. The air-coupled microphone has the benefit of having little impact on the chest wall and a very straightforward fabrication. The disadvantage is that the air-coupled microphones have a poor impedance match with the chest wall and are susceptible to noise from the surroundings. Till now, many researchers to capture heart sounds using air-coupled microphones [39-43]. Thinklabs released an electronic stethoscope based on the Electromagnetic Diaphragm theory in 2003. The diaphragm of the stethoscope has a

conductive surface coating. There is a metal plate behind the diaphragm. Depending on the distance between them, the diaphragm and the plate function as a capacitor with a variable capacitance. Recent research on the acoustic detection of heart sound [44-46], utilized the Thinklabs stethoscope. Piezoelectric contact sensors [47], which Chen et al. employed in studies of cardiac sounds [48], are another transducer principle. Dr. Salvatore Mangione, MD, of Philadelphia's Allegheny University of Health Sciences [29], in his study, stated that medical students are more challenging to train for detecting heart sound problems with a stethoscope.

These drawbacks can be overcome by the MEMS microphone-based heart sound detection system, which is more compact and has an embedded digital interface that is simple to integrate with any system without a lot of additional electronic overhead. The experiments [48-49] revealed that sensors based on MEMS microphones recorded the highest-quality heart sounds when the acoustic sensor was placed in the area of the right second intercostal space. The frequency range of the signal recorded was 60-140 Hz [50]. Signals contain useful information and the least amount of noise, limiting the diagnosis process in auscultation. Due to high sensitivity, immune to noise characteristics, and ease of implementation, the MEMS microphones were considered for the present multichannel phonocardiography system.

2.4 Cardiac sound sensor placements and detection

Heart sound detection at multi-site recording has been done for 25 years. In 1978, B. Hök et al. detected the chest-surface vibrations induced by heart action using holographic interferometry [51-54]. However, that is unsuitable for catching time-related changes such as vibration propagation. After that, in 1980, K. Chihara et al. measured the first heart sound at 25 points on the chest surface with each of four phone microphones [54]. In 1982, M. Okada repeated the recording of cardiac sounds at every 36 positions of the chest surface concurrently with a 2-channel electrocardiogram and analyzed the recorded phonocardiogram, which synchronized to the time reference point R-wave peak of the ECG [55]. In 1983, J. Verburg simultaneously measured the heart sounds at 12 places on the chest wall. Results of examining the propagation velocity of heart sound indicated propagation at almost 10 (m/s) [56]. It surmised that generation and propagation of the heart sound often show a dipolar relation. In 1989, H. Vermarien repeated the simultaneous recording of heart sounds at all eight positions on the chest wall; a phonocardiogram that synchronized 49 positions was obtained, and the heart sound's intensity distribution confirmed the dipole pattern [57]. In 1998, M. Cozic et al.

implemented simultaneous sampling of the envelope for heart-sound at 22 sites on the chest wall using analog circuits [58]. Recently, visualization of the current distribution in cardiac muscle [59] and the spatial analysis of the radio magnetic field [60] was reported using a 64-channel magnetocardiography system. These measurements used bulky, heavy, and expensive equipment utilized for specialized magnetic sensing of a superconducting quantum interference device.

Sound source localization techniques in this sector may generally be categorized into four major groups: methods based on time difference of arrival (TDOA) [61-62], methods based on beam formation [63-64], approaches based on high-resolution processing [65-66], and techniques that need a training phase [67-68]. The TDOA approach is highly accurate at locating static sound sources, particularly transient events (69). To accurately measure TDOA, the Generalized Cross Correlation (GCC) and its variations, including the Cross Power Spectrum Phase (CSP) and Generalized Cross Correlation utilizing Phase Transform (GCC-PHAT), can be used [70-72]. The TDOA and beamforming techniques could not be successfully used for localization purposes and have a poor performance when a microphone array is faced with multiple sound sources. The high side lobe level of the employed beam pattern reduces the accuracy of the method for narrow-band signals since the resolution of source localization via beamforming is incredibly reliant on the source frequency [73]. The subspace localization techniques work with higher resolution results and make use of spectrum estimation. Some well-known techniques in this category include (MUSIC) [74], Estimation of Signal Parameters through the Rotational Invariant Technique (ESPRIT) [75], and root-MUSIC [76]. These methods will perform less well when sources are incoherent since the covariance matrix is assumed in these methods to be in maximum order.

In the first step, a set of Time Difference Of Arrivals (TDOAs) is estimated using measurements across different combinations of microphones [77-82]. In the second step, when the position of the sensors and the speed of sound are known, the source positions can be estimated using geometric considerations and rough estimators. This widely used method is known as the indirect method. Using a least squares solution, close-formed estimators, and Iterative maximum likelihood estimators [83-89]. The position of the sources can be directly determined, and spatial probability functions can be defined from the area's acoustic map produced by the direct technique. Accurate localization of the sources of cardiac sounds can provide valuable insights into cardiac dynamics and aid in diagnosing cardiovascular conditions. The localization of cardiac sources within PCG signals provides valuable insights

into the underlying physiological processes. Localization of sound sources allows clinicians to monitor changes in cardiac function over time. By tracking the spatial distribution of specific sound sources, the effectiveness of therapeutic interventions can be assessed, and appropriate follow-up care can be provided.

2.5 Cardiac sound signal processing methods for classification and analysis

Every time a medical professional takes auscultation, he or she tries to distinguish the different cardiac components and is trained to evaluate relevant parameters, including rhythm, temporal instants, intensity of heart sound components, splitting of S2, etc. Using this approach, he or she can look for murmurs and audio anomalies that might be related to particular heart diseases. Auscultation may not be effective for determining a diagnosis if there are poor listening conditions (such as in a crowded healthcare ward), other noises or murmurs are present, the heart is beating quickly, or there are non-cardiac sounds, such as chest wheeze or lung sounds, are present [90-91]. Growing semiconductor technology in the digital era makes it possible to address these issues from raw signal capture through final processing to identify anomalies [92-93].

In the literature, a number of signal processing procedures have been proposed for cardiac sound segmentation, classification, and feature extraction for finding abnormalities. A number of studies are researching a wide range of approaches to create a tool that can deliver steady and dependable findings conveniently and affordably [94]. Many different types of noise and artifacts from numerous sources frequently affect the collected PCG signals. A PCG segmentation method's accuracy may suffer from the presence of noise and artifacts. Therefore, to mitigate the impact of high-frequency disturbances, the recorded PCG signal was first filtered. A digital low-pass filter (LPF) with a cutoff frequency of 900 KHz and a wavelet decomposition method was employed in the majority of PCG segmentation techniques [95-98]. For cardiac sound segmentation, a number of parameters have been proposed in the literature [97-104], including amplitude, energy, the square of energy, average Shannon energy, average three-order Shannon energy, instantaneous amplitude, energy, and frequency, as well as an ideal signal envelope. In past studies, wavelet transforms have been frequently used for the segmentation of heart sounds [105–106][107]. To find the low frequency cardiac sound components, we can use the time-frequency representation [108- 109]. The time and

frequency resolutions of TFR techniques like the short-time Fourier transform (STFT) and Wigner-Ville distribution (WVD) are demonstrated [110 - 116]. In cardiac sound analysis, the Stockwell transform is a preferred method to the STFT [117-118]. The STFT's key drawback is its trade-off between chronological and spectral accuracy [119-120]. The wavelet transform was often employed to categorize biological signals based on the literature [121–126]. Wavelet denoising technique allowed for independent modification of the recorded PCG signal and didn't necessitate any further measuring procedures [127-133]. As a result, it was possible to make the measurement apparatus smaller, and the patients were more comfortable throughout the examination. Analyses of models [134–136] demonstrated the superiority of wavelet denoising techniques among alternative adaptive algorithms.

Artificial neural networks (ANNs), which are based on the cognitive system of the human, are frequently employed in pattern recognition and computer learning [137-138]. These networks have a critical role in a number of fields, such as biomedical engineering, control engineering, and electronic systems [139-140]. Cardiac sounds have been categorized using Multi-Layer Perceptron -Back Propagation in [141] and [142]. Three cases of cardiac sounds were used to train a two-dimensional self-organizing map [143], but sufficient performance was not reported. The selection of input features for the multi-layer perception can take some time [144-146], making the deployment of Artificial Neural Networks (ANN) time-consuming. The properties of the input also affected the number of layers and neurons in each layer. It takes inspiration from efforts to simulate organic networks of neurons. Here, the nodes are connected using weighted linkages. The network learns throughout the learning phase by modifying the weights to enable the prediction of the correct class labels for the input sequence. Fuzzy neural networks based on wavelets have also been utilized to identify coronary artery disease. To distinguish between normal and abnormal phonocardiogram data from the human heart, deep convolutional neural networks, and mel-frequency spectrum coefficients were used. The experiment's data set includes heart sound data from PhysioNet.org. The accuracy of the suggested method is 84.15%. 80.63% and 87.66%, respectively, were the sensitivity and specificity [147]. Automatically detecting urban noises was examined in [148] using feature extraction based on the short-time Fourier transform (STFT) spectrogram, feed-forward artificial neural networks (ANN), and k-nearest neighbor (kNN) classifiers. Similar to [149], local binary pattern (LBP) features taken from spectrogram transforms were used to train an SVM to classify environmental noises. Convolutional neural networks (CNN) were used as the classifier to assess speech emotions in a similar manner [150-154].

The features of heart sounds were extracted using the wavelet transform and classified using a neural network with 64.7% of sensitivity and 70.5% specificity [155]. Analyzed the doppler signals of heart valves using wavelet transform and short-time Fourier transform and classified the cardiac sounds using HMM with sensitivity of 97% and 92% of specificity [106]. The least-squares support vector machine categorized the heart sounds into two groups with a 94.5% of specificity of 94.5% and a 90% of sensitivity.

Traditional approaches have primarily focused on time-frequency analysis and feature extraction techniques. This study presented a multi-channel phonocardiography system that simultaneously recorded the heartbeat at four different sites using MEMS-based microphones as sensors. By measuring the time delays and identifying the sensor location using a good the signal to noise ratio, heart sound localization is used to determine where to place the sensors. The segmentation of heart sounds was done using the proposed wavelet analysis. To identify abnormal heart sounds, the classification of cardiac sound components is carried out using neural network training from the derived feature set. The proposed algorithms were developed on SoC FPGA, and the outcomes were evaluated against MATLAB simulations.

Chapter 3. Development of MEMS Microphone based Multi-Channel Phonocardiography system

3.1 Introduction

In recent years, phonocardiography systems have become popular for recording cardiac sounds and studying structural abnormalities in heart sounds. However, the detection and processing of low-frequency signals from an adult's heart, or detection of the cardiac signal from a single/multiple fetus of a pregnant patient, or detection and analysis of low-frequency respiratory, gastric bio-signals and their effects on cardiac, is complicated by issues such as sensor placement. This calls for a need for a high-sensitivity phonocardiogram (PCG) sensor with robust characteristics, sensor portability, and the need for multichannel signal detection and processing. In general, various acoustic sensors are required for each new or modified application to detect low-frequency sounds, which causes system portability and evaluation issues. Also, the current medical systems for diagnosis, such as the electronic noninvasive phonocardiography system and related point of care (POC) medical systems, may not have multichannel or multimodal safe computations embedded for effective detection of the low-frequency cardiac signal or continuous noninvasive monitoring of the patients' health [156-163].

The detection of structural heart defects such as aortic insufficiency or the existence of a ventricular septal defect (VSD) remains a significant clinical challenge. Although precise auscultation can detect many of these anomalies, only experienced cardiologists can consistently detect crucial yet subtle auscultatory findings. Echocardiography is excellent at detecting and describing such anomalies, and it is costly and unsuitable for bulk screening or continuous monitoring. Furthermore, its operation demands a great deal of expertise and experience. The current research work addresses these issues using a multichannel phonocardiography system and methods to analyze the cardiac sounds to find the abnormalities.

Acoustic MEMS (microelectromechanical systems) microphones present unique prospects for healthcare diagnostics and treatments due to their small size, lightweight, and ability to be shaped into an array over a limited area. Because of its small size, MEMS microphones have a high surface-to-volume ratio that can be used in a surface-reaction-based medical diagnostic tool. Furthermore, there are other advantages like the tiny size and weight

of fewer reagents, accurate (and digital) reagent control, the potential to implant acoustic MEMS in the human body, improved functional aspects not feasible with macro systems, and low power consumption [164-171].

Noise reduction is used to raise the Signal Noise Ratio (SNR), which allows for a more accurate assessment of the source position in significant conditions with low SNR. All of the signals from the network arrays are processed using algorithms that provide the source positions during localization [172-182]. Finally, post-processing is an important step that improves the precision of location data and aims to reduce or eliminate the effects of reflection, reverberation, and incorrect measurements [183].

In real contexts, the presence of a noise source and echo effects substantially reduce the performance of a PCG system. Some channels will have lower signal-to-noise ratios (SNR) than others, depending on the distance between each microphone and the noise source signal, mainly when a large microphone array is used [184]. The resonance effects varied between the sensors as well. As a result, deploying as many microphones as possible in an actual situation may not necessarily improve speech enhancement performance. Furthermore, in microphone array processing, it is commonly assumed that all microphones have the same characteristics. Differences in the system operation from the microphone to the analog-to-digital converter (ADC) [185-186] may invalidate this assumption. The SNR-based method is easy and quick to calculate but relies on cardiac activity monitoring and is hence challenging in chaotic environments.

Himawan et al. addressed the issue of microphone placement on an ad hoc basis [187]. As a result, microphone clustering must be done without prior knowledge of microphone placements. In contrast, we examine a situation where the microphones are strategically placed, and the locations are known ahead of time. This assumption allows us to simplify the problem significantly. In general, we can use the multichannel cross-correlation coefficient (MCCC) [188-189] as a method for evaluating whether channels are reliable. The cross-correlation coefficient can be viewed as a specific case of the MCCC calculated with more than one channel. We choose the maximum MCCC criterion for channel selection, although Benesty et al. developed the MCCC for the speaker localization problem [190]. Using the classical Cross-Correlation, the Generalized Cross-Correlation (GCC) [189], multichannel signal processing for sound localization estimates the Time Difference Of Arrival (TDOA) between a microphone pair.

The present algorithm is aimed at extracting the signal from unreliable channels which are mutually independent of those from other channels. We first use the phase transform (PAHT) to adjust for the signals' delays for computational efficiency [191-192]. Next, we compute the large MCCC once the multichannel signal has been aligned and then select a set of channels with the large MCCC. Lastly, the selected channels were subjected to post-filtering. Through a series of cardiac signal identification studies using real data acquired with real microphones, we demonstrate the efficiency of our channel selection technique.

3.2 Materials and Methods

3.2.1 High-Performance Multichannel phonocardiography system Design

The proposed high-performance phonocardiography system was developed based on the advanced MEMS microphone to capture the low-frequency components and analyze the captured data using the proposed algorithm based on the inverse delayed function model of neurons. The proposed algorithm was implemented on Xilinx Zynq-7 System on chip Field-programmable Gate Array which has dual-core ARM Cortex -A9 for application software and programmable logic for algorithm complex computations [193]. The detailed block diagram for the high-performance phonocardiography system is shown in Figure 3-1.

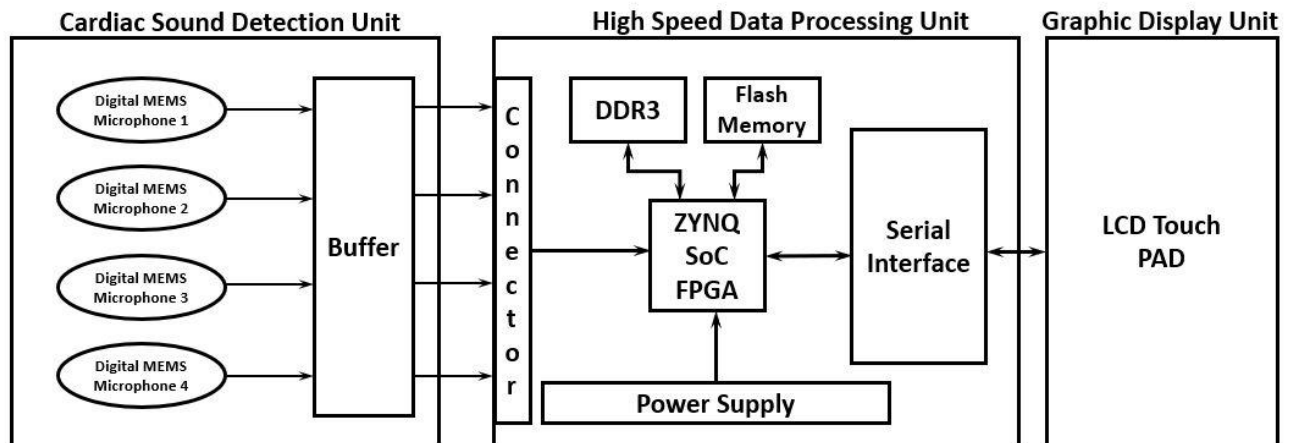


Figure 3-1: Phonocardiography System Block Diagram

Cardiac Sound Detection (CSD) unit consists of a MEMS microphone, a tiny Integrated circuit with a sound transducer, an analog front end, and signal conditioning circuit [194-195]. The MEMS microphone has a high Signal Noise Ratio (SNR) of 70 dB and a good frequency response from 10 Hz to 10 kHz, as shown in Figure 3-2. Due to its flat response and high SNR

in the lower region more suitable for detecting the third and fourth heart sounds and murmurs. The CSD module has four microphones placed based on sound source localization to cover the four heart valves (Aortic valve, Tricuspid valve, Mitral valve, and Pulmonary valve), which are the origins of the cardiac sounds.

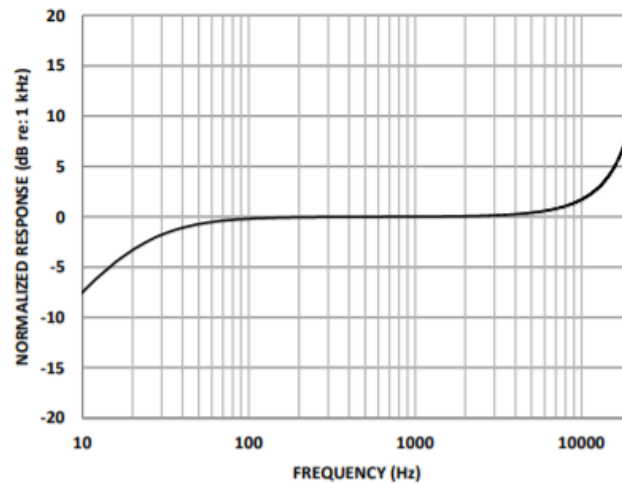


Figure 3-2: MEMS microphone Frequency response

Figure 3-3a shows the microphone sensor jacket developed for capturing heart sound signals. Figure 3-3b. shows the hardware board developed for the systems development. High-Speed Data Processing (HSDP) unit consists of Xilinx Zynq-7 System on chip Field-programmable Gate Array which has dual-core ARM Cortex -A9 processor for application software, programmable logic for algorithm complex computations. The HSDP module is responsible for separating cardiac sounds based on the frequencies and processes using the proposed ANN-based ID model neuron. The Graphical Display Recorder (GDR) unit consists of an LCD touchpad for parameter configuration and a display for analyzing the results for further diagnosis. Apart from dynamic analysis, the GDR Module also stores the original signal in non-volatile memory (SD Card) for future offline analysis and reference for training purposes. The application software was developed on an ARM cortex-A9 processor and interfaced with the GDR module.

The current system is implemented in two phases. In the first phase, the proposed algorithm was modeled using MATLAB, simulated with different test parameters, and baselined as a golden reference for further hardware system development. The proposed algorithm was implemented on FPGA in the second phase compared to the MATLAB model.

The cardiac sounds detected by the CSD unit are passed to the HSDP unit to extract the cardiac feature set. These feature sets are given to respective processed blocks for further analysis.

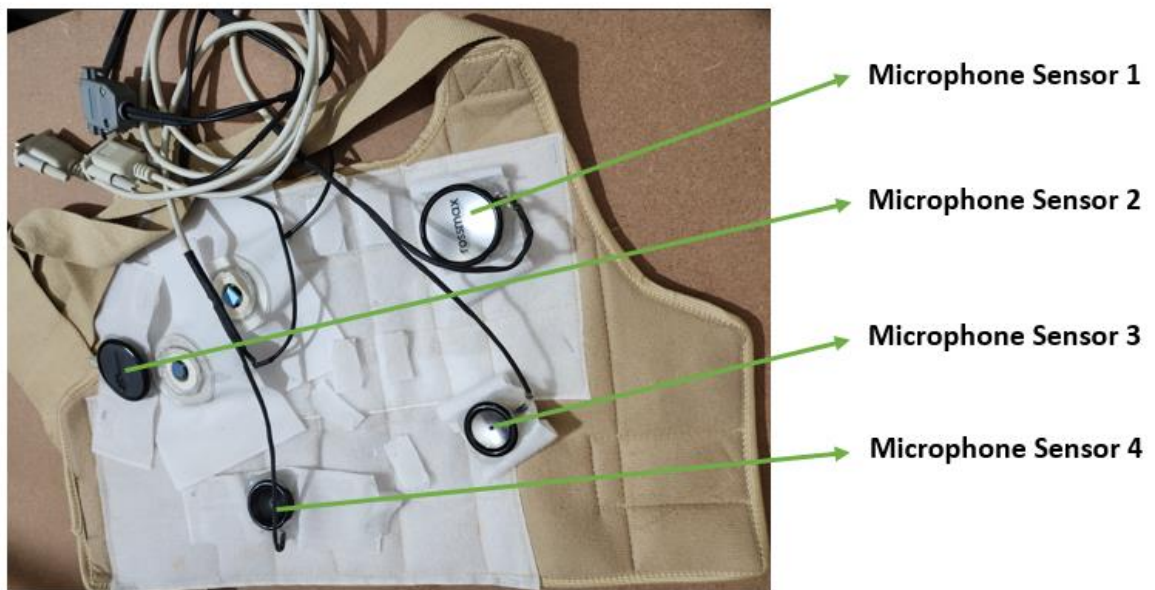


Figure 3-3a: Cardiac sound detection jacket with four sensors

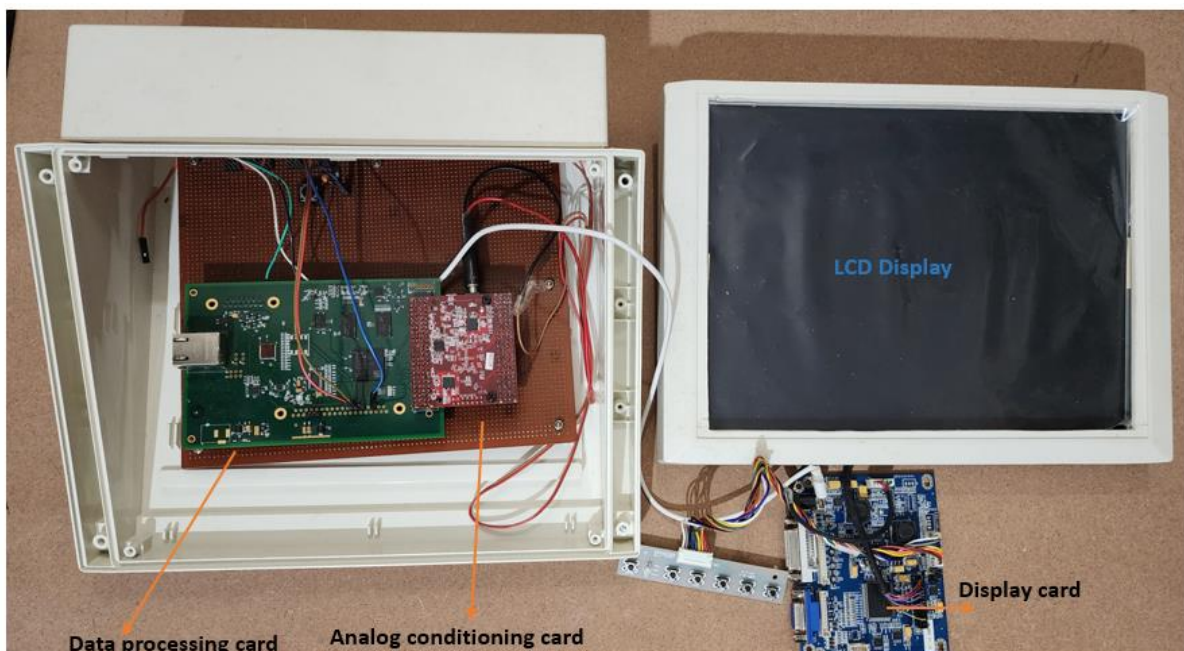


Figure 3-4b: High speed data processing unit with LCD Display

3.2.2 Heart sound localization and microphone placement

The localization of the heart sound and placement of the MEMs microphones are computed based on the Time Delay of Arrival (TDOA) method [196-209]. The digital MEMs microphones are placed at four heart valves in a fixed location, as shown in Figure 3-5. Let the four microphones' Cartesian coordinates be designated as (x_1, y_1) , (x_2, y_2) , (x_3, y_3) , (x_4, y_4) , and the heart sound source at (x_s, y_s, z_s) . The \vec{r}_1 , \vec{r}_2 , \vec{r}_3 , \vec{r}_4 and \vec{r}_s are the vector representation of four microphones and heart sound sources from the origin of the coordinate system. The heart sound source reaches the microphone at different time intervals t_1 , t_2 , t_3 , and t_4 .

The mathematical relationship between the heart sound source and four microphones is as follows:

$$\|\vec{r}_s - \vec{r}_i\| = \|\vec{r}_s - \vec{r}_1\| + c\Delta t_{1i} \quad (1)$$

Where $\Delta t_{1,i}$ ($i = 2, 3, 4$) is the TDOA between the i^{th} microphone and the first microphone, obtained using the generalized cross-correlation (GCC) method [106]. A positive $\Delta t_{1,i}$ means i^{th} microphone is far from the sound source than the first microphone, while negative $\Delta t_{1,i}$ means i^{th} microphone is near the sound source. c is the heart sound velocity, and the symbol $\|\cdot\|$ represents the length of a vector.

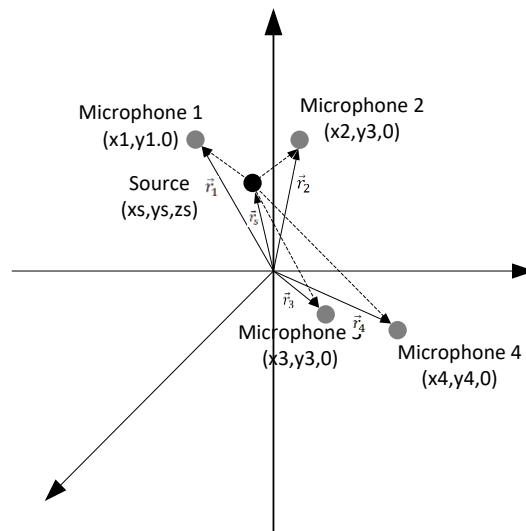


Figure 3-5: Microphone Placement for Heart sound source Localisation

Eq. (1) can be rewritten as

$$\sqrt{(x_s - x_i)^2 + (y_s - y_i)^2 + z_s^2} = \sqrt{(x_s - x_1)^2 + (y_s - y_1)^2 + z_s^2} + c\Delta t_{1,i} \quad (2)$$

Substitute the microphone locations (x_1, y_1) , (x_2, y_2) , (x_3, y_3) , (x_4, y_4) in Equation 2.

$$\sqrt{(x_s - x_2)^2 + (y_s - y_2)^2 + z_s^2} = \sqrt{(x_s - x_1)^2 + (y_s - y_1)^2 + z_s^2} + c\Delta t_{1,2} \quad (3)$$

$$\sqrt{(x_s - x_3)^2 + (y_s - y_3)^2 + z_s^2} = \sqrt{(x_s - x_1)^2 + (y_s - y_1)^2 + z_s^2} + c\Delta t_{1,3} \quad (4)$$

$$\sqrt{(x_s - x_4)^2 + (y_s - y_4)^2 + z_s^2} = \sqrt{(x_s - x_1)^2 + (y_s - y_1)^2 + z_s^2} + c\Delta t_{1,4} \quad (5)$$

Where c is the velocity of sound, $\Delta t_{1,2}$ is the time interval between the first and second microphones, $\Delta t_{1,3}$ is the time interval between the first and third microphones, $\Delta t_{1,4}$ is the time interval between the first and fourth microphone.

Squaring equation 3 and canceling the similar terms on both sides.

$$\begin{aligned} (x_s - x_2)^2 + (y_s - y_2)^2 + z_s^2 &= (x_s - x_1)^2 + (y_s - y_1)^2 + z_s^2 + 2((x_s - x_1)^2 + (y_s - y_1)^2 + z_s^2)(c\Delta t_{1,2}) \\ &\quad + (c\Delta t_{1,2})^2 \end{aligned}$$

$$\begin{aligned} x_2^2 + y_2^2 - x_1^2 - y_1^2 - (c\Delta t_{1,2})^2 &= -2x_s(x_1 - x_2) - 2y_s(y_1 - y_2) + 2C\Delta t_{1,2}\sqrt{(x_s - x_1)^2 + (y_s - y_1)^2 + z_s^2} \end{aligned} \quad (6)$$

$$\text{Substituting } x_2^2 + y_2^2 - x_1^2 - y_1^2 - (c\Delta t_{1,2})^2 = C2$$

$$C2 + 2x_s(x_1 - x_2) + 2y_s(y_1 - y_2) = 2C\Delta t_{1,2}\sqrt{(x_s - x_1)^2 + (y_s - y_1)^2 + z_s^2} \quad (7)$$

Similar operation is performed on equation 4 and equation 5.

$$C3 + 2x_s(x_1 - x_3) + 2y_s(y_1 - y_3) = 2C\Delta t_{1,3}\sqrt{(x_s - x_1)^2 + (y_s - y_1)^2 + z_s^2} \quad (8)$$

$$C4 + 2x_s(x_1 - x_4) + 2y_s(y_1 - y_4) = 2C\Delta t_{1,4}\sqrt{(x_s - x_1)^2 + (y_s - y_1)^2 + z_s^2} \quad (9)$$

Where $C3 = x_3^2 + y_3^2 - x_1^2 - y_1^2 - (c\Delta t_{1,3})^2$ and $C4 = x_4^2 + y_4^2 - x_1^2 - y_1^2 - (c\Delta t_{1,4})^2$

Dividing equation 7 by Equation 8 gives

$$\begin{aligned} C2\Delta t_{1,3} + 2\Delta t_{1,3}[x_s(x_1 - x_2) + 2y_s(y_1 - y_2)] \\ = C3\Delta t_{1,2} + 2\Delta t_{1,2}[x_s(x_1 - x_3) + 2y_s(y_1 - y_3)] \end{aligned} \quad (10)$$

Dividing equation 7 by Equation 9 gives

$$\begin{aligned} C2\Delta t_{1,4} + 2\Delta t_{1,4}[x_s(x_1 - x_2) + 2y_s(y_1 - y_2)] \\ = C4\Delta t_{1,2} + 2\Delta t_{1,2}[x_s(x_1 - x_4) + 2y_s(y_1 - y_4)] \end{aligned} \quad (11)$$

Rearrange the Equation 10 and Equation 11.

$$x_s \left[\frac{(x_1 - x_3)\Delta t_{1,2} - (x_1 - x_2)\Delta t_{1,3}}{(y_1 - y_3)\Delta t_{1,2} - (y_1 - y_2)\Delta t_{1,3}} \right] + y_s = \frac{1}{2} \left[\frac{C2\Delta t_{1,3} - C3\Delta t_{1,2}}{(y_1 - y_3)\Delta t_{1,2} - (y_1 - y_2)\Delta t_{1,3}} \right] \quad (12)$$

$$x_s \left[\frac{(x_1 - x_4)\Delta t_{1,2} - (x_1 - x_2)\Delta t_{1,4}}{(y_1 - y_4)\Delta t_{1,2} - (y_1 - y_2)\Delta t_{1,4}} \right] + y_s = \frac{1}{2} \left[\frac{C2\Delta t_{1,4} - C4\Delta t_{1,2}}{(y_1 - y_4)\Delta t_{1,2} - (y_1 - y_2)\Delta t_{1,4}} \right] \quad (13)$$

Consider

$$a_1 = \frac{(x_1 - x_3)\Delta t_{1,2} + (x_1 - x_2)\Delta t_{1,3}}{(y_1 - y_2)\Delta t_{1,3} + (y_1 - y_3)\Delta t_{1,2}}, \quad a_2 = \frac{(x_1 - x_4)\Delta t_{1,2} + (x_1 - x_2)\Delta t_{1,4}}{(y_1 - y_2)\Delta t_{1,4} + (y_1 - y_4)\Delta t_{1,2}}$$

$$b_1 = \frac{c_3\Delta t_{1,2} + c_2\Delta t_{1,3}}{2[(y_1 - y_2)\Delta t_{1,3} + (y_1 - y_3)\Delta t_{1,2}]}, \quad b_2 = \frac{c_4\Delta t_{1,2} + c_2\Delta t_{1,4}}{2[(y_1 - y_2)\Delta t_{1,4} + (y_1 - y_4)\Delta t_{1,2}]}$$

Substitute a_1, a_2, b_1, b_2 in equation 12 and equation 13.

$$b_1 = a_1 x_s + y_s \quad (14)$$

$$b_2 = a_2 x_s + y_s \quad (15)$$

Equation 14 and Equation 15 are solved for the values of x_s and y_s , which represent the coordinates of the sound source.

$$x_s = \frac{b_2 - b_1}{a_1 - a_2}, \quad y_s = \frac{a_1 b_2 - a_2 b_1}{a_1 - a_2}$$

$$z_s = \pm \sqrt{\left(\frac{2(x_1 - x_2)x_s + 2(y_1 - y_2)y_s + c_2}{2c\Delta t_{1,2}} \right)^2 - (x_s - x_1)^2 + (y_s - y_1)^2} \quad (16)$$

Equation 16 represents the localization of the heart sound source with respect to four microphones.

The sensor module has four individual channels, and each channel was developed using Digital MEMS microphone modules to cover the four heart valves (Aortic, Tricuspid, Mitral, and Pulmonary) [210-212]. Figure 3-6. shows the placement of the four PCG sensors on the body to capture the data. Figure 3-7. shows the printed circuit board for the PCG sensor used in the present work. A first microphone was placed at the aortic valve to cover the right side of the 2nd intercostal space, just lateral to the sternum. The second microphone was placed at the pulmonic valve to cover the left side of the 2nd intercostal space, just lateral to the sternum. The third microphone was placed at the Tricuspid valve to cover the left side of the 4th-5th intercostal space over the left sternal border. Finally, the Fourth microphone was placed at the Mitral valve to cover the 5th intercostal space, the midclavicular line.

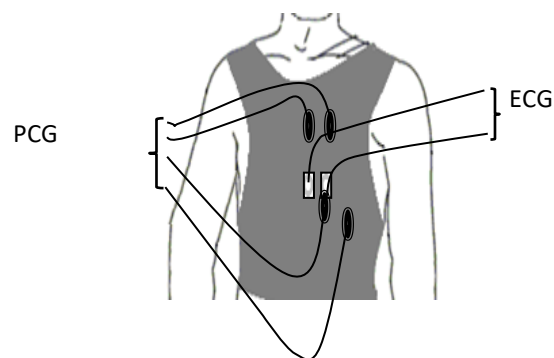


Figure 3-6: PCG sensors placement for the experiment



Figure 3-7: PCG Sensor Printed Circuit Board (10x10mm)

The First heart sound is best heard at the mitral and tricuspid valves more stridently than other components. The second heart sound is best heard at the aortic and pulmonary valves. The Third and Fourth sounds are best heard at the mitral valve low-pitched blowing

sound during the early and late diastole cycle. During pathology, systolic and diastolic murmurs heard with low-pitched sounds at the valve indicate the dysfunction of the respective heart valve.

3.2.3 Cross-Correlation methods for TDOA calculation

Cross-Correlation (CC) is a measure of two signals' similarity. The CC is defined as the product of two wide-sense stationary signals. y_1 and y_2 .

$$C_{y_1, y_2}(p) = E[y_1(k)y_2(k + p)] \quad (17)$$

$E[\cdot]$ denotes mathematical expectation, and the relative time delay is calculated using a cross-correlation function estimation of the highest peak detection.

$$\hat{\tau} = \operatorname{argmax} C_{y_1, y_2}(p) \quad (18)$$

Because of the restricted observation period and the non-stationary nature of the acoustic source, the CC is determined by its time-averaged estimate at time k on observed samples of length $k+L$; hence, the CC in digital implementation becomes

$$C_{x_1, x_2}(p) = \begin{cases} \frac{1}{L-p} \sum_{l=0}^{L-1} y_1(k+l)y_2(k+l+p), p = 0, \dots, \tau_{max} \\ \frac{1}{L-p} \sum_{l=0}^{L-1} y_2(k+l)y_1(k+l+p), p = -\tau_{max}, \dots, -1 \end{cases} \quad (19)$$

where τ_{max} is the maximum TDOA of the microphone pair and depends on the distance between microphones

$$\tau_{max} = \frac{d_{12}}{c} \quad (20)$$

The Pearson Correlation Coefficient (PCC) can normalize the CC. The PCC measures the correlation between two signals, with values ranging from +1 to -1. The PCC is calculated by multiplying the covariance of two variables by the product of their standard deviations.

$$\rho_{y_1, y_2} = \frac{\text{cov}(y_1, y_2)}{\sigma_{y_1} \sigma_{y_2}} = \frac{E[(y_1 - E[y_1])(y_2 - E[y_2])]}{\sigma_{x_1} \sigma_{x_2}} \quad (21)$$

Many factors, such as signal self-correlation and reverberation, might reduce the CC's performance. As a result, it is inappropriate to use it in a real-world setting.

The Generalized Cross-Correlation (GCC) is the classic method to estimate the relative time delay associated with acoustic signals received by a pair of microphones in a moderately reverberant and noisy environment. The GCC consists of a cross-correlation followed by a filter to reduce the performance degradation caused by additive noise and multipath channel effects. The GCC in the frequency domain is

$$C_{y_1, y_2}^{GCC}(k) = \frac{1}{L} \sum_{f=0}^{L-1} \Psi(f) S_{y_1, y_2}(f) e^{\frac{2\pi j f k}{L}} \quad (22)$$

where $\Psi(f)$ is the frequency domain-general weighting function, and the cross-spectrum of the two signals is defined as

$$G_{y_1, y_2}(f) = E[Y_1(f)Y_2^*(f)] \quad (23)$$

where $Y_1(f)$ and $Y_2(f)$ are the DFT of the signals and $*$ denotes the complex conjugate. GCC is used to minimize the influence of moderate uncorrelated noise and moderate multipath interference, maximizing the peak in correspondence with the time delay. The relative time delay τ is obtained using an estimation of the maximum peak detection in the filter cross-correlation function

$$\hat{\tau}^{GCC} = \text{argmax} C_{y_1, y_2}(k) \quad (24)$$

The CC is computed when $\Psi(f)CC = 1$. The CC is estimated using the DFT and the IDFT, which can be efficiently implemented with the Fast Fourier Transform (FFT). The most used and effective weighting function is the Phase Transform (PHAT). It places equal importance on each frequency by dividing the spectrum by its magnitude. The

PHAT normalizes the amplitude of the spectral density of the two signals and uses only the phase information to compute the GCC.

$$\Psi_{PHAT}(f) = \frac{1}{G_{y_1, y_2}(f)} \quad (26)$$

In acoustic and noisy situations, the GCC efficiently enhances time delay estimation between microphone pairs [213-214]. The GCC approaches are fast and accurate, making them ideal for monitoring real-time systems that require an estimate. Furthermore, in periodic sounds, or generally quasi noises, the GCC performance is significantly lowered. When applied to a quasi-sound, the GCC is less effective in reducing the negative impacts of noise and reverberation. [191] provides a thorough examination of PHAT performance for both broadband and narrowband signals. The findings show that the PHAT can improve detection accuracy for one or more locations in noisy and acoustic situations when the sound occupies most of the frequency band.

The Multichannel Cross-Correlation Coefficient (MCCC) approach [215] is a spatial correlation-based method that uses redundant data from many sensors. Using the spatial prediction (or interpolation) error, the aim is to evaluate the correlation between many signals [216]. We can formulate the signal model using the microphone placement indicated in Fig. 3, a single source, ignoring the noise terms.

$$y_n(k + \tau_n) = \alpha_n G(k - t) \quad (27)$$

The time-aligned signal is as follows once the time delays of M signals are determined using the PHAT.

$$Y = [y_1(k), y_2(k + \tau_n) \dots y_n(k + (N - 1)T_n)]^T \quad (28)$$

We'll need a spatial correlation (covariance) matrix of observations to construct the MCCC. The spatial correlation matrices can be written as follows:

$$C_N = E\{Y_{d,N}[k]Y_{d,N}^T[k]\} \quad (29)$$

Then, given the TDOA estimates, the MCCC can be computed as

$$\rho_N^2 = 1 - \frac{\det[C_N]}{\prod_{i=1}^M \sigma_i^2} \quad (30)$$

where $\det[.]$ denotes the determinant and σ_i^2 denotes the C_N spatial correlation matrix i^{th} diagonal component. In the case of $M = 2$, the MCCC is easily proved to be comparable to the cross-correlation coefficient normalized by the energy.

In the present study, MCCC with constant time delays for channel selection using the TDOA based on the PHAT results in a significant computational decrease in the case of the near-field assumption.

3.2.4 Feature sets for cardiac sound assessment

The assessment of the cardiac sound components involves the different parameters, and a set of features defers these to sort out the components from the heart sounds. In the current research, the segmentation algorithm by Springer et al. 2016. was used to differentiate the heart sound using timing intervals of S1, S2, Systole, and diastole. The following parameters (Table 3-1) are used as feature sets to identify the low-frequency abnormal and normal heart sound components.

Table 3-1: Cardiac sounds Feature sets

S. No	Feature	Description
1	F1	Mean of the Systolic to diastolic time interval ratio of each heart sounds.
2	F2	Mean of the S1, S2 intervals ratio.
3	F3	Mean of the heart sound peak energy in the systolic cycle to total cardiac cycle energy of each heartbeat.
4	F4	Mean of the heart sound peak energy in the diastolic cycle to total cardiac cycle energy of each heartbeat.
5	F5	The mean of spectral frequencies from 10 Hz to 900 Hz with a window resolution of 10 Hz in the systole cycle of each heartbeat.
6	F6	Mean spectral frequencies from 10 Hz to 900 Hz with a window resolution of 10 Hz in the diastolic cycle of each heartbeat.

3.2.5 Performance Evaluation

The proposed system performance is assessed using statistical values, like Repeatability, Reproducibility, and error in coordinate positions with respect to SNR. Repeatability and reproducibility are the two aspects of precision measurement. Repeatability refers to the variability in repeated measurements by one observer when all other factors are assumed constant. Reproducibility refers to the variability in repeated measurements when one or more factors, such as observer, instrument, calibration, environment, or time are varied. The current guidelines from the British and International Standards recommend the expression of repeatability and reproducibility estimates in terms of standard deviations. The random-effects model was used to compute the standard deviation (ρ), Variation coefficient (VC), and repeatability Coefficient (RC).

$$VC = \frac{\rho}{\sigma} \quad (31)$$

σ means overall mean,

$$RC = \sqrt{2} * 1.96\rho \quad (32)$$

The source coordinates are estimated using this input data, and the accuracy of the output is assessed using L-2 norm errors specified with the benchmark coordinates.

$$err = \frac{|\vec{r} - \vec{r}_{ref}|^2}{|\vec{r}_{ref}|^2} * 100\% \quad (33)$$

Where \vec{r}, \vec{r}_{ref} represents the measured and reference positions, respectively.

3.3 Experimental results

Heart sounds are captured using the proposed phonocardiography system in section 3.2.1 under the supervision of a doctor to ensure that the measurements are accurate. All tests on human subjects follow the Declaration of Helsinki. The proposed localization algorithm was implemented in a zynq SoC FPGA and evaluated on captured signals at a 2 kHz sampling rate.

The heart sounds of 50 patients with normal and abnormal sounds were recorded. *Figure 3-8.* shows the captured data from the four channels. We applied cross-correlation signal processing to detect cardiac sounds to identify dominating channels. Based on the lag durations between channels, cross-correlation analysis determines the dominant region and estimates the relationship between channels. The propagation impact and dominating patterns in the Cardiac sounds were also confirmed by visual inspection. The cross-correlation between channels was analyzed to see which channels were dominant and how they interacted. The study revealed delays between channels in the area of interest and throughout the measuring probe. These signal delays indicate that leading signals are the dominating channels. It is plausible to infer that the delays represent the movement of activated areas to surrounding areas based on the delays between channels. Furthermore, our findings revealed that the dominant channel had one of the most robust responses. *Figure 3-9.* shows the final output of the signal derived from the four channels after applying the proposed correlation analysis to reduce the noise level

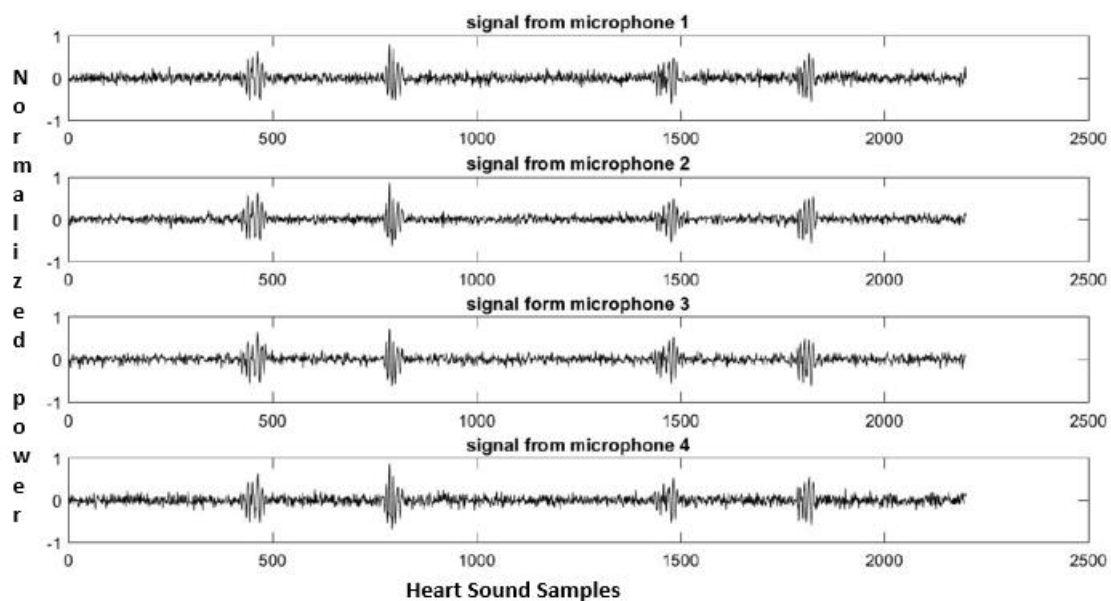


Figure 3-8: Signal capture from four channels

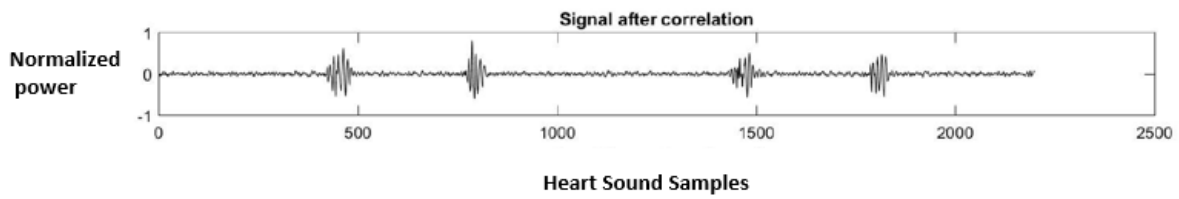


Figure 3-9: Signal after correlation

Table 3.2 shows the values of standard deviation (ρ), repeatability coefficient (RC), and variance coefficient (VC) for repeatability and reproducibility computed from the random-effects model for the feature set. Considering the mean intervals of the systole to diastole cycle, the repeatability is below 4%, and the VC and RC were 2.7 – 3.9%, 6.4 – 8.9%. For reproducibility, the ρ was around 2-3%, and the VC and CR were 2.8 – 4%, 6.4 – 8%, respectively. The VC for both repeatability and reproducibility are below 4%, indicating the results are within the standard limits.

Table 3-2: Repeatability and Reproducibility Results

Feature	Mean	Repeatability			Reproducibility		
		ρ	VC	RC	ρ	VC	RC
F1	0.85	0.023	0.027	0.064	0.024	0.028	0.066
F2	0.83	0.027	0.033	0.075	0.029	0.034	0.080
F3	0.75	0.023	0.030	0.064	0.026	0.035	0.072
F4	0.81	0.026	0.032	0.072	0.027	0.033	0.075
F5	0.79	0.031	0.039	0.086	0.023	0.029	0.064
F6	0.84	0.029	0.034	0.080	0.025	0.040	0.069

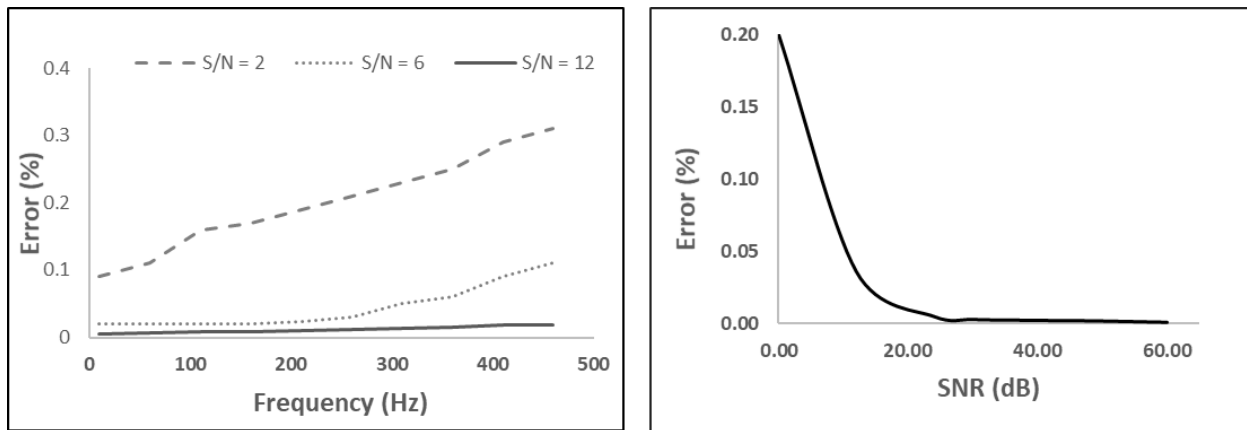


Figure 3-10: Error vs. Frequency with different S/N values

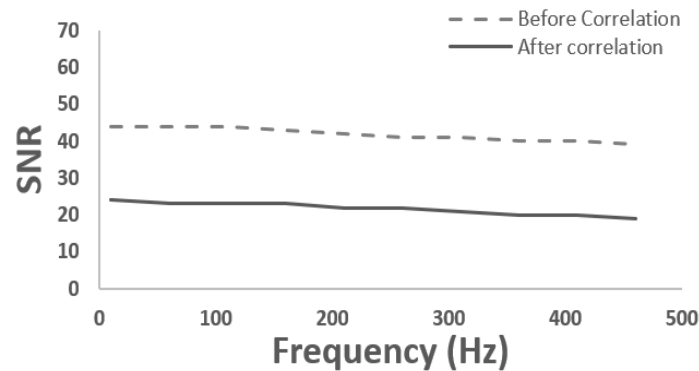


Figure 3-11: S/N vs. Frequency before and after correlation

Figure 3-10. depicts the results of the cross-correlation approach and the received signal. For the set of signals used in the correlation approach, the S/N ratio increases significantly (at least 25 dB). This enhancement is critical for accurate signal detection. However, as shown in Figure 3-11., the received signal-to-noise ratio expression and the growth in the S/N ratio obtained by the cross-correlation approach can be analyzed. These measurements show that utilizing the cross-correlation method. Therefore, it is possible to reliably get the signal amplitude and obtain an increase of 18 to 25 dB in the S/N ratio, resulting in an improvement in cardiac detection.

The origin of the Cartesian coordinate is (0,0,0). The four sensors are situated at (1, 4, 0), (-2, 4, 0), (2, -2, 0), and (3, 4, 0) cm, respectively, to cover the four heart valves. In the plane of 5cm x 5 cm, the origins of cardio sounds from mitral, aortic, tricuspid, and pulmonary valves reach four sensors at different time intervals at a constant speed. Figure 3-11 shows the deviation of the sensor placement with respect to the reference coordinates, which varies the intensity of the sound and, thus, the S/N ratio of the microphone.

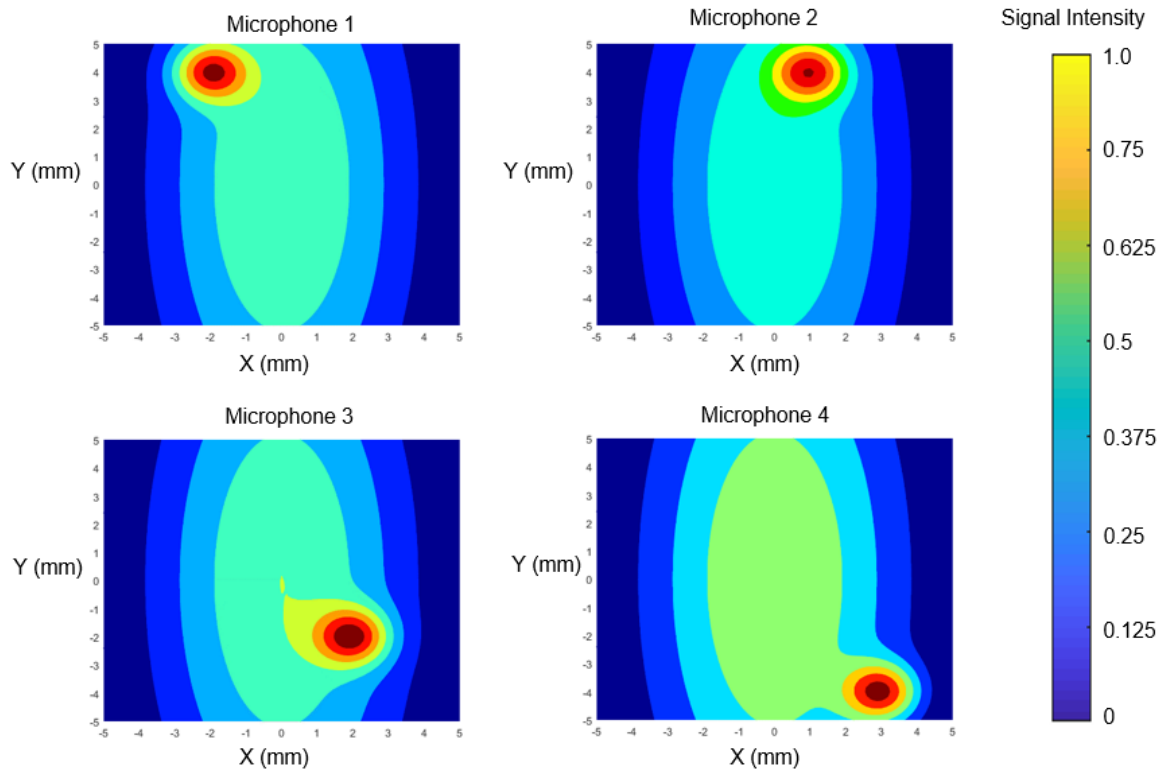


Figure 3-12: Microphone co-ordinates placement Deviation index

A significant observation of the cross-correlation study is that the noise can be decreased by removing irrelevant data. Channels with deficient activation after stimulation, for example, can be removed from the database because they don't indicate any interaction within the experiment. As a result, signal processing techniques like cross-correlation are critical for identifying important channels that accurately depict activations following a stimulus.

3.4 Summary

A phonocardiography system has been developed using four MEMS microphones for cardiac signal capturing, and parallel data processing at high speeds is achievable with an SoC FPGA. This enables the implementation of a real-time multichannel phonocardiography system. In addition, most of the required data processing is performed by an SoC FPGA (ZYNQ SoC), which eliminates the need for robust and expensive computer systems.

In comparison to other occurrences, the position on the chest wall where a specific sound or murmur is best observed may aid in determining the source of the sound or murmur. These positions are influenced by the vibration direction and the distance to the source. For

example, aortic valve sounds, or murmurs should be explored at the second intercostal space to the right of the sternum. In contrast, pulmonary sounds or murmurs should be investigated to the left of the sternum. The lower half of the sternum at the fourth intercostal space level corresponds to the right ventricular region. In contrast, the left ventricular area corresponds to the sternum and the heart's apex point (fifth intercostal space level). Additionally, particular physiological techniques that affect cardiac hemodynamics can be employed to improve the examination of heart sounds and murmurs.

Finally, the presence, timing, location on the chest wall, duration, amplitudes and amplitude pattern, and harmonic components of murmurs and abnormal sound complexes serve as the foundation for auscultatory and phonocardiography assessment of cardiac problems. The time delays are estimated by measuring cross-correlations of the signals collected in different channels, which leads to mistakes in source localizations. For repeatability, the ρ is below 4%, the Variation coefficient was 2.7% to 3.9%, Repeatability coefficient was 6.4 to 8.9%. For reproducibility, the ρ was around 2-3%, the Variation coefficient was 2.8% to 4 %, Repeatability coefficient was 6.4% to 8%, respectively. The VC for both repeatability and reproducibility is below 4%, indicating the results are within the standard limits. Furthermore, the results show that the accuracy and spatial resolution of source localization using this method are practically frequency independent. Also, the relationship between the cross-peak correlation's value and the amplitude of the received signal synthesizes and optimizes the signal analysis. The repeatability and reproducibility of the device for the feature set are measured.

Chapter 4. Classification of Abnormal and normal cardiac sounds using wavelet decomposition and Shannon energy

4.1 Introduction

Digital MEMS can capture low-frequency components of the heart sound signal for analysis and sub-segment diagnosis of the heart. Also, advanced digital signal processing techniques are available to analyze heart sounds. Heart sounds are non-stationary, so heart sound analysis in frequency and time domain provides much information to diagnose heart abnormalities [217]. Many signal processing techniques like Fast Fourier Transform (FFT) [218], Short Time Fourier Transform (STFT) [219], Wigner Ville Distribution (WVD) [220], and Wavelet Transforms (WT) [221] are available to measure the Time and frequency components of the heart sound. FFT provides the frequency domain information, not the time domain information. The WVD and STFT provide both time and frequency, but there is a tradeoff in window selection for frequency and time resolution [222-223] On the other hand, WT provides high time resolution and low-frequency resolution for high frequencies, low time resolution, and high-frequency resolution for low frequencies. This matches the human ear time-frequency resolution features. So, WT is the more appropriate technique for heart sound analysis to capture both frequency and time information.

The analysis of heart sound signals consists of classifying heart sound signals into individual components and extracting features for the pathophysiological information [224-226]. The present work aims to develop a high-performance phonocardiography system to help physicians capture and analyze heart sounds at the bedside. The current work includes hardware development, data recording, results display, and algorithm development to classify different pathological events using digital signal processing techniques. Based on these techniques performance of the system has been evaluated.

4.2 Theoretical Framework

4.2.1 Daubechies Wavelet Transform:

The wavelet transform (WT) of a signal $x(t)$ has the following expression:

$$x(t) = \sum C_{jk} \varphi_{jk}(t) + \sum_j \sum_k d_{jk} \psi_{jk} \quad (1)$$

Where C_{jk} is approximation coefficients, φ_{jk} is scaling function, d_{jk} is a detailed term, ψ_{jk} – is a wavelet function.

Equation 1 shows that there are two terms. The first is the ‘approximation term,’ and the second is the ‘details term.’

In Equation (1), the detailed term is represented below —

$$d_{jk} = \int x(t) \psi_{jk}^*(t) dt \quad (2)$$

And $\psi_{jk}(t)$ is called the wavelet function and is given below –

$$\psi_{jk}(t) = \frac{1}{\sqrt{2^j \psi\left(\frac{t - k2^j}{2^j}\right)}} \quad (3)$$

The approximation coefficients are given by:

$$C_{jk} = \int x(t) \varphi_{jk}^*(t) dt \quad (4)$$

$\varphi_{jk}^*(t)$ is called a scaling function and is given by:

$$\varphi_{jk}(t) = \frac{1}{\sqrt{2^j \varphi\left(\frac{t - k2^j}{2^j}\right)}} \quad (5)$$

Daubechies wavelets [227] are a family of wavelets with the highest number (A) of vanishing moments, with support width $N=2A$, and among the $2A-1$ possible solutions, the one chosen whose scaling filter has an extremal phase. This family contains the Haar wavelet, db1, the most straightforward and oldest wavelet. It is discontinuous, resembling a square form. Except for db1, the wavelets of this family do not have an explicit expression.

The names of the Daubechies family wavelets are written as dbN, where N denotes the order, and db is the wavelet "surname." For example, the db1 wavelet mentioned above is the name of the Haar wavelet. Here are the wavelet functions Ψ of the ten members of the family, as shown in Figure 4-1.

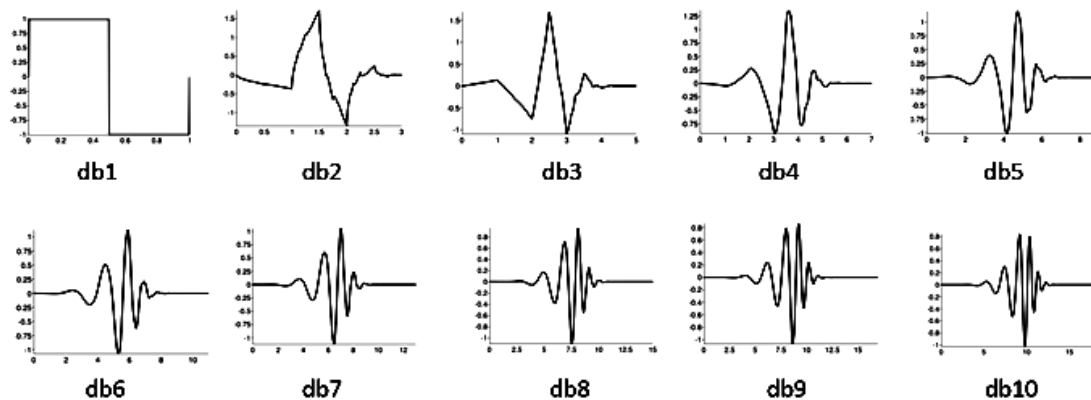


Figure 4-1: The members of the Daubechies wavelet family [db1 to db10]

This family has the following properties:

The ψ and ϕ support length is $2N-1$. The number of zero moments of ψ is N ;

dbN wavelets are asymmetric (in particular for low values of N) except for the Haar wavelet;

The regularity increases with the order. When N becomes very large, ψ and ϕ belong to $C_{\mu N}$ where $\mu \approx 0.2$. This value μN is too pessimistic for relatively small orders, as it underestimates the regularity; The analysis is orthogonal.

The above four properties of the Daubechies wavelets are well set to analyze non-stationary heart sound signals. Also, Daubechies wavelets are ideal for minimum size support for a given number of vanishing moments. Daubechies wavelet db9 was used in the proposed algorithm to

decompose the heart sound signal. In the wavelet analysis technique, the signal under inspection is filtered successively using one low-pass (LP) and one high-pass (HP) filter alternately. The output of the HP filter gives the 1st level detail coefficients, while the output of the LP filter gives the 1st level approximation coefficients. Decomposing the derived approximate and independent detail coefficients gives the respective approximation for all successive levels, as illustrated in Figure 4-2., and is called multilevel decomposition.

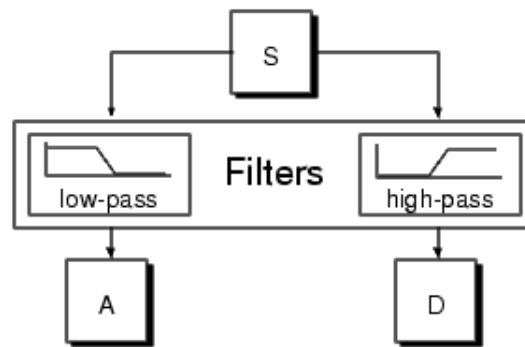


Figure 4-2: Multilevel decomposition of wavelet analysis

4.2.2 Shannon energy

Shannon energy is used to generate an envelope of the heart sound for estimating systole and diastole periods [228-229]. This technique is used in the detection of heart sound peaks. The Shannon energy, S_n , is formulated by

$$S_n = -N_n^2 \log N_n^2 \quad (6)$$

Where N_n , is the normalized PCG signal after noise removal.

The Shannon energy can better emphasize the low and medium heart sound intensities than the conventional square energy operation. As a result, the heart sound signal after processing with Shannon energy does not have significant differences in terms of amplitude, and it makes use of a single thresholding technique in the heart sound peak detection algorithm possible.

4.3 Materials and Methods

4.3.1 Algorithm for Heart sound data analysis

The heart sound algorithm consists of segmentation and feature extraction using wavelet transforms. Figure 4-3. shows the flow diagram of the proposed algorithm for the high-performance phonocardiography system for cardiac diagnosis.

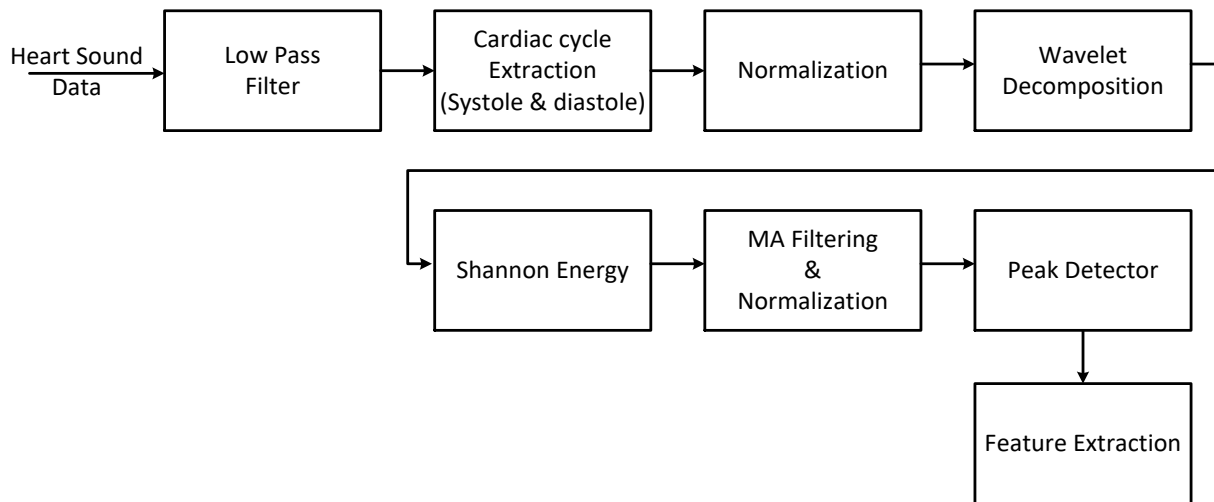


Figure 4-3: Algorithm for high-performance phonocardiography system

The segmentation of the cardiac auscultations and the detection of the different heart sounds, precisely normal heart sounds (S1, S2, S3, and S4), and abnormal heart sounds (Systolic and diastolic murmurs) play a vital role in diagnostics. The segmentation classifies each of these heart sound components and allows for the murmurs' time-based localization. The proposed segmentation algorithm will accurately detect the heart sounds with no false positives inline to the dataset being tested and identify each sound as S1, S2, S3, and murmurs.

The first level of segmentation is done on heart sound to divide the signal into several cardiac cycles (systole and diastole) based on the ECG signal captured along with the PCG signal and applied the QRS detection. The second level of segmentation is done on one cardiac cycle to segment heart sound components. The second level of segmentation is done by normalizing the heart sound intensity level and then decomposed by wavelet transform to extract peaks of the cardiac components.

One cardiac cycle with systole and diastole is considered for the segmentation. In general, the intensity level of heart sounds varies from patient to patient, depending on the physiological

conditions. So, to get the constant intensity level of different subjects, the intensity of the heart sound is normalized on a scale of 0 to 1.

$$I_{norm} = \frac{|I|}{|I_{max}|} \quad (7)$$

The Normalized heart sound output passed through the wavelet decomposition module for sub band decoding. The wavelet decomposition was performed using a 2000 Hz sampling frequency and the 9th order Daubechies (db) wavelet Level 7 for decomposition, as shown in Figure 4-4. The S1 and S2 heart sound band of 20Hz to 150 Hz matches the sum of sub bands' 4th, 5th, and 6th decomposition detail coefficients (31.25 Hz to 250Hz). The S3 and S4 gallop heart sound band of 20Hz to 70 Hz matches the sum of the subbands' 6th and 7th decomposition detail coefficients (15.625 Hz to 62.5 Hz). Stenosis murmurs in the heart sound band of 200Hz to 500 Hz match the sum of subbands' 3rd and 4th decomposition detail coefficients (125 Hz to 500 Hz). Ejection murmurs in the heart sound band of 110Hz to 500 Hz match the sum of the subband's 3rd, 4th, and 5th decomposition detail coefficients (61.25 Hz to 500Hz). Regurgitation murmurs in the heart sound band of 110Hz to 900 Hz match the sum of the subband's 2nd, 3rd, and 4th decomposition detail coefficients (125 Hz to 500Hz).

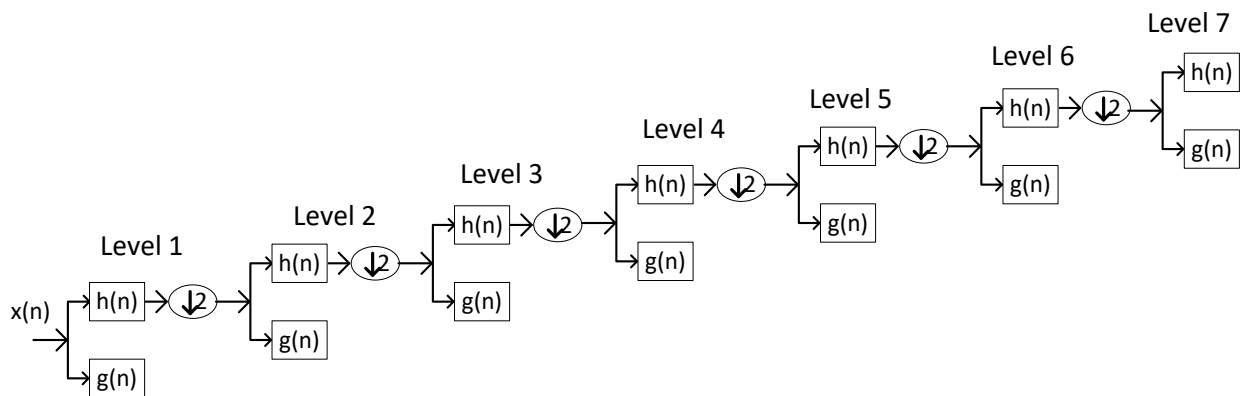


Figure 4-4: 7-level wavelet decomposition

The Shannon energy computed on the outputs of the sum of the subband decomposition detail coefficients of cardiac components S1- S2; S3-S4 gallop, Stenosis murmurs, regurgitation

murmurs. The Shannon energy output passes through the moving average filter with a window length of 50, and then normalization is performed.

A threshold mechanism performs peak detection to determine the max peaks on each sub-band coefficient value and the threshold value for S1-S2 peaks taken from the maximum-minimum approximation. Other abnormal heart sounds have lower intensity than the S1-S2, so the threshold value is computed to an S1-S2 threshold value. Then, feature extractions are performed by dividing the total cardiac cycle interval into equal parts of 0.01 sec. Figure 4-5. shows normal and abnormal heart sounds extraction based on the Shannon high-intensity peaks.

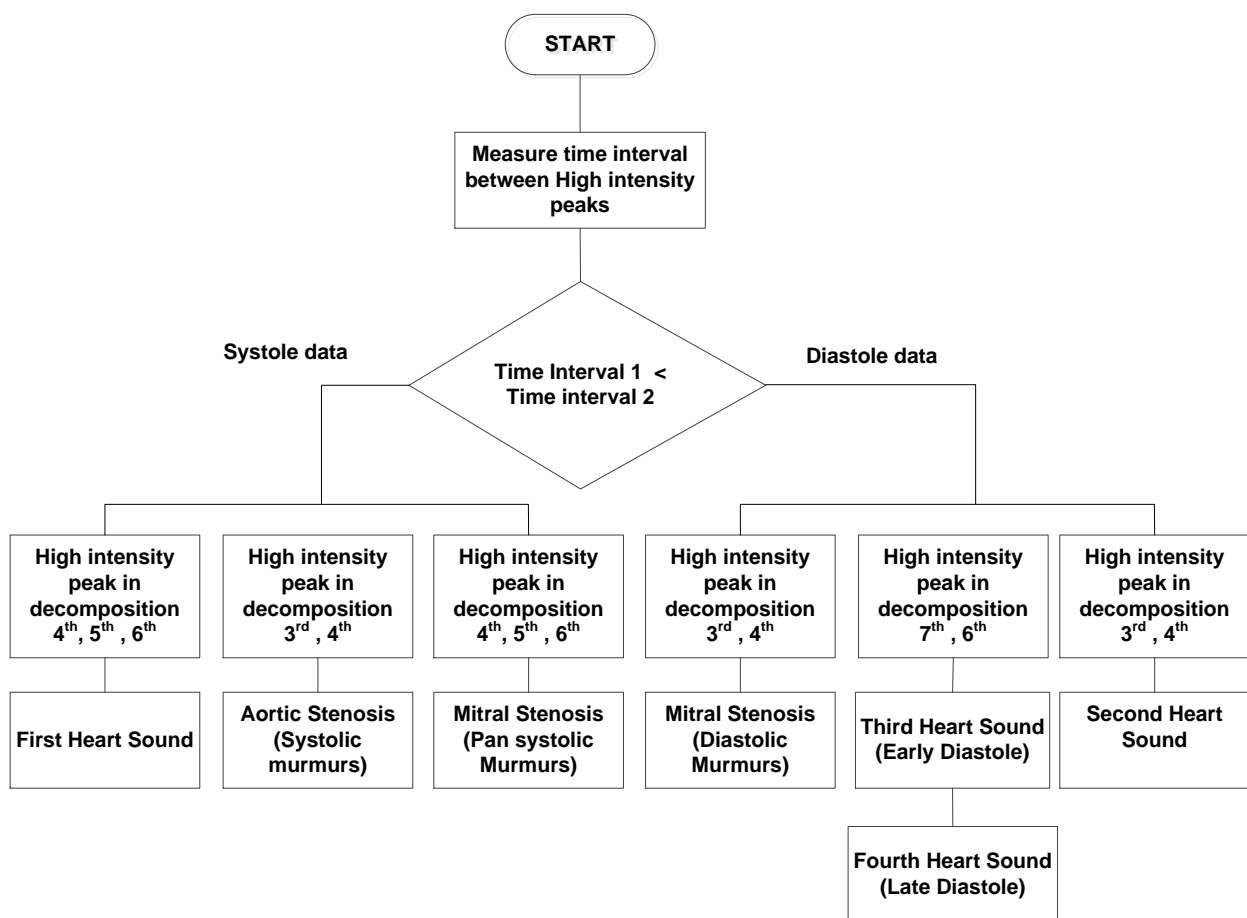


Figure 4-5: Extraction of normal and abnormal heart sounds

4.3.2 Performance Evaluation

The proposed algorithm performance is assessed using statistical values, like the positive predictive rate (PPR), the sensitivity (SEN), and the detection error rate (DER). These values can be computed as follows.

$$SEN = \frac{TP}{TP + FN} \times 100\%$$

$$SPF = \frac{TN}{TN + FP} \times 100\%$$

$$PPR = \frac{TP}{TP + FP} \times 100\%$$

$$DER = \frac{FN + FP}{TP + FN} \times 100\%$$

(8)

Where the true-positive (TP) is the number of correct heart sound peaks detected by the algorithm, true-negative (TN) is the number of correct heart sound peaks rejected by the algorithm, false-negative (FN) is the number of missing heart sound peaks detected, and false-positive (FP) is the number of incorrect heart sounds peaks detected by the algorithm.

4.4 Experimental results

The Heart sounds are collected from the patients using the proposed phonocardiography system under the doctor's supervision to correct the measurements. All the tests on human subjects conform to the Declaration of Helsinki. The proposed algorithm has been executed on the captured sounds at a sampling frequency of 2 kHz. Heart sounds were collected from 50 patients with normal and abnormal heart sounds. From this total, 1756 cardiac cycles were considered for the experiment. The rest of this section describes the results obtained from the experiment mentioned in the previous section. Table 4-1 shows the SEN, PPR, and DER of different components of the heart sound.

Table 4-1. Performance Evaluation of phonocardiography system

Components*	SEN	PPR	DER
S1	99.27%	99.81%	0.09%
S2	99.45%	99.45%	1.09%
AS	99.33%	98.68%	1.98%
MS	98.78%	99.3%	1.81%
MR	99.42%	98.85%	1.73%
S3/S4	98.75%	99.37%	1.86%

*S1- First heart sound, S2-Second heart sound, AS- Aortic Stenosis, MS-Mitral Stenosis, MR- Mitral Regurgitation, S3/S4- Third and Fourth heart sound.

Table 4-2. Comparison of Performance Evaluation of other states of art algorithms

Algorithms	Sensitivity	Specificity	Accuracy
DFT-PCA-HMM [114]	70.3%	93.3%%	0.09%
DWT-ISOM [115]	-	-	95%
DWT-Shannon Energy-ANFIS [113]	100%	95.24%	-
Fourier Bessel-Least square SVM [112]	-	-	94.01%
STFT/WT- HMM [146]	97%	92%	-
WT-GAL / MLP-BP [155]	-	-	96.52% /97.02%
GAL Network [145]	-	-	99%
WPT-Entropy-Bayes Net [116]	-	-	96.4%
WT-PCA-NN [138]	64.7%	70.5%	-
Proposed algorithm	99.16%	98.4%	98.6%

4.4.1 Study 1: Normal cardiac sounds S1 and S2.

The diastole duration between the S2 peak and the next immediate S1 peak is greater than the systole duration between the S1 peak and the next immediate S2, indicating that the S1 and S2 cardiac sounds are high-intensity peaks. Using this criteria, S1 and S2 components are identified, and then other components are identified. Figure 4-6. shows the decomposition details of the S1 and S2. Figure 4-7. shows the Shannon energy peaks of S1 and S2. Out of 1756 cardiac cycles, a total of 551 S1 components and 549 S2 components have been identified with a Sensitivity of 99.27% and 99.45%, respectively.

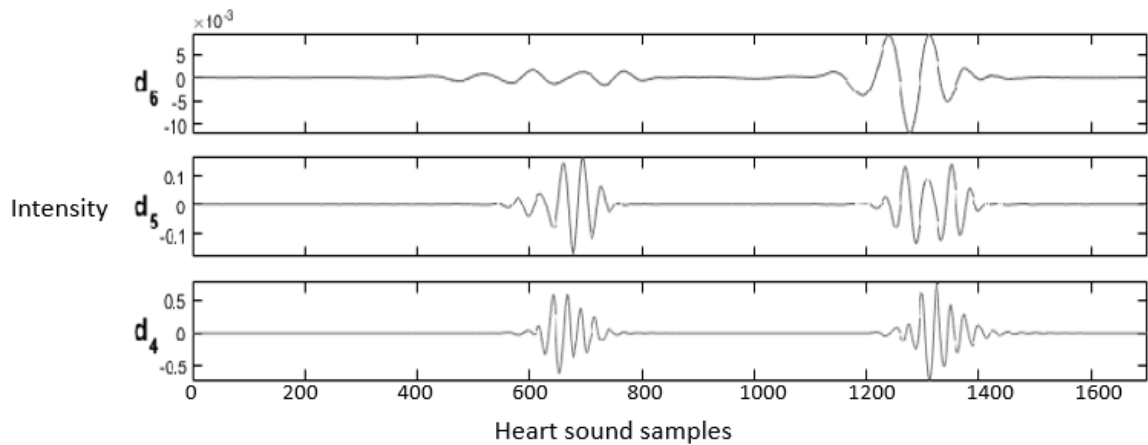


Figure 4-6: Decomposition detail of S1 and S2

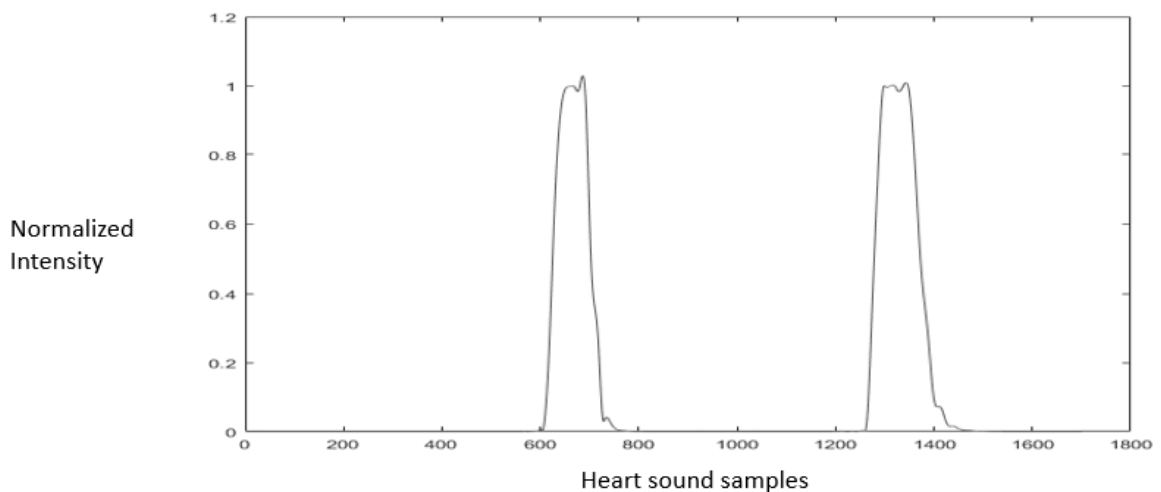


Figure 4-7: Shannon Energy peaks of S1 and S2

4.4.2 Study 2: Aortic stenosis cardiac sounds.

Aortic stenosis is a high-frequency diastolic murmur seen immediately after the second cardiac sound peak. Figure 4-8. shows the decomposition details of Aortic stenosis. Figure 4-9. shows the Shannon energy peaks of Aortic stenosis. Out of 1756 cardiac cycles, 153 Aortic stenosis components were processed with a Sensitivity of 99.33%.

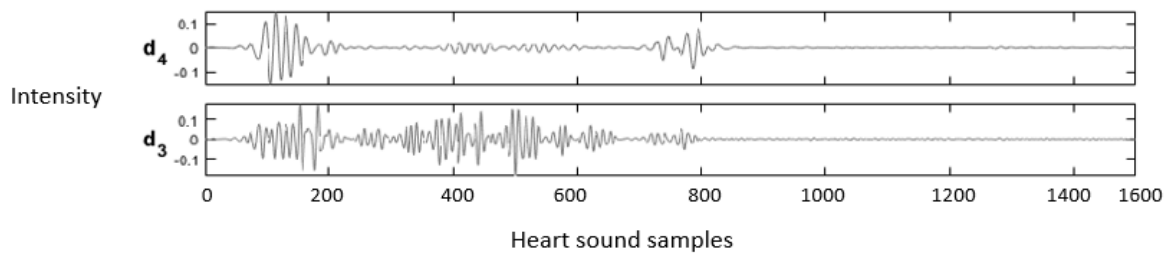


Figure 4-8: Decomposition detail of Aortic stenosis

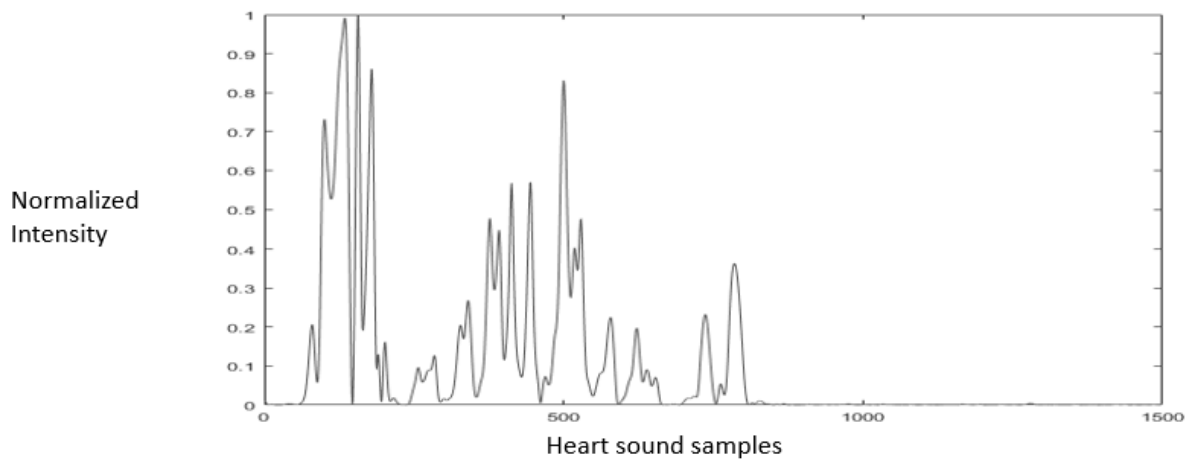


Figure 4-9: Shannon Energy peaks of Aortic stenosis

4.4.3 Study 3: Mitral stenosis cardiac sounds.

Mitral stenosis is a diastolic murmur seen in the last two-thirds of diastole *Figure 4-10*. shows the decomposition details of the Mitral stenosis. *Figure 4-11*. shows the Shannon energy peaks of Mitral stenosis. Out of 1756 cardiac cycles, 166 mitral stenosis components were processed with a Sensitivity of 98.78%.

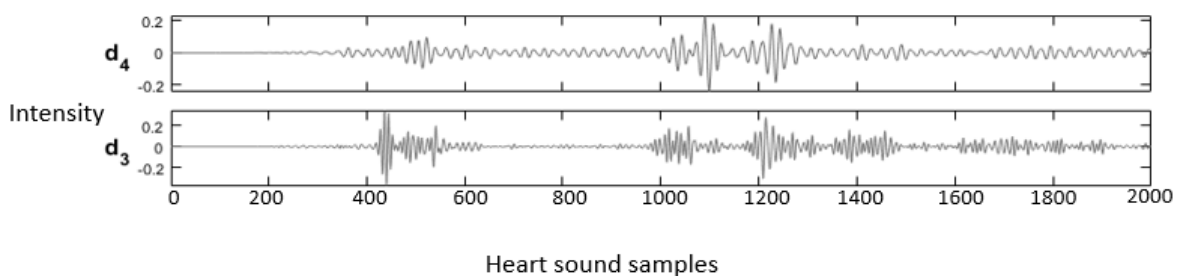


Figure 4-10: Decomposition detail of Mitral stenosis

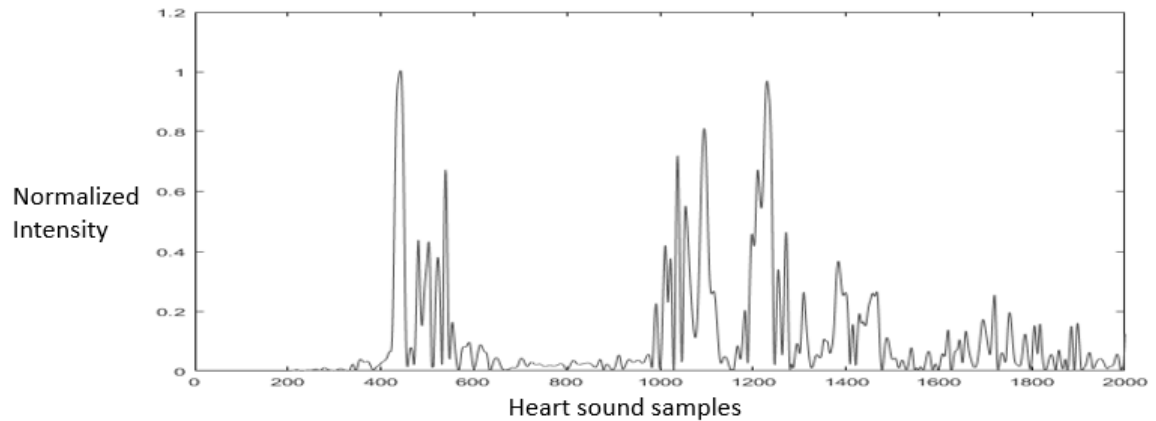


Figure 4-11: Shannon Energy envelope of Mitral stenosis

4.4.4 Study 4: Mitral Regurgitation heart sounds.

The mitral regurgitation is a low frequency, low amplitude peak seen in the diastole cycle. Figure 4-12. shows the decomposition details of the Mitral Regurgitation. Figure 4-13. shows the Shannon energy peaks of Mitral Regurgitation. Out of 1756 cardiac cycles, a total of 175 Mitral regurgitation components were processed with a Sensitivity of 99.42%.

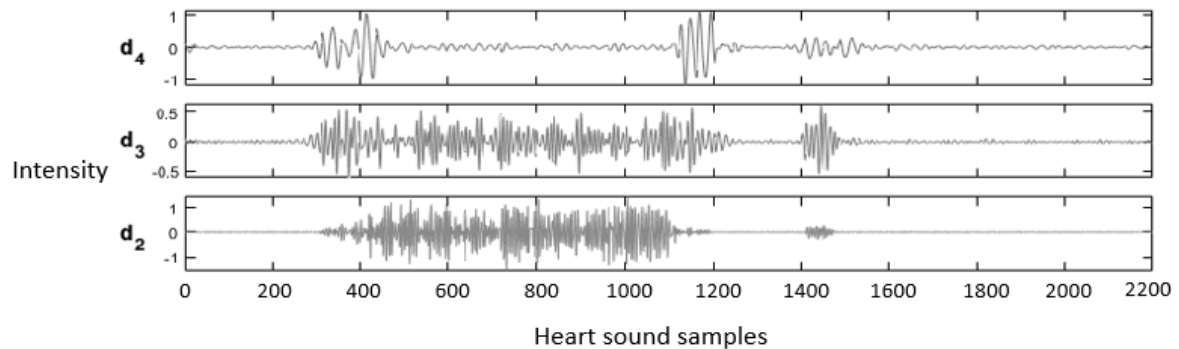


Figure 4-12: Decomposition detail of Mitral regurgitation

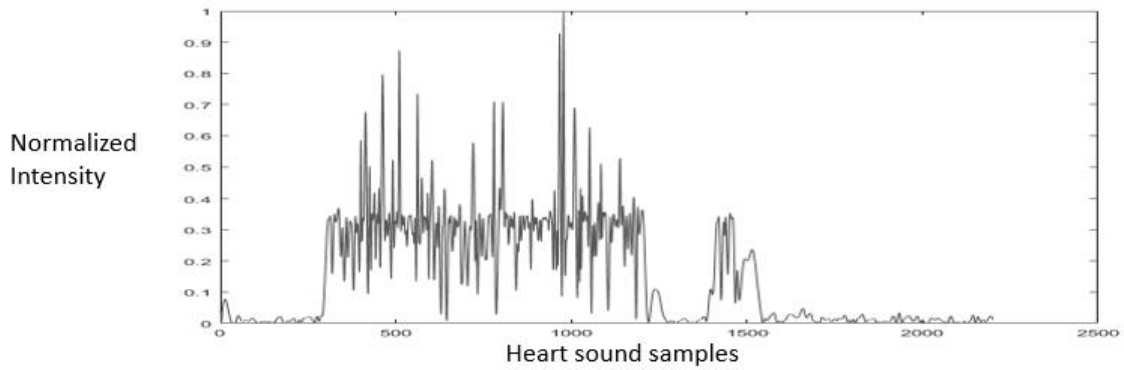


Figure 4-13: Shannon Energy peak of Mitral regurgitation

4.4.5 Study 5: S3 and S4 gallop cardiac sounds.

The S3 is a low frequency, low amplitude peak seen in the pre-diastole cycle just after the S2 peak. The S4 is a low frequency, low amplitude peak seen in the early-systole cycle before the S1 peak. Figure 4-14., Figure 4-16., shows the S3, S4 heart sound decomposition. Figure 4-15., and Figure 4-17., shows the Shannon energy peaks of S3, S4 heart sounds. Out of 1756 cardiac cycles, a total of 162 S3-S4 gallop components were processed with a Sensitivity of 98.75%.

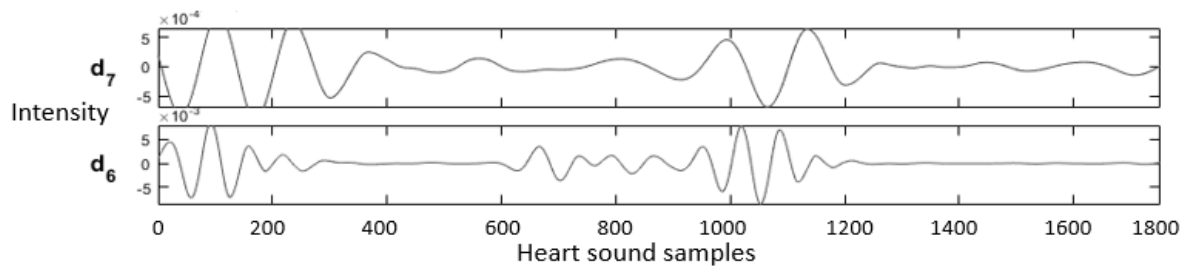


Figure 4-14: Decomposition detail of third heart sound(S3)

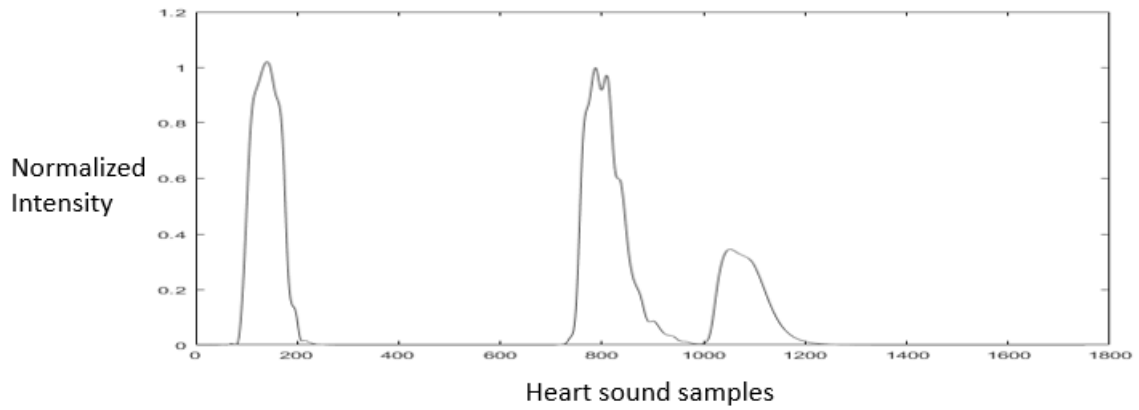


Figure 4-15: Shannon Energy envelope of Third heart sound (S3)

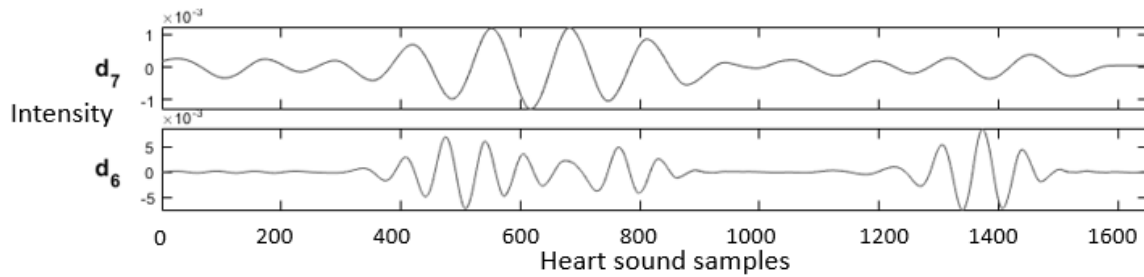


Figure 4-16: Decomposition detail of Fourth heart sound (S4)

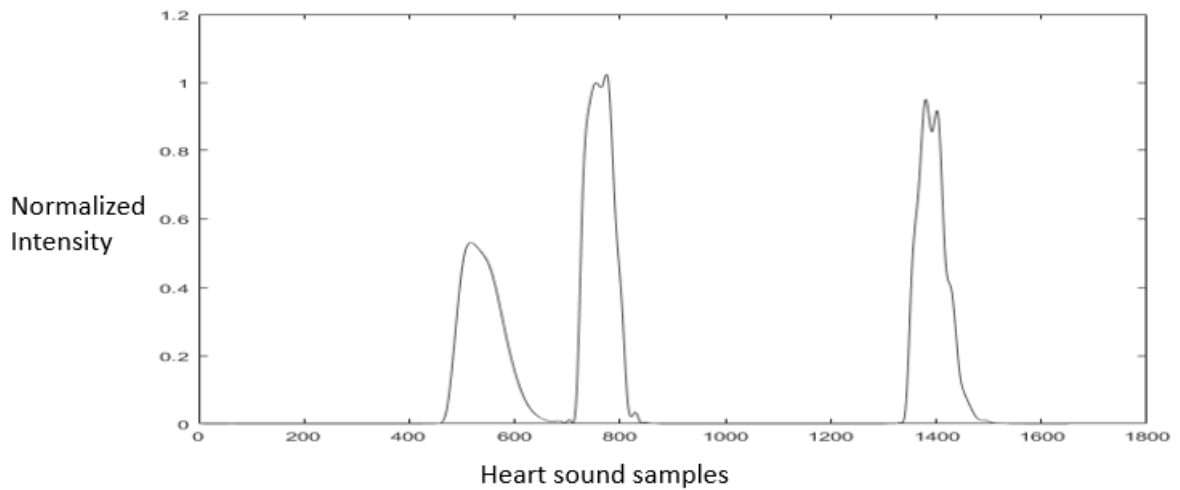


Figure 4-17: Shannon Energy envelope of Fourth heart sound (S4)

4.5 Summary

An algorithm for the classification of normal and abnormal heart sound analyses has been proposed and implemented in the developed phonocardiography system that helps the physician with primary heart failure diagnosis at the bedside by capturing heart sounds and providing a detailed analysis report for the heart sound pathophysiological information on the display. The performance of the phonocardiography system has been evaluated using 1756 cardiac cycles of PCG from a cohort of 50 patients with different pathophysiological conditions. Table 4.2 shows the comparison of Performance Evaluation of other state-of-the-art algorithms. A comparison between the result of this algorithm and those identified by experienced cardiologists shows a high degree of agreement. However, more subjective segmentation carried out by experts is being investigated to express this agreement statistically.

Chapter 5. Extraction cardiac sound components based on Inverse neuron delayed neuron model

5.1 Introduction

The cardiac auscultations are nonlinear and analyzed using artificial neural networks (ANN). Artificial Neural Networks are more useful for the approximation of nonlinear functions. The neural network models are mainly classified by their architecture, activation function, and learning algorithm. Instead of directly emulating the biological behavior, the traditional neuron network models translate it into time-averaging techniques [230-237]. The inverse Delayed (ID) function model of neuron that has been proposed by Nakajima [238-240] is a universal neuron model that includes characteristics of both the Bonhoeffer Van der Pol model and Hopfield model [237]. In addition, the inverse delay function model uses the inverse function of the tan sigmoidal activation function rather than the traditional tan sigmoidal activation function and features a finite conversion time from the internal state of the element to the output.

The energy function of the Inverse delay function model with symmetric synapse weights is similar to that of the Hopfield model. The ID model's negative resistance can free the neural network state from such local minima. Unlike the chaotic neural network, the ID model does not need to transform the output vector, record the output vector during calculation, or control the dynamics by changing the network parameters. We only need to wait for it to become an inactive state to find a solution using the ID neural network and a simple implementation method. The ID model is capable of resolving combinatorial optimization problems [240]. The negative resistance of the ID model can destabilize a neural network's stable equilibrium points, reducing the possibility of unknown values in suboptimal synaptic weight solutions obtained using an ANN-based on a traditional neuron model. The ANN implementation using the ID neuron model needs a lot of parallel computations to solve the complex real-time data for the extraction of components. The Field Programmable Gate Arrays (FPGAs) handle these complex real-time computations effectively and improve performance.

The current study concentrated on the noninvasive detection of cardiac component abnormalities in raw samples collected with MEMs-based microphones. Wavelet decomposition algorithms were used to generate the featured set. The ID neuron function was

used to create the ANN model, which extracts the cardiac components from the feature set obtained. The neuron's inverse delayed function model was used to optimize the weights of the synapses between the neurons. The entire algorithm was implemented on a Xilinx SoC FPGA XC7Z020CLG400. The proposed system has been validated using the cardiac components' sensitivity, specificity, and accuracy, and it has been justified using receiver operating characteristic curve analysis. This chapter is structured as follows. Section 2 focuses on the material, methods, and theory supporting the proposed method using the inverse delayed function model of neuron, illustrating the feature sets for cardiac sound assessment and realization of the inverse delayed function model of neuron. Section 3 focuses on the experimental results. Finally, a summary is presented in section 4.

5.2 Materials and Methods

5.2.1 Inverse delayed function model of neuron

The ANN has been realized using the ID function model of a neuron. Nakajima and Hayakawa proposed the ID function model of neuron by the following set of Equations.

$$\tau \frac{du_i}{dt} = \sum_{j, j \neq i} w_{ij} x_j - a_{ii} x_i - u_i \quad (1)$$

$$\tau_x \frac{dx_i}{dt} = u_i - g(x_i) \quad (2)$$

$$g(x_i) = f^{-1}(x_i) - K x_i \quad (3)$$

Where u_i is the i^{th} neuron internal state, x_j is the j^{th} neuron output, W_{ij} is the synaptic weight between j^{th} and i^{th} neurons, h_i is the bias input, a_{ii} is the self-connection synaptic weight, τ is the internal state time constant, and τ_x is the neuron output time constant.

From Equation (3). $f(x)$ is the neural network sigmoid function, then $g(x) = f^{-1}(x)$ is the N-shaped inverse output function. $g(x)$ can be changed with a positive value of K times the output of the neuron. The transition time from u to x is less than τ , and thus $\tau_x \ll \tau$. In general, the transition time should be considered if it is significantly less than τ . For the present problem, we used the self-connection less neurons to devoid the hysteresis effects[137]. So $a_{ii} = 0$ in Equation (1).

Differentiating Equation (2) with respect to time t, we get

$$\tau_x \frac{d^2 x_i}{dt^2} = \frac{du_i}{dt} - \frac{dg(x_i)}{dx_i} \frac{dx_i}{dt} \quad (4)$$

Let us consider

$$\varphi_i = \frac{dg(x_i)}{dx_i} + \frac{\tau_x}{\tau} \quad (5)$$

Substitute Equation (5) in Equation (4) gives

$$\tau_x \frac{d^2 x_i}{dt^2} + \varphi_i \frac{dx_i}{dt} - \frac{\tau_x}{\tau} \frac{dx_i}{dt} = \frac{du_i}{dt} \Leftrightarrow \tau_x \frac{d^2 x_i}{dt^2} + \varphi_i \frac{dx_i}{dt} = \frac{1}{\tau} \left(\sum_j (w_{ij} x_j - g(x_i)) \right) \quad (6)$$

$$\text{Let, } \frac{\partial U_i}{\partial x_i} = \frac{1}{\tau} (g(x_i) - \sum_j w_{ij} x_j)$$

Equation (6) becomes

$$\tau_x \frac{d^2 x_i}{dt^2} + \varphi_i \frac{dx_i}{dt} = \frac{\partial U_i}{\partial x_i} \quad (7)$$

$$\text{Where } U_i = \frac{1}{\tau} \left(\int_0^x g(x_i) dx_i - x_i \sum_j w_{ij} x_j \right)$$

U_i denotes the potential of the ID function model of the neuron. In Equation (7), the first term denotes inertia, and the second term denotes friction. If $g(x_i)$ is an N-shaped function, then the area where $\frac{dg(x)}{dx_i}$ is less than $\frac{-\tau_x}{\tau}$ for specific values of x_i is called negative resistance region.

From the Lyapunov function, the energy of the ID function model is

$$E = -\frac{1}{2\tau} \sum_i \sum_j w_{ij} x_i x_j + \frac{1}{\tau} \sum_i \int_0^x g(x_i) dx_i + \frac{\tau_x}{2} \sum_i \left(\frac{dx_i}{dt} \right)^2 \quad (8)$$

The self-connections between neurons are ignored since the proposed neuron network has fewer neurons self-connection. The last term in Equation (8) shows the time delay in the ID function model.

Differentiating both sides of Equation (8) with respect to time t, we get

$$\frac{dE}{dt} = -iv \sum_i \frac{dx_i}{dt} \left\{ \frac{1}{\tau} w_{ij} x_j - \frac{1}{\tau} g(x_i) - \tau_x \frac{d^2 x_i}{dt^2} \right\} \quad (9)$$

$$\frac{dE}{dt} = - \sum_i \left(\frac{dg(x_i)}{dx_i} + \frac{\tau_x}{\tau} \right) \left(\frac{dx_i}{dt} \right)^2 \quad (10)$$

$$\frac{dE}{dt} = - \sum_i \varphi_i \left(\frac{dx_i}{dt} \right)^2 \quad (11)$$

From Equation (11), The energy (E) of the ID model, like that of the Hopfield model, decreases with time if the network state is in the positive resistance region ($\varphi_i > 0$). However, in the negative resistance region ($\varphi_i < 0$), the energy (E) increases with time, so even if the state is in the minima region, it quickly exits this region. Therefore, it is necessary to have this feature to avoid local minima. As a result, if the network is an inverse delayed function model, it is expected to increase the likelihood of escaping the local minima.

5.2.2 Prediction model using ID function model of neuron

The proposed ANN algorithm is based on a feedforward network with three layers, as shown in Figure 5-1. The first layer has six inputs for six feature sets mentioned in Table 3-1. The second layer is the hidden layer consisting of 12 hidden neurons, and the third layer is the output layer, which consists of 5 output neurons. The hidden layer contains a neuron that computes the delayed weighted sum of inputs and the inverse tangent sigmoid nonlinear function for the feature extraction. The output layer is a logical net to reduce the error in extraction and sends the output based on the input from the hidden layer.

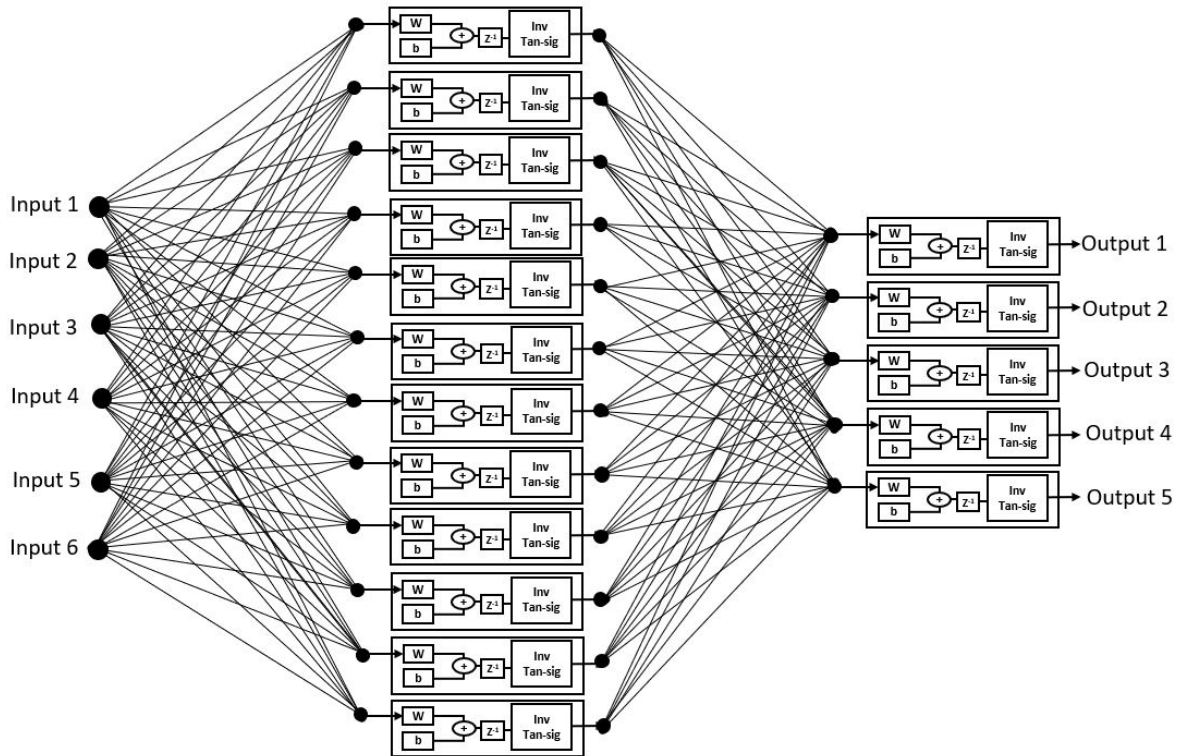


Figure 5-1: ANN using ID function neuron model

5.2.3 Realization of inverse activation function

An activation function is to present non-linearity into the output of the neuron. The inverse tan hyperbolic function is an activation function for current work.

$$f(x) = \tan^{-1}h(x) = \frac{1}{2} \ln \left(\frac{1+x}{1-x} \right) \quad (12)$$

$$f(x) = \frac{1}{2} (\ln(1+x) - \ln(1-x)) \quad (13)$$

$$f(x) = \frac{1}{2} \left(2x + \frac{2}{3}x^3 + \frac{2}{5}x^5 + \dots \right) \quad (14)$$

$$f(x) = x + \frac{x^3}{3} + \frac{x^5}{5} + \dots \quad (15)$$

Neglecting the higher terms $f(x)$ becomes

$$f(x) = x + \frac{x^3}{3} \quad (16)$$

Equation (16) realized using constant (1/3), adder, and multiplier. The activation limits the output in the range of [1, -1].

Figure 5-2 shows that the activation function in the ID model is an N-shaped transfer function.

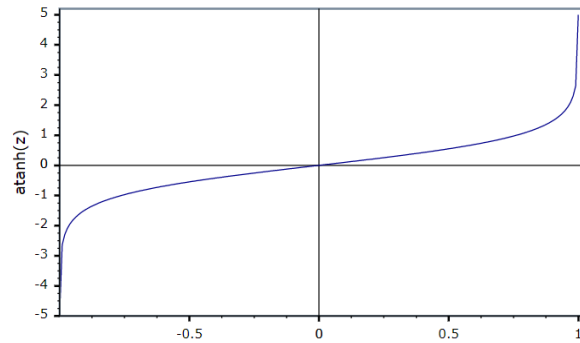


Figure 5-2: Transfer function

The ID network consists of 12 hidden neurons in the hidden layer. The neural network is trained using MATLAB, and learning is accomplished using the Levenberg-Marquardt backpropagation algorithm. First, backpropagation is used to obtain the input and layer weight matrices by incorporating the derivatives of the inverse functions. Next, these matrices are used to replicate the ID network onto the FPGA. Finally, the neural network is trained using the ID function model, and the result of the regression coefficient 'R' is shown in Figure 5-10.

The cleaned data is processed through the cardiac cycle separation engine to differentiate the systole diastole cycles. Feature Extraction module extracts the features mentioned in Table 1 from systole and diastole. The extracted six featured sets passed through the ANN model to classify the five heart sound component groups. The Decision logic outputs the true negative (TN), true positive (TP), false negative (FN), and false positive (FP) for corresponding heart sound components. Figure 5-3. shows the real-time experimental setup for the proposed hardware. Figure 3-6. shows the placement of the four PCG sensors on the body to capture the data.

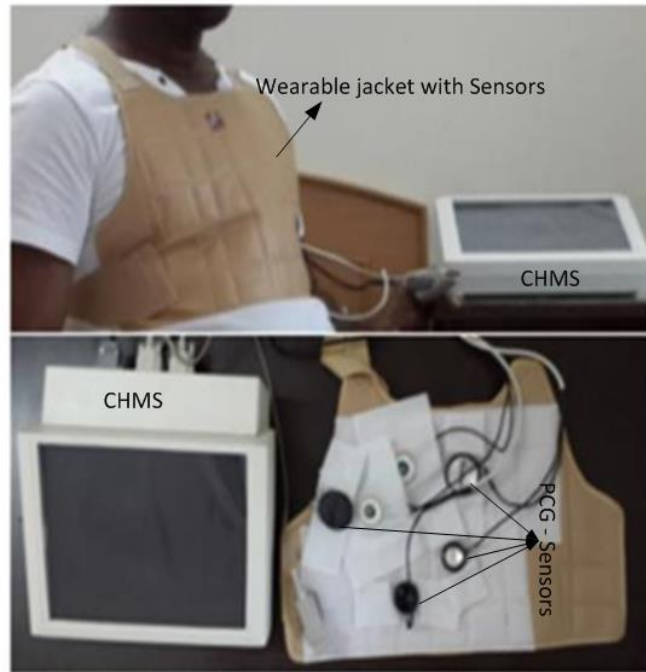


Figure 5-3: Real-time experimental setup with proposed hardware

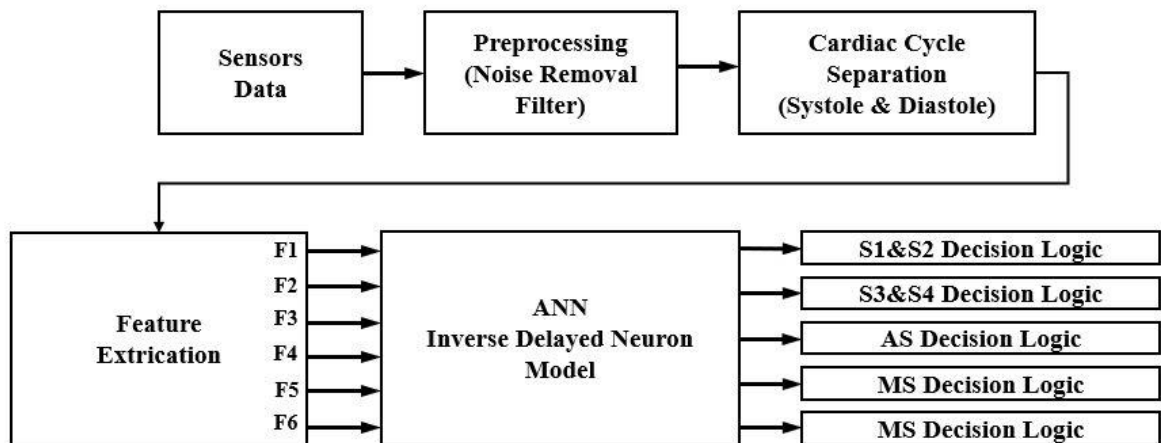


Figure 5-4: Flow diagram for extraction of Cardiac Sound components

As discussed in previous sections, the ANN with inverse delayed neuron model is implemented in MATLAB using the neural network toolbox and the fixed-point toolbox. The model is simulated to check the functionality and calculate the synaptic weights and bias required for the hidden and output layers. The simulated fixed-point MATLAB model is a golden reference for further hardware realization using FPGA.

The Xilinx System generator tool is used to implement and generate Verilog code for the system integration. As discussed in earlier sections, the ANN model is realized using three stages; in the first stage, the input layer, the inputs are scaled with weights and passed to hidden neurons. The bias is added to the summed weights by the hidden layer, which then passes through the delayed activation function. The output layer computes the output value from all hidden neurons and the output bias and activation function. The sigmoid activation function is a building block used in both the hidden and output layers. Equation (16) is used to implement the inverse activation function, which consists of an adder, multiplier, and constant value. As shown in Figure 5-5., the neuron model is realized using a Mult-Add block, a constant block for bias, and an activation function.

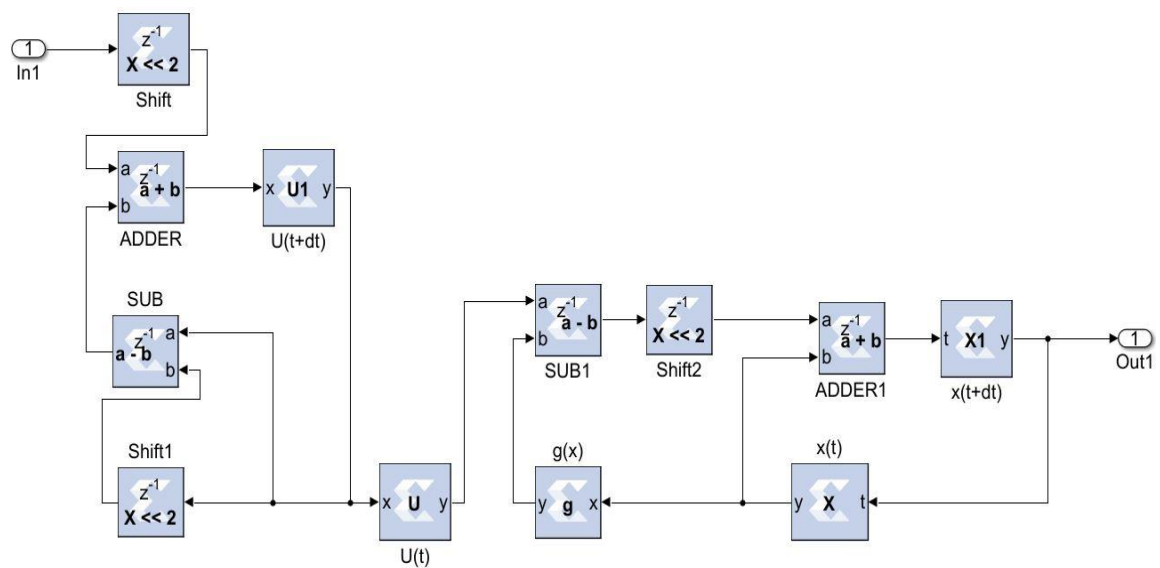


Figure 5-5: Neuron Model

Figure 5-6. depicts the proposed ANN model implementation. The estimated sigmoid value is closer to the real sigmoid value obtained from MATLAB, allowing the approximation effect to be reduced for improved accuracy when implemented in hardware.

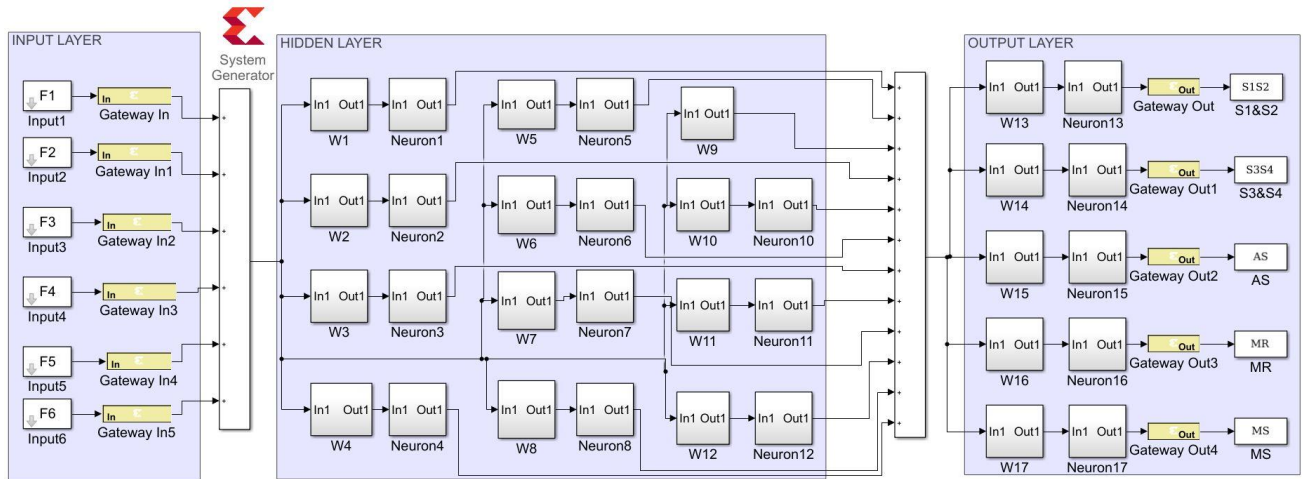


Figure 5-6: System Generator Implementation of ANN Model

5.3 Experimental results

The extraction of cardiac sounds from the MEMS-based high performance phonocardiography system using a neural network based on the ID function model of neurons. The neural networks based on the ID function model and the conventional neuron models are realized on FPGA, and the hardware requirements and performance of the two models are compared. The proposed system was validated using the data of 30 patients in accordance with the Declaration of Helsinki. After obtaining informed consent, a total of 60 patients were made available for evaluation, with 30 patient data used for training the neural networks and the remaining 30 patient's data for testing the proposed system.

The neural networks were trained offline using data from 30 patients in MATLAB and then implemented on FPGA to reduce design circuitry. The MATLAB model weights and biases are used as hardcoded values in the FPGA ANN model to reduce computational cycles and achieve the accuracy obtained in simulation. The FPGA implementation of the inverse tangent sigmoid function, which requires the realization of an N-shaped activation function, involves multiplication but not division. The multiplier is all that is required for the ID model's functional units. This dramatically reduces hardware complexity. The system generator FPGA netlist files are used to run the synthesis, implement, and generate the bit file needed to program the FPGA. Figure 5-7. depicts the RTL schematic for the neuron model following RTL synthesis. The physical layout of the proposed system is depicted in Figure 5-8.

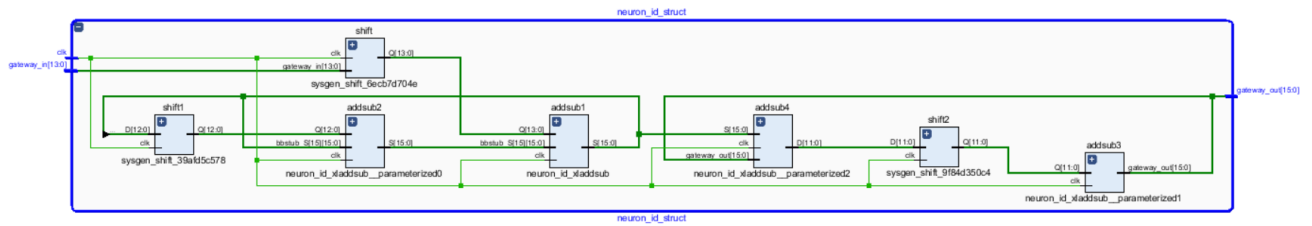


Figure 5-7: RTL Schematic – Neuron Model

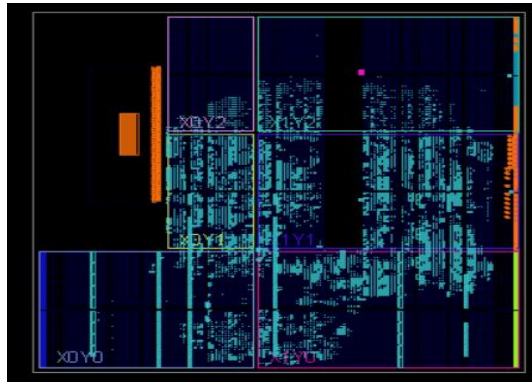


Figure 5-8: Physical layout for the proposed system

Figure 5-9. shows the FPGA Resource utilization of the after place and route.

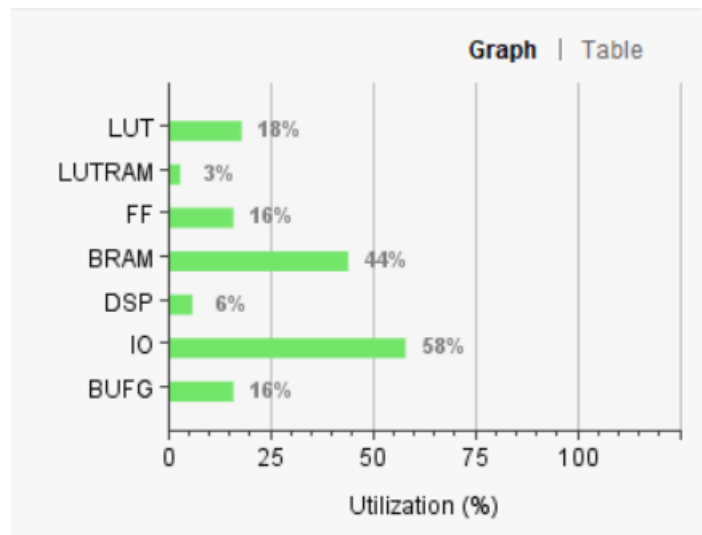


Figure 5-9: Resource utilization of the proposed system

The mean square error in extracting cardiac sound components detection rate using neural networks with 12 neurons in the hidden layer is 0.9. Regression analysis is performed on the input and target datasets, and the mean square error is 4.4×10^{-5} . Figure 13 depicts the

regression analysis of the network's training and validation. In the regression analysis, the parameter 'R' equal to 0.99 represents the correlation between extracted cardiac components and essential cardiac components.

The regression analysis showing the training and validation of the network is depicted in Figure 5-10. The parameter 'R' which is equal to 0.99 in the regression analysis, signifies the correlation between extracted cardiac components with actual cardiac components. Figure 5-11. depicts the training state analysis of a neural network based on the ID function model of a neuron. Figure 5-12. depicts a neural network for performance analysis. Training analysis was performed for epoch 11, with a gradient factor of 9.0661×10^{-5} and validation checks equal to 6.

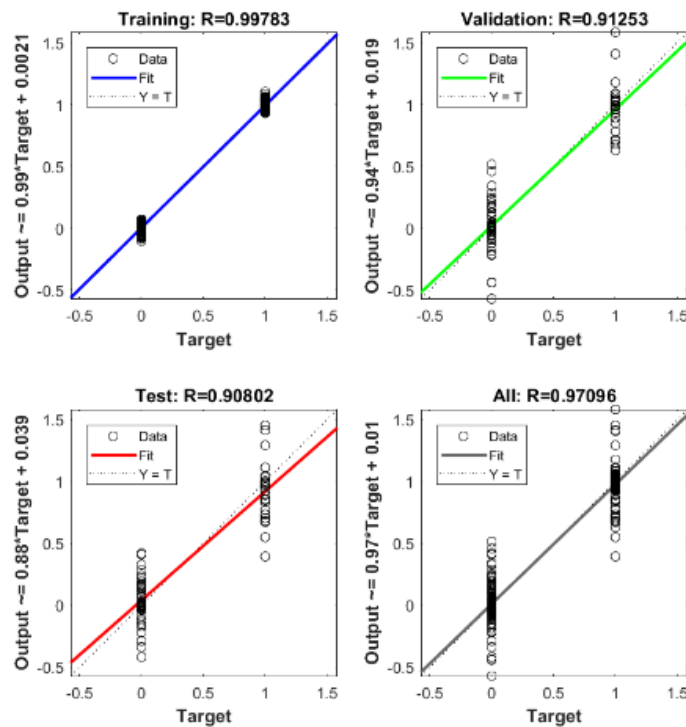


Figure 5-10: Regression analysis of neural network based on ID Function model of neuron

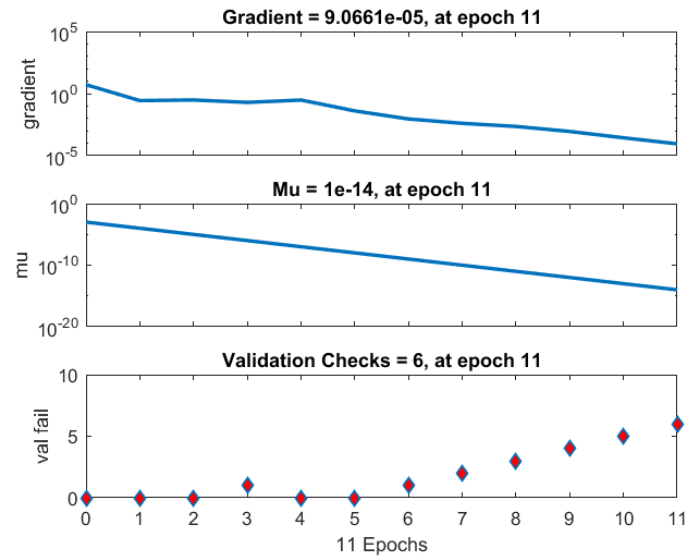


Figure 5-11: Training state analysis of neural network based on ID Function model of neuron

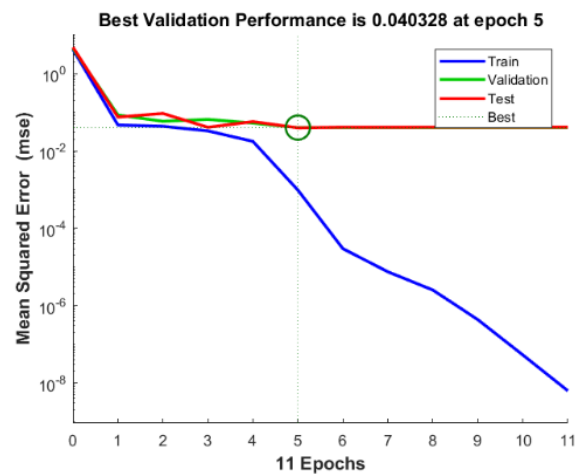


Figure 5-12: Performance analysis of neural network based on ID Function model of neuron

Clinical trials were conducted on 30 patients in accordance with the Declaration of Helsinki (1964), using the proposed high performance phonocardiography system, and the results were compared to the known test results from the medical practitioner. The prevalence of disease in the tested population, the outcome of the diagnostic test, and the sensitivity and specificity of the test all impact the reliability of any diagnostic test result. The sensitivity, the specificity rate, and the accuracy. These values can be computed as follows.

$$\text{Sensitivity} = \frac{\text{TP}}{\text{TP} + \text{FN}} \times 100\%$$

(17)

$$\text{Specificity} = \frac{\text{TN}}{\text{TN} + \text{FP}} \times 100\%$$

(18)

$$\text{Accuracy} = \frac{\text{TP} + \text{TN}}{\text{TP} + \text{TN} + \text{FP} + \text{FN}} \times 100\%$$

(19)

Where True-negative (TN) represents the number of correct heart sound components rejected, True-positive (TP) represents the number of correct heart sound components detected by the proposed system, False-negative (FN) represents the number of incorrect heart sound components rejected, and False-positive (FP) represents the number of incorrect heart sound components detected by the proposed system. Table 5-1. displays the sensitivity, specificity, and accuracy of cardiac component detection for a healthy individual and under specific disease conditions. Table 5-2 shows the comparison of performance evaluation of Inverse delay of neuron model with the other states of art algorithms.

Table 5-1. Accuracy of the proposed system for different cardiac components in heart sounds

Heart sound Components	Sensitivity	Specificity	Accuracy
S1 & S2	99.1%	99.3%	0.99
S3 & S4	98.1%	98.6%	0.98
Aortic Stenosis	98.3%	98.7%	0.98
Mitral Stenosis	98.5%	98.7%	0.98
Mitral Regurgitation	98.2%	98.4%	0.98

Table 5-2. Comparison of Performance Evaluation of ID model with other states of art algorithms

Algorithms	Sensitivity	Specificity	Accuracy
DFT-PCA-HMM [114]	70.3%	93.3%%	0.09%
STFT/WT- HMM [146]	97%	92%	-
WT-GAL / MLP-BP [155]	-	-	96.52% /97.02%
GAL Network [145]	-	-	99%
WPT-Entropy-Bayes Net [116]	-	-	96.4%
WT-PCA-NN [138]	64.7%	70.5%	-
Proposed ID algorithm	98.44%	98.74%	98.2%

The proposed method's performance was evaluated using the Receiver Operating Characteristic (ROC) curve AUC (Area Under Curve) value. This validates the extraction of cardiac components from the captured data using the proposed algorithm. The Receiver Operating Characteristic curve for the extraction of cardiac component accuracy for the proposed ID neuron model system is shown in Figure 16. The accuracy of S1&S2, S3&S4, Aortic stenosis, Mitral Stenosis, and Mitra regurgitation is 99.3%, 98.6%, 98.7%, 98.7%, and 98.6% based on AUC values in Figure 5-13(a),(b),(c),(d) and (e).

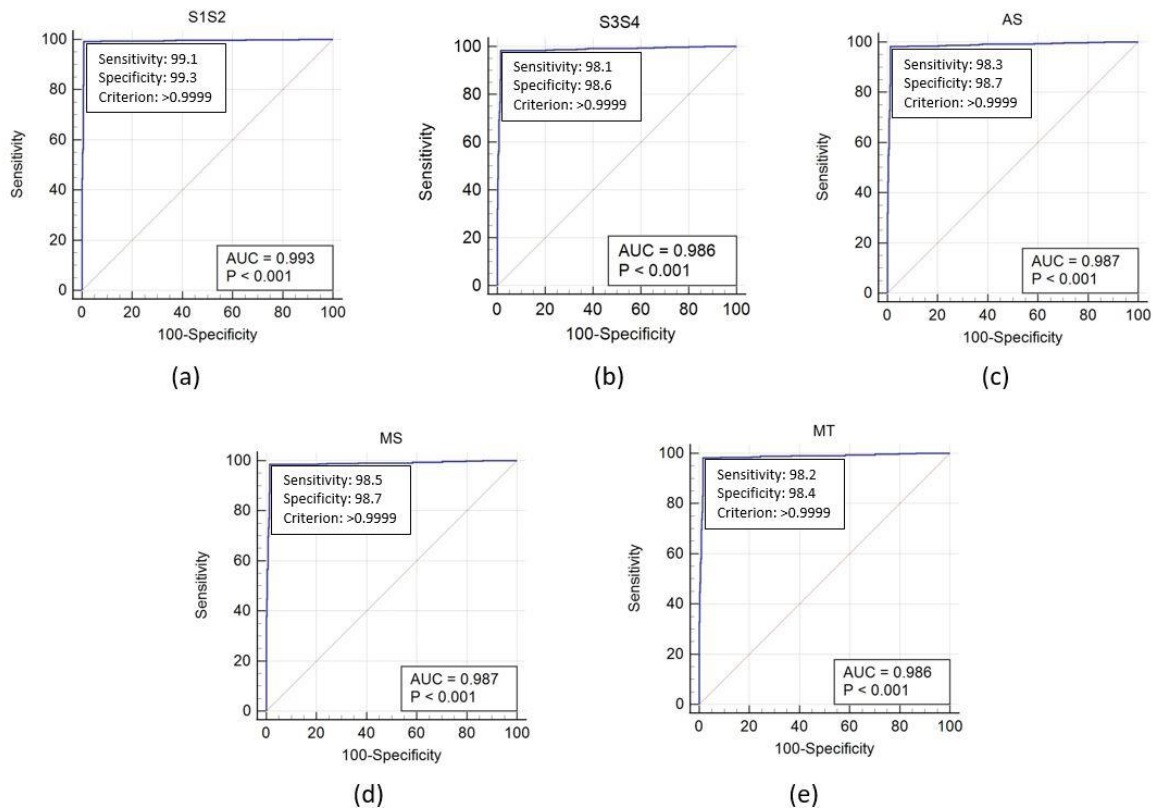


Figure 5-13. ROC Curve Analysis of Heart Sound components with the inverse delayed function of Neuron Model (a) First and Second Heart sound (b) Third and Fourth Heart sound (c) Aortic Stenosis (d) Mitral Stenosis (e) Mitral Regurgitation

5.4 Summary

The current research focused on developing a multichannel MEMS-based phonocardiography system to capture the heart sounds and process the acquired sample to remove the unwanted noise and derive the feature set using wavelet transforms and, after that, extract the low-frequency cardiac sounds using ANN based on the ID function of the neuron model. The realization of the activation function covers the implementation of the inverse tan sigmoidal

function. Hardware implementation of the proposed algorithm implemented using the Xilinx system generator model of neuron function and the total ANN model. The neural network was trained using real known data, and the proposed system was tested using patient test data. The experimental results show the RTL schematic of the neuron model and implemented resource utilization of the device, training state analysis of neuron network based on ID function model of a neuron, Mean square error of different 11 epochs and selection of best valid epoch, regression analysis of ID function model of a neuron. The performance of the phonocardiography system has been evaluated using 2150 cardiac cycles of PCG from a cohort of 30 patients with different pathophysiological conditions with good sensitivity of 99% and an accuracy of 0.9. The accuracy of S1&S2, S3&S4, Aortic stenosis, Mitral Stenosis, and Mitral regurgitation is 99.3%, 98.6%, 98.7%, 98.7%, and 98.6% based on AUC values from Receiver Operating Characteristics (ROC) curve. The developed ANN-based phonocardiography system is helpful for the physician to know abnormal low-frequency heart sounds with a simple diagnosis setup similar to the stethoscope and visualize graphical data for better medical diagnosis.

Chapter 6. Conclusion

6.1 Summary of the present work

Phonocardiography is the primary non-invasive technique for diagnosing the human heart. PCG signals have a number of nonstationary or transient characteristics, including the timing of heart sounds, their composition, and their location in the cardiac cycle. Particularly, the PCG signals are characterized by sudden and fast frequency changes across time. Due to the source of generation in the cardiac cycle, the auscultation approach that uses a single acoustic sensor might not provide sufficient detail in the identification of low-frequency signals. In this research, cardiac auscultations will be captured with a multichannel acoustic sensor, and the signal will be analyzed using segmentation, feature extraction, and classification.

A multichannel high-performance phonocardiography system hardware has been developed using the MEMS microphone for heart sound acquisition and SoC FPGA for proposed algorithms implementation. The developed system is helpful in computing high-end signal processing for cardiac sounds and eliminates the need for robust and expensive computer systems. The location on the chest wall where a particular sound or murmur is best heard may aid in establishing the source of the sound or murmur compared to other occurrences. The microphone positions are influenced by the vibration direction and the distance to the source. The location, timing on the chest wall, duration, amplitudes and amplitude pattern, and harmonic components of murmurs and abnormal sound complexes serve as the foundation for auscultatory and phonocardiography assessment of cardiac problems. A mathematical model has been developed for the heart sound localization to place the sensor to get the high signal-to-noise ratio and increase the system's sensitivity to detect the low-frequency signals like S3 and S4. The time delays are estimated by measuring cross-correlations of the signals collected from different channels, leading to improved heart sound quality. The results show that source localization accuracy and spatial resolution using this method are practically frequency independent.

Time intervals of S1, S2, systole, and diastole events are taken and used to create a feature set with six features that detect low-frequency heart sounds. The precision of the multichannel phonocardiography system is measured by computing the repeatability and reproducibility using the feature set parameters. The repeatability coefficient ranged from 6.4%

to 8.9%, and the variation coefficient ranged from 2.7% to 3.9% for repeatability. For reproducibility, the standard deviation was between 2% to 3%, the Variation coefficient was between 2% to 4%, and the Repeatability coefficient was between 6% to 8%. When the variance coefficient for repeatability and reproducibility is less than 4%, the findings are considered to be within acceptable bounds. The outcomes also demonstrate that this method's source localization accuracy and spatial resolution are essentially frequency independent. Additionally, the cross-peak correlation between the received signal's amplitude and its value synthesizes and improves the signal analysis.

A segmentation algorithm for normal and abnormal heart sound analyses has been proposed and implemented in the developed system. The performance of the proposed segmentation algorithm has been evaluated using different pathophysiological conditions. A complete analysis report for the heart sounds pathophysiological information on the display for the captured data.

We have investigated the ANN based on the ID function of neuron model. The neural network was trained using real known data, and the proposed system was tested using patient test data. Regression analysis is performed on the captured data set. Performance was evaluated using the Receiver Operating Characteristic (ROC) curve AUC (Area Under Curve) value. This validates the extraction of cardiac components from the captured data using the proposed algorithm. As a result, the developed ANN-based phonocardiography system is useful to the physician to know the abnormal low-frequency heart sounds with a simple diagnosis setup similar to a stethoscope and visualize graphical data for better medical diagnosis.

6.2 Conclusion

A new heart sound localization method has been proposed for the placement of PCG sensors for multi-channel phonocardiography. The system provides more opportunities to support medical researchers who work with enormous amounts of data. The exploration of hidden cardiac sound components from data sets has a lot of potential to find cardiac abnormalities. Detection of future outcomes based on past experiences is made possible by the recognition and categorization of patterns in multivariate patient attributes. We can use these patterns to make a clinical diagnosis. It aids in providing high-quality healthcare services based on the needs, symptoms, and preferences of the patient. It also reduces the amount of time that patients must wait for medical attention. The data analysis is helpful for improving existing clinical cardiac auscultation instruction and training. Predictive clinical investigations are

crucial because they have the power to confirm or deny the applicability and significance of the methodology presented for assessing heart abnormalities. The following is a summary of the research's findings on using multi-channel phonocardiography to identify cardiac abnormalities early on:

- A multi-channel phonocardiography system has been developed using MEMS microphones to capture cardiac sound data from four valves.
- A novel cardiac sound source localization was developed using MCCC with constant time delays for channel selection and TDOA based on the PHAT.
- The variance coefficient for repeatability and reproducibility is less than 4%, which shows that the findings are within standard limits. The precision of the system is good to use for the capture of cardiac sounds.
- Out of 1756 cardiac cycles, a total of 551-S1 components, 549-S2 components have been identified with a Sensitivity of 99.27% and 99.45%, respectively, 153-Aortic stenosis components were processed with a Sensitivity of 99.33%, 166 mitral stenosis components were processed with a Sensitivity of 98.78%, a total of 175 Mitral regurgitation components were processed with a Sensitivity of 99.42%, a total of 162 - S3S4 gallops components were processed with a Sensitivity of 98.75%.
- The prediction model based on the ID function of the neuron model has been evaluated with different pathophysiological conditions with good sensitivity of 99% and an accuracy of 0.9. and the mean square error of 4.4×10^{-5} .

6.3 Scope of future work

Continuing the present work, more data analytics methods are planned to improve accurate parameter derivation. Safety-related features will implement for the effective detection of faults and reducing spurious fault alarms, which improves practical nursing by reducing alarm fatigue. The proposed system enhances the capability to predict a cardiac-related illness by processing the multi-signal input data and performing data analytics on the data collected from these various multi-sensors for pathological Completeness.

The present research work is done in a constrained, noise-free environment with limited human trails, but in a realistic environment surrounding noises may influence the captured data, and final results may vary, and more research needs to be done on the mechanical housing of

sensors so that noise can be filtered at capturing stage itself instead of using more pre-processing filters.

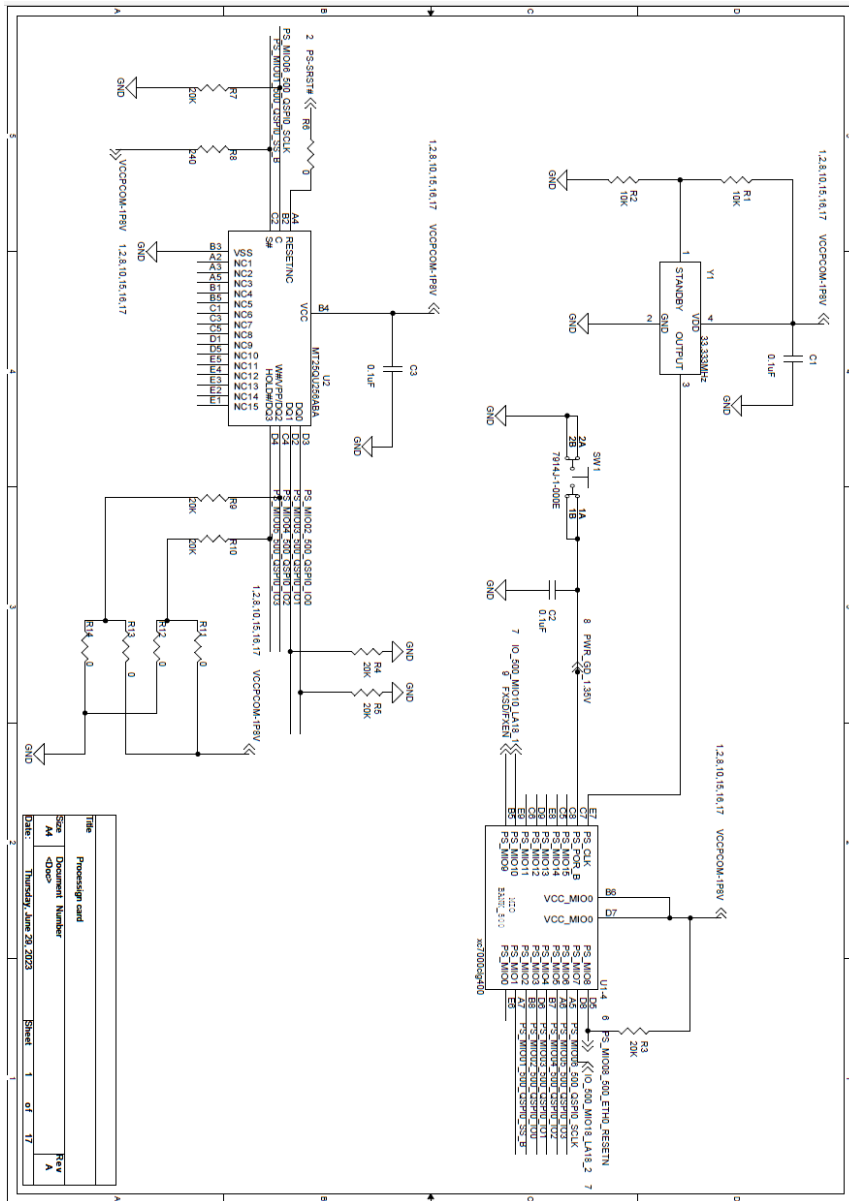
A lot of research working is going on the multi-channel phonocardiography systems, and the placement of sensors is crucial in finding heart abnormalities. More research needs to be done by increasing the number of sensors and applying the proposed algorithm to enhance captured data quality and find more low-frequency components.

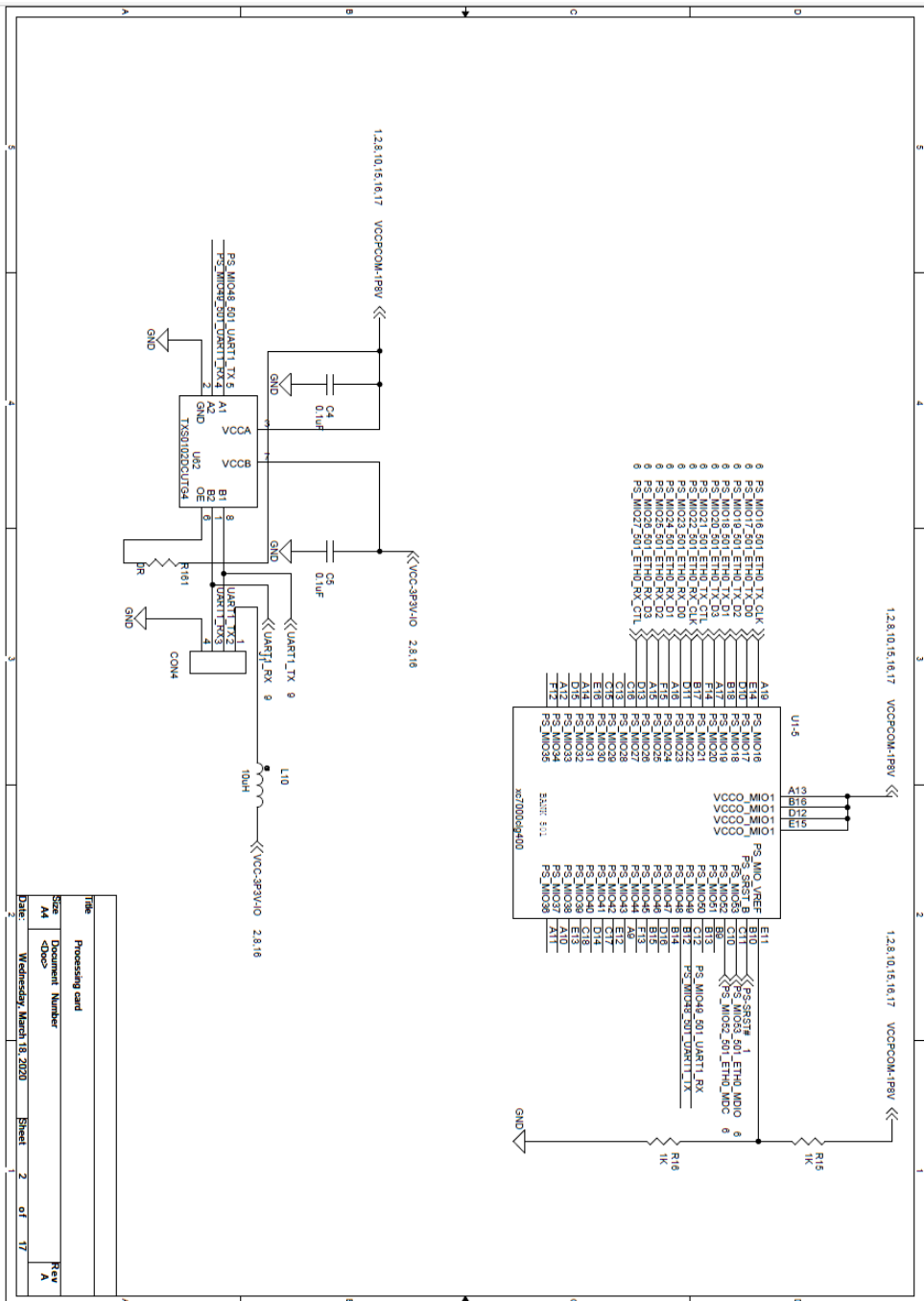
The present research work proposes the source localization algorithms based on MCCC with constant time delays for channel selection and TDOA based on the PHAT using four sensors. In the literature, there are other sound source localization methods like beam formation [63-64], approaches based on high-resolution processing [65-66], and ANN techniques that need a training phase. Continuing with the current research, there is potential for researchers to use the methodologies described above for heart sound localization.

The present research work covers the extraction of cardiac sounds S1, S2, Mitral stenosis, Mitral regurgitation, Aortic stenosis, and S3/S4 gallops. Extending these heart sound components, the present system can be used for other cardiac sound murmurs with little algorithms modifications.

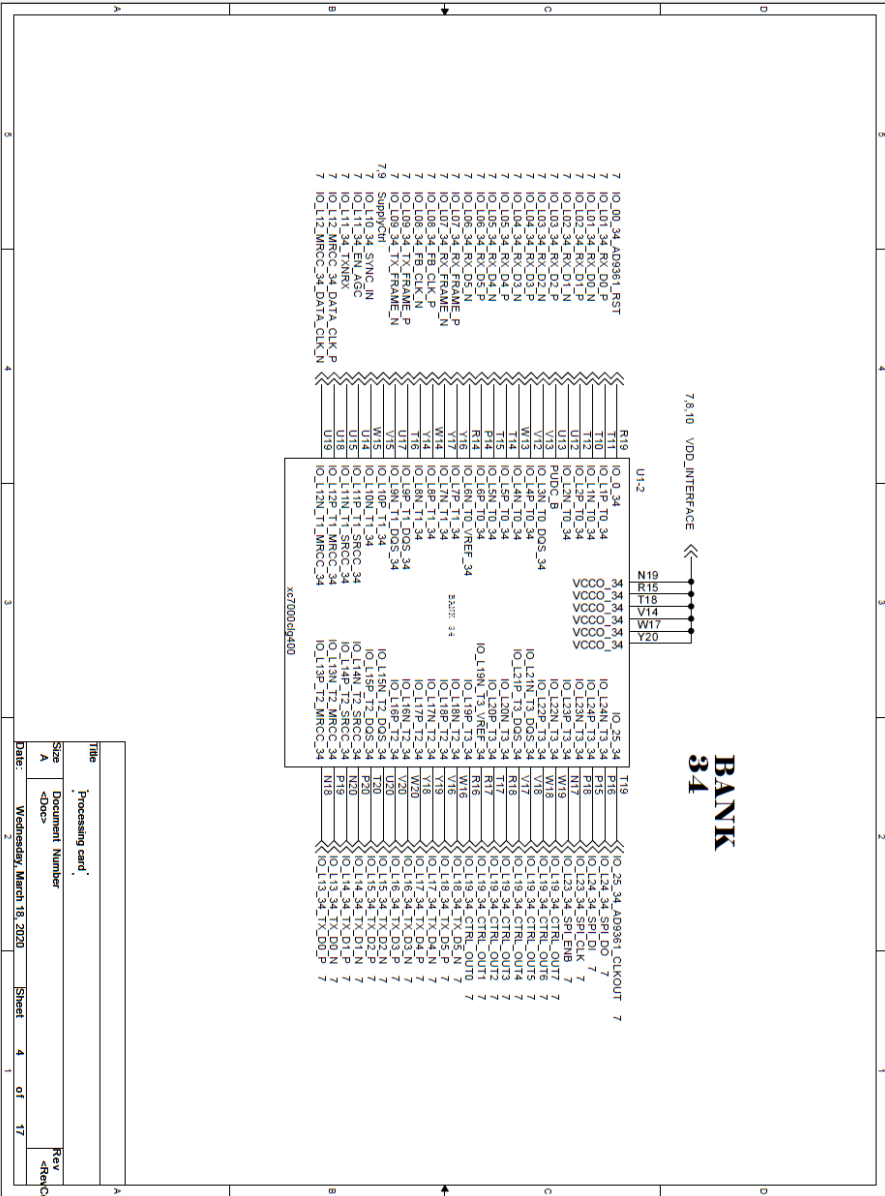
Work must be done to comprehend the underlying physiology of an individual that influences the measurement, and a standard solution must be put forth to have a prediction model that can be used for everyone without the need for periodic calibration from person to person. By expanding the patient group, there is potential to increase the measurement's sensitivity.

Appendix A- Processing Board Schematics

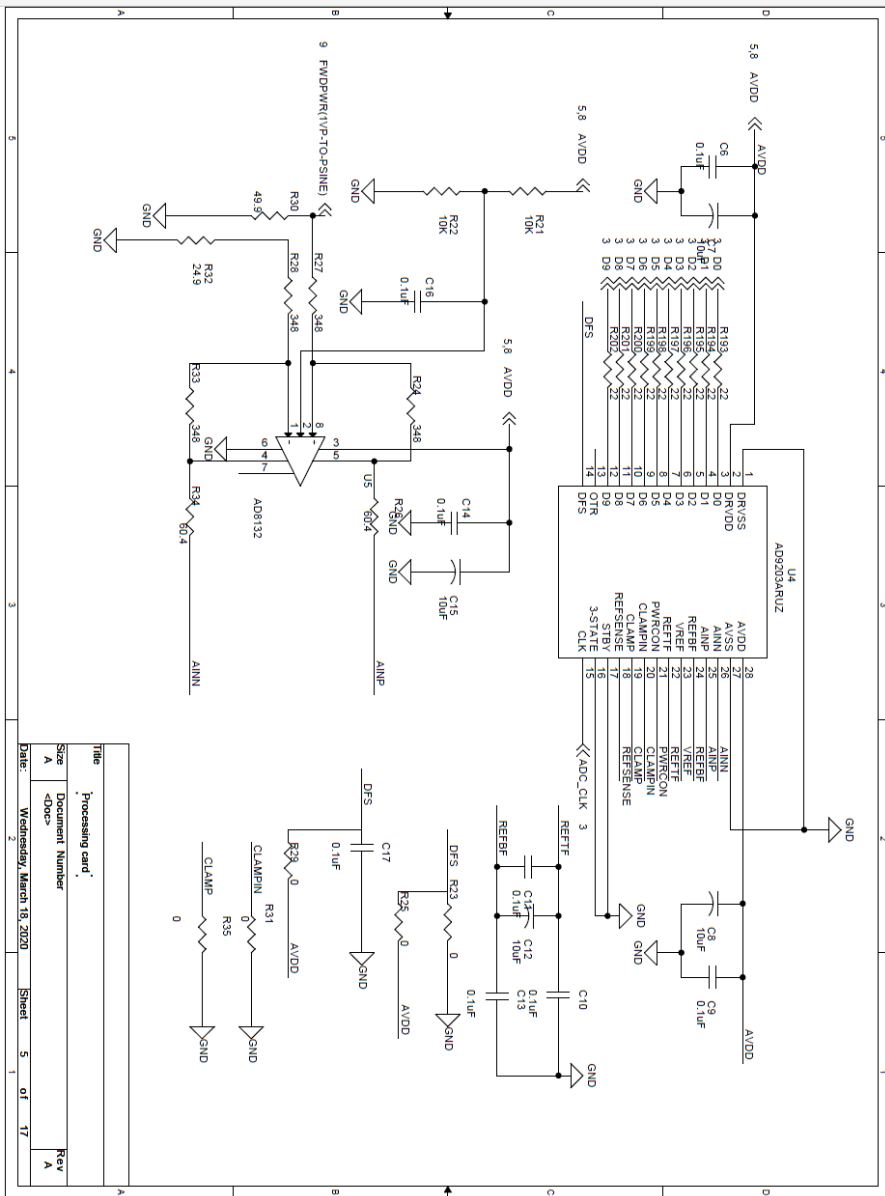


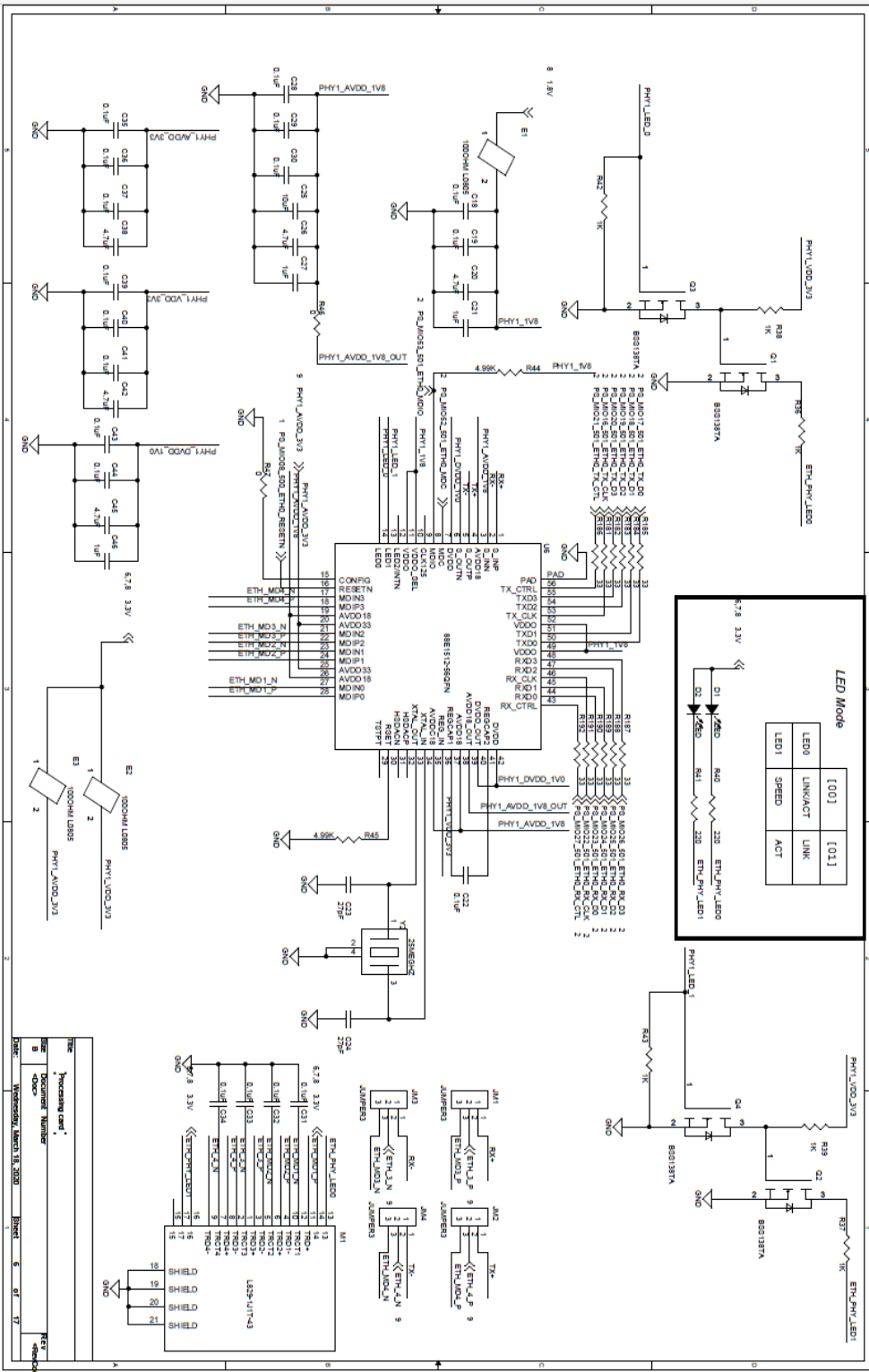


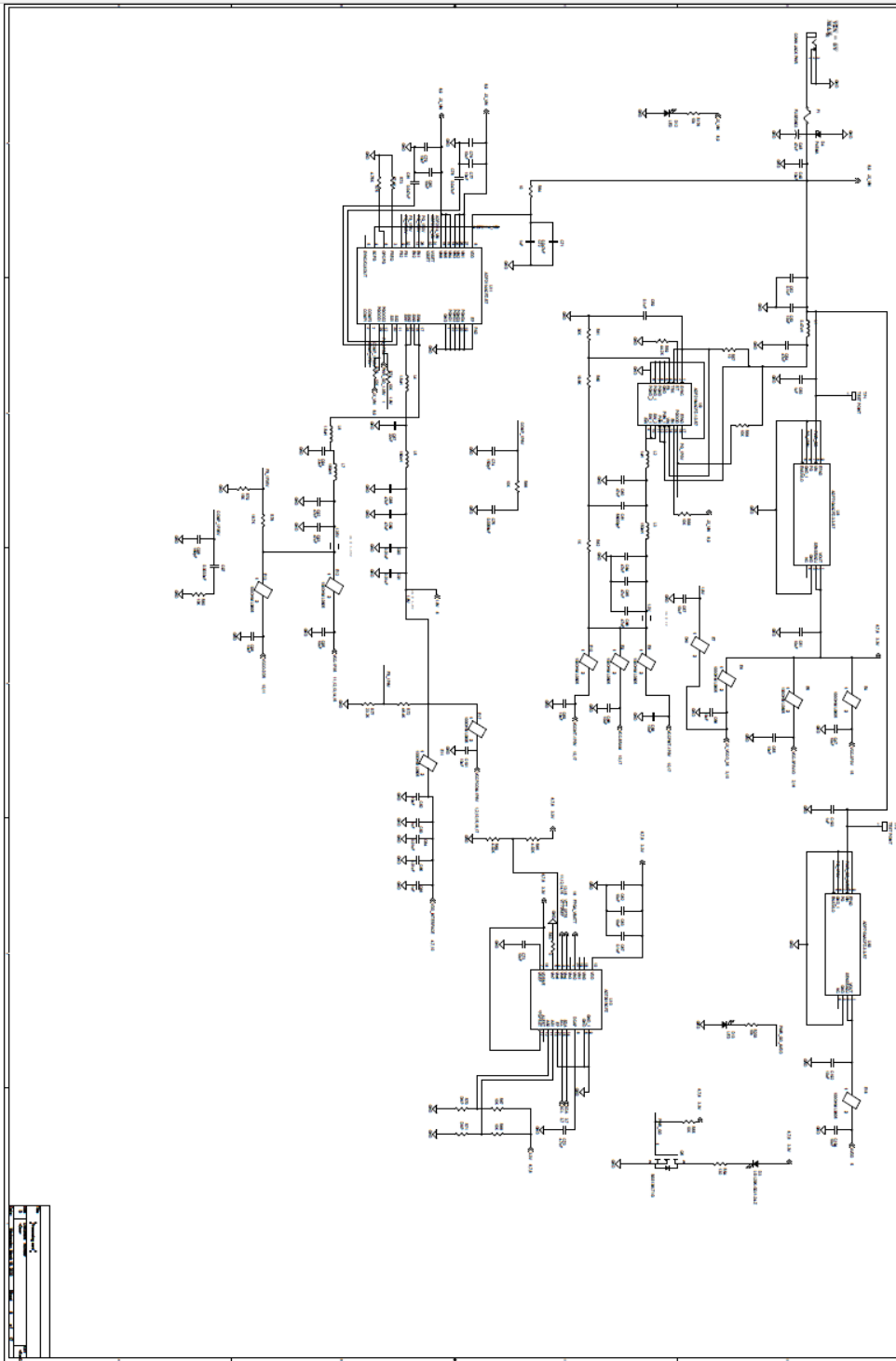
Title: Processing card
 Size: Document Number
 Rev: Rev A
 Date: Wednesday, March 18, 2020 Sheet 2 of 17

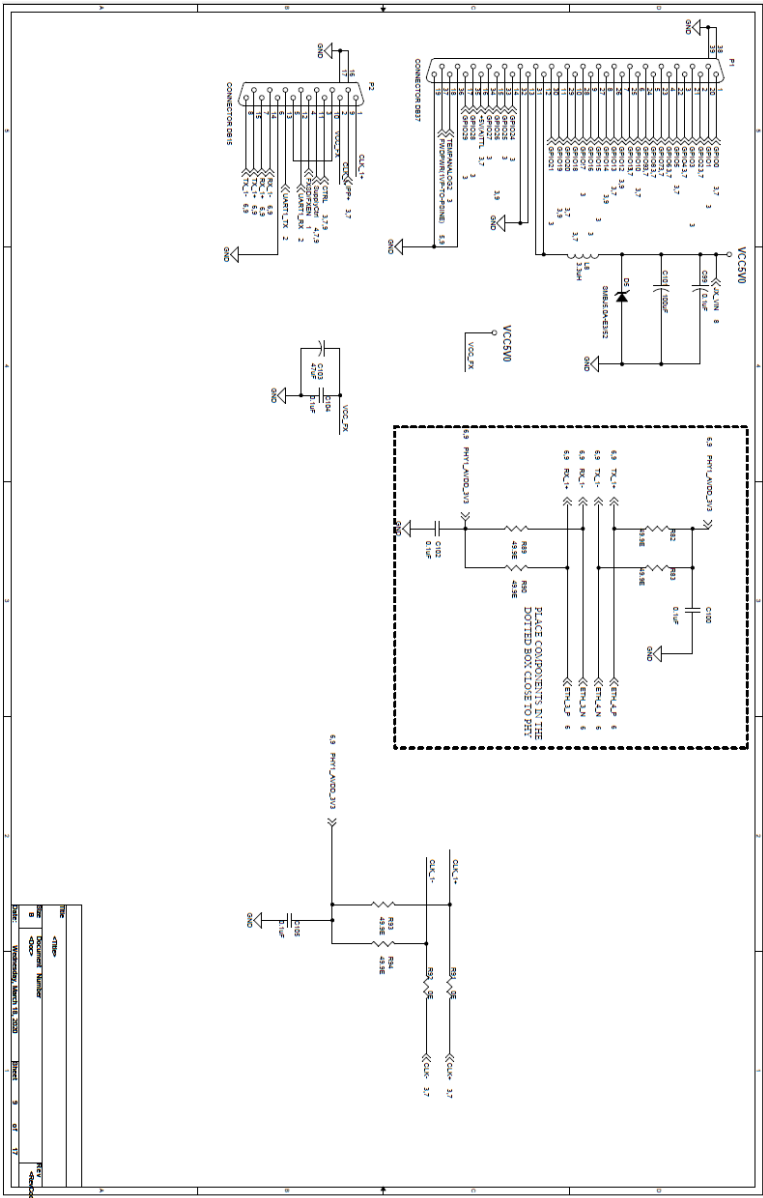


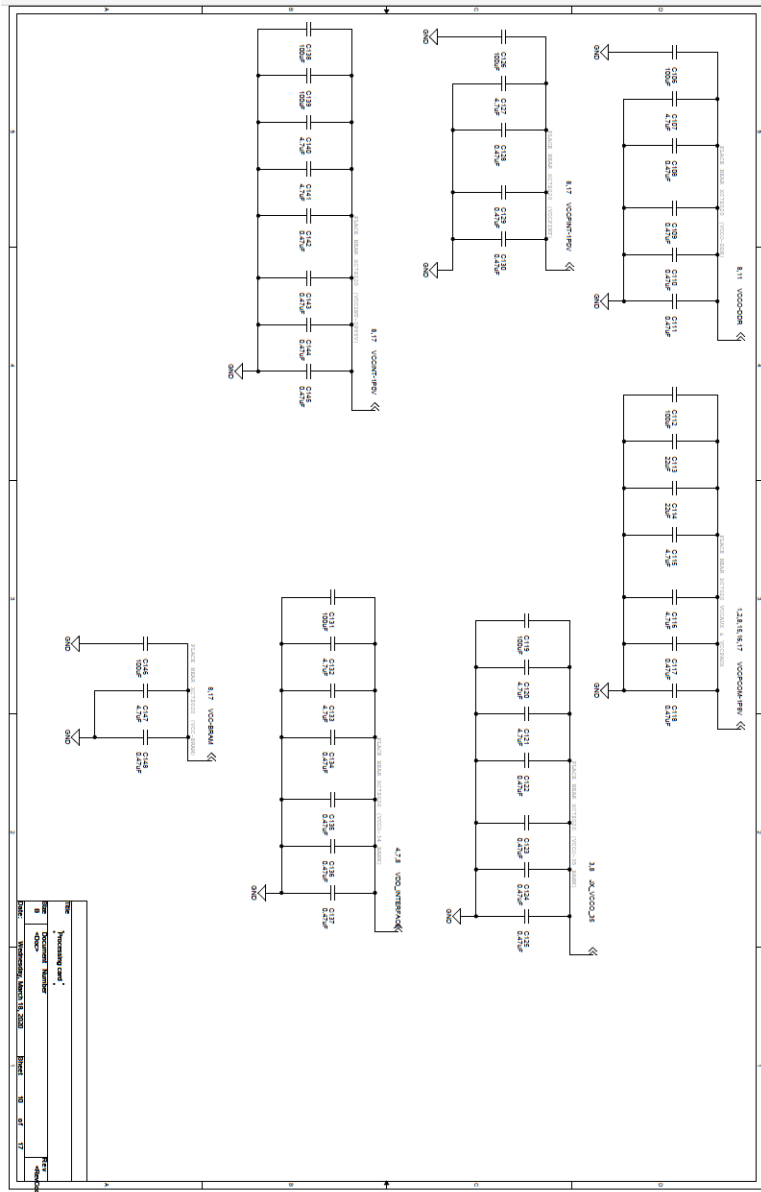
Title	Processing card
Size	A
Document Number	<Doc>
Date:	Wednesday, March 16, 2020
Sheet	4 of 17
Rev	<Rev>

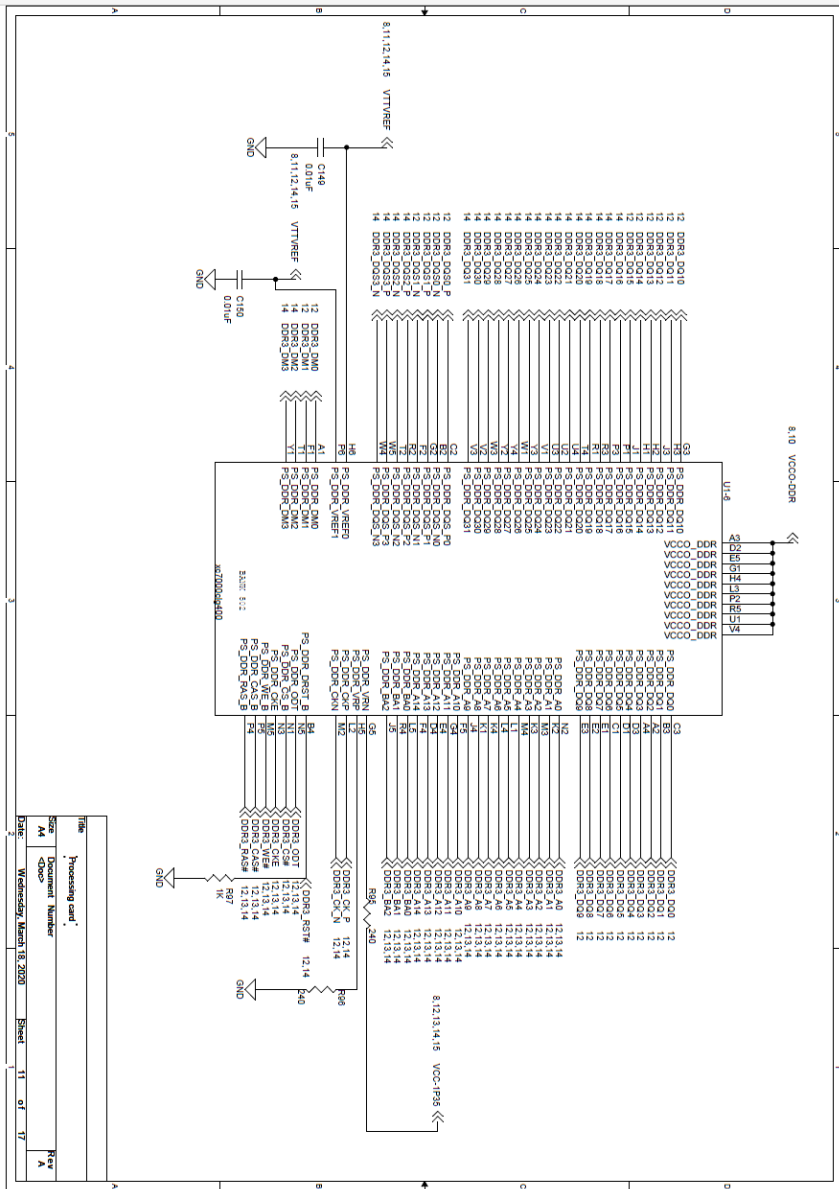


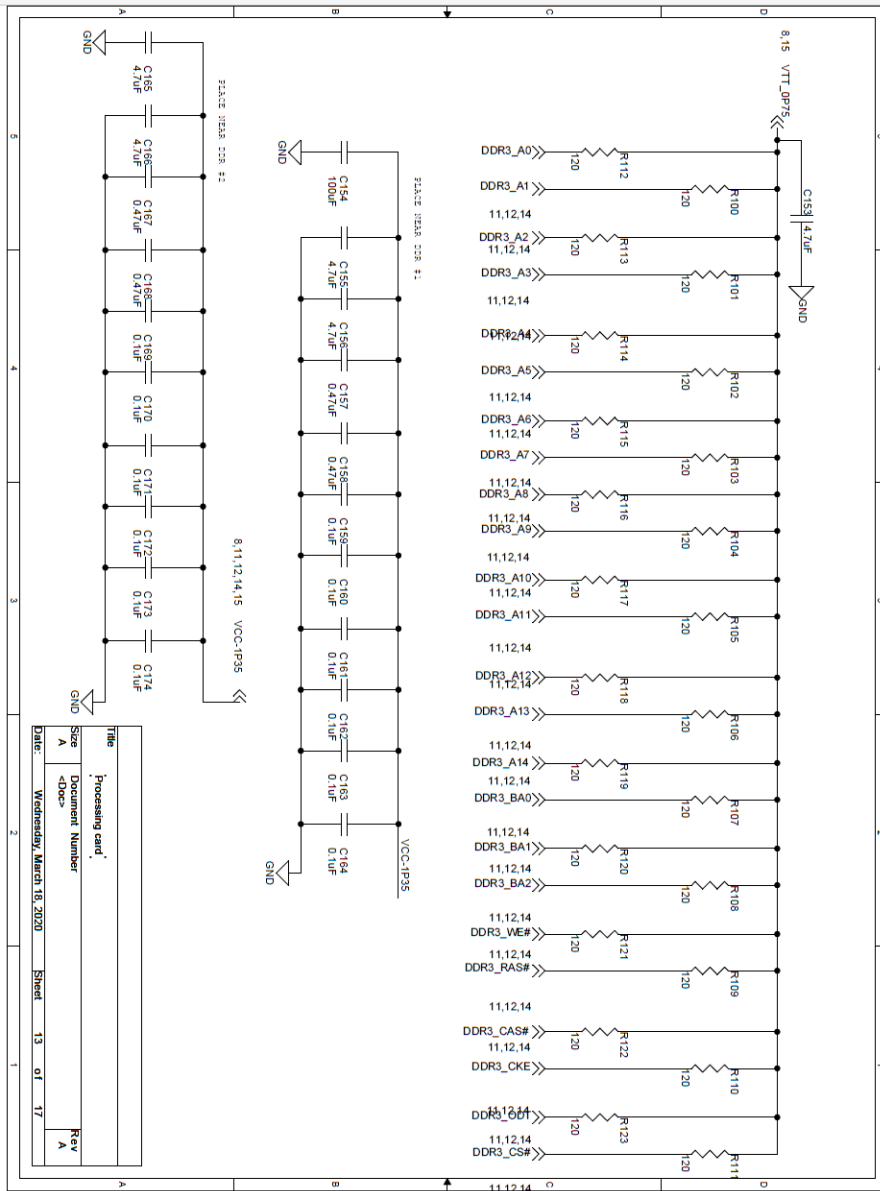












List of Publications

Journals:

- [1] Anumukonda, M., Lakkamraju, P. and Chowdhury, S.R., 2021. FPGA-Based High-Performance Phonocardiography System for Extraction of Cardiac Sound Components Using Inverse Delayed Neuron Model. **Frontiers in Medical Technology**, p.38.
- [2] Lakkamraju, P., Anumukonda, M. and Chowdhury, S.R., 2020. Improvements in Accurate Detection of Cardiac Abnormalities and Prognostic Health Diagnosis Using Artificial Intelligence in Medical Systems. **IEEE Access**, 8, pp.32776-32782.

Conferences:

- [3] Anumukonda, M., Ramasahayam, S., Raju, L.P. and Chowdhury, S.R., 2015, December. Detection of cardio auscultation using MEMS microphone. In 2015 9th **International Conference on Sensing Technology (ICST) (pp. 173-177). IEEE.**
- [4] Anumukonda, M., Lakkamraju, P.R. and Chowdhury, S.R., 2020, January. Classification of Abnormal and Normal Heart Sounds Using the MEMS-based High Performance PhonoCardioGraphy System. In 2020 International Conference on **Artificial Intelligence and Signal Processing (AISP) (pp. 1-7). IEEE.**
- [5] Prasada Raju, L.; Anumukonda, M. and Roy Chowdhury, S. (2019). Safety-related Studies on Non-Invasive Biomedical Signals and Its Aptness Usage in Design of Fault Tolerant Multimodal Human Health Monitoring System. In **Doctoral Consortium - DCBIOSTEC**, ISBN, pages 3-14

Book chapter:

- [6] Anumukonda M., Chowdhury S.R. (2017) "**Heart Sound Sensing Through MEMS Microphone.**" In: Postolache O., Mukhopadhyay S., Jayasundera K., Swain A. (eds) "Sensors for Everyday Life. Smart Sensors, Measurement and Instrumentation", vol 22. Springer, Cham
- [7] S. Roy Chowdhury, G. Sharma, Y. Arora, L.V.R. Prasadaraju, M. Anumukonda, S. Ramasahayam, "Smart circuits for signal conditioning of wearable medical sensors", **Chapter-3 in the book titled Wearable Sensors: Application, Design and Implementation**, edited by S.C. Mukhopadhyay and T. Islam, pp. 3.1-3.28, **IoP Publishing**, 2017

List of Patents

- [1] L.V.R. Prasadaraju, A. Madhubabu, S. Roy Chowdhury, “Wearable Hemoglobin Monitoring Device”, Indian Patent Application No. 201643036895, dated 26-10-2016. FER – Submitted in July’21
- [2] L.V.R. Prasadaraju, A. Madhubabu, S. Roy Chowdhury, “Wearable Cardiac Health Monitoring System”, Indian Patent Application No. 201641036083, dated 21-10-2016.
- [3] L.V.R. Prasadaraju, A. Madhubabu, S. Roy Chowdhury, “Wearable Fetal Cardiac Health Monitoring System”, Indian Patent Application No. 201643042957, dated 16-12-2016. FER – Submitted in Nov’21

Bibliography

- [1] The top 10 causes of death from WHO. <https://www.who.int/en/news-room/factsheets/detail/the-top-10-causes-of-death>.
- [2] A. Bloch, J Crittin, A. Jaussi, "Should functional cardiac murmurs be diagnosed by auscultation or by Doppler echocardiography?" *Clin Cardiol*, 24(12), 767-9, 2001.
- [3] Koymen, Hayrettin et al. "A Study of Prosthetic Heart Valve Sounds." *IEEE Transactions on Biomedical Engineering BME-34* (1987): 853-863.
- [4] S.Mangione, "Cardiac auscultatory skills of physicians-in-training: a comparison of three English-speaking countries," *Am J Med*, vol. 110, pp. 210–216, 2001.
- [5] Karnath B, Thornton W. Auscultation of the heart. *Hospital Physician* September 2002, pp. 39–43.
- [6] A. Tlkian and M. Conover, *Understanding Heart Sounds and Murmurs: With an Introduction to Lung Sounds*, W. B. Saunders Co., Philadelphia, 2001.
- [7] March SK, Bedynek JL Jr, Chizner MA, "Teaching cardiac auscultation: effectiveness of a patient-centered teaching conference on improving cardiac auscultatory skills." in *Mayo Clinic Proceeding*, vol. 80, no. 11, Nov 2005, pp.1443-1448.
- [8] D.L. Mann, et al., *Braunwald's Heart disease: A Textbook of Cardiovascular Medicine*, Elsevier Health Sciences, 2014.
- [9] Pronichev IV (2004). *Lectures on Physiology of Central Nervous System*. Moscow: Swift, p. 214.
- [10] A. Manson, S. J. Kovacs, A. F. Hall, and S. Nudelman, "The relationship of the third and fourth heart sounds to transmitral flow," *Proceedings of 16th Annual International Conference of the IEEE Engineering in Medicine and Biology Society*, 1994, pp. 95-96 vol.1, doi: 10.1109/IEMBS.1994.412087.
- [11] J. E. Hebden and J. N. Torry, "Identification of aortic stenosis and mitral regurgitation by heart sound analysis," *Computers in Cardiology 1997*, 1997, pp. 109-112, doi: 10.1109/CIC.1997.647842.
- [12] Bickley, L.S., *Bates' Guide to Physical Examination and History Taking*. 10th Edition ed. 2009, Philadelphia: Wolter Kluwer | Lippincott Williams & Wilkins.
- [13] J. Wynne, —The clinical meaning of the third heart sound,|| *Amer. J. Med.*, vol. 111, no. 2, pp. 157–158, Aug. 2001.
- [14] Harris IS, Lee E, Yeghiazarians Y, Drew BJ, Michaels AD: Phonocardiographic timing of third and fourth heart sounds during acute myocardial infarction. *J Electrocardiol* 2006, 39:305-309.
- [15] Y.-L. Tseng, P.-Y. Ko and F.-S. Jaw, "Detection of the third and fourth heart sounds using hilbert-huang transform," *Biomedical engineering online*, vol. 11, no. 1, pp. 1-13, 2012.
- [16] N. J. Mehta, and I. A. Khan, —Third heart sound: genesis and clinical importance,|| *Int. J. Cardiology*, vol. 97, no. 2, pp. 183–86, Nov. 2004.

- [17] E. Schwammenthal, C. Chen, F. Benning, M. Block, G. Breithardt, and R. A. Levine, "Dynamics of mitral regurgitant flow and orifice area. Physiologic application of the proximal flow convergence method: clinical data and experimental testing," *Circulation*, pp. 307–322, 1994.
- [18] Pelech, A.N., 2004. The physiology of cardiac auscultation. *Pediatric Clinics*, 51(6), pp.1515-1535.
- [19] R.E. Klabunde. "Cardiovascular physiology concepts." Lippincott Williams and Wilkins. Baltimore, 2011.
- [20] S. Leng, R. San Tan, K.T.C. Chai, C., Wang, D. Ghista and L. Zhong. "The electronic stethoscope." *Biomedical engineering online*, 14(1), 2015, p.66.
- [21] E. Kaniusas, H. Pfutzner, and B. Saletu, "Acoustical signal properties for cardiac/respiratory activity and apneas," in *IEEE Transactions on Biomedical Engineering*, vol. 52, no. 11, pp. 1812-1822, Nov. 2005, doi: 10.1109/TBME.2005.856294.
- [22] P. Wang, Y. Kim, L. H. Ling, and C. B. Soh, "First Heart Sound Detection for Phonocardiogram Segmentation," *2005 IEEE Engineering in Medicine and Biology 27th Annual Conference*, 2005, pp. 5519-5522, doi: 10.1109/IEMBS.2005.1615733.
- [23] V. Nigam and R. Priemer, "A procedure to extract the aortic and the pulmonary sounds from the phonocardiogram," in *Proceedings of the 28th IEEE EMBS Annual International Conference*, New York City, USA, Aug 30-Sep 3 2006.
- [24] B. Silverman, M. Balk, Digital stethoscope-improved auscultation at the bedside, *Am. J. Cardiol.* 123 (6) (2019) 984–985.
- [25] Vermarien, H., van Vollenhoven, E. The recording of heart vibrations: a problem of vibration measurement on soft tissue. *Med. Biol. Eng. Comput.* 22, 168–178 (1984). <https://doi.org/10.1007/BF02446821>
- [26] S.Y. Li, F. Li, S.J. Tang, W.J. Xiong, A review of computer-aided heart sound detection techniques, *Biomed Res. Int.* 2020 (2020) 1–10.
- [27] Y. Cheng, Y. Zhang, S. Dai, Design and feature recognition of 4-channel synchronous heart sound signal acquisition device, *J. Nanjing Univ. Posts Telecommunication*. (Natural Science Edition) 39
- [28] Bill Gardner and Keith Martin, HRTF Measurements of a KEMAR Dummy-Head Microphone, MIT Media, Aug 2000.
- [29] Salvatore, S. (1997). "Study: Most New Doctors Can't use Stethoscope," <http://edition.cnn.com/HEALTH/9709/02/nfm.heart.sounds/> (14 July 2012).
- [30] Amiri AM, Armano G. An intelligent diagnostic system for congenital heart defects. *IJACSA.* 2013;4:93–97.
- [31] K. Ajay Babu, B. Ramkumar, Automatic recognition of fundamental heart sound segments from PCG corrupted with lung sounds and speech, *IEEE Access.* 8 (2020) 179983–179994.
- [32] S. E. Schmidt et al., "Detection of coronary artery disease with an electronic stethoscope," *Comput. Cardiol.*, vol. 34, pp. 757–760, 2007.
- [33] Veytsenfeld A (2000) Microphones. *Zvukorezhisser* 1: 4-8.

- [34] L. Nowak and N. Nowak, "Sound differences between electronic and acoustic stethoscopes," *BioMedical Engineering OnLine*, vol. 17, no
- [35] J. Kirchner, S. Souilem, G. Fischer, Wearable system for measurement of thoracic sounds with a microphone array, presented at IEEE Sensors, Glasgow, Scotland, Oct.–Nov. (2017).
- [36] M.S. Afzal, H. Shim, Y. Roh, Design of a piezoelectric multilayered structure for ultrasound sensors using the equivalent circuit method, *Sensors* 18 (12) (2018) 4491.
- [37] J.Wang et al., "Modeling sound generation in stenosed coronary arteries," *IEEE Trans. Biomed. Eng.*, vol. 37, no. 11, pp. 1087–94, Nov. 1990.
- [38] D. Shen, J. L. Semmlow and W. Welkowitz, "Automated identification of artifact-free diastolic heart sounds," in *Proceedings of the Annual Conference on Engineering in Medicine and Biology*, 1990, pp.569-570.
- [39] M. Akay, J. L. Semmlow, W. Welkowitz, M. D. Bauer and J. B. Kostis, "Detection of coronary occlusions using autoregressive modeling of diastolic heart sounds," *IEEE Trans. Biomed. Eng.*, vol.37, pp. 366-373, Apr 1990.
- [40] M. Akay, J. L. Semmlow, W. Welkowitz, M. D. Bauer and J. B. Kostis, "Noninvasive detection of coronary stenoses before and after angioplasty using eigenvector methods," *IEEE Trans. Biomed. Eng.*, vol. 37, pp. 1095-1104, 11, 1990.
- [41] M. Akay, M. Bauer, J. L. Semmlow, W. Welkowitz, and J. Kostis, "Analysis of diastolic heart sounds before and after angioplasty," *Proceedings of the Annual International Conference of the IEEE Engineering in Medicine and Biology Society*, New Orleans, LA, USA, 1988, pp. 257-259 vol.1, doi: 10.1109/IEMBS.1988.94505.
- [42] M. Akay, M. Bauer, J. L. Semmlow, W. Welkowitz, and J. Kostis, "Autoregressive modeling of diastolic heart sounds," *Proceedings of the Annual International Conference of the IEEE Engineering in Medicine and Biology Society*, New Orleans, LA, USA, 1988, pp. 172-174 vol.1, doi: 10.1109/IEMBS.1988.94463.
- [43] M. Akay, J. L. Semmlow, W. Welkowitz, and J. Kostis, "Parametric modeling of diastolic heart sounds before and after angioplasty," *Images of the Twenty-First Century. Proceedings of the Annual International Engineering in Medicine and Biology Society*, Seattle, WA, USA, 1989, pp. 51-52 vol.1, doi: 10.1109/IEMBS.1989.95566.
- [44] M. Akay, Y. M. Akay, D. Gauthier, R. G. Paden, W. Pavlicek, F. D. Fortuin, J. P. Sweeney and R. W.Lee, "Dynamics of diastolic sounds caused by partially occluded coronary arteries," *IEEE Trans.Biomed. Eng.*, vol. 56, pp. 513-517, Feb, 2009.
- [45] D. Gauthier, Y. M. Akay, R. G. Paden, W. Pavlicek, F. D. Fortuin, J. K. Sweeney, R. W. Lee, and M.Akay, "Spectral analysis of heart sounds associated with coronary occlusions," in *Proceedings of the IEEE/EMBS Region 8 International Conference on Information Technology Applications in Biomedicine*, ITAB, 2008, pp. 49-52.
- [46] D. Gauthier, Y. M. Akay, R. G. Paden, W. Pavlicek, F. D. Fortuin, J. K. Sweeney, R. W. Lee, and M.Akay, "Spectral analysis of heart sounds associated with coronary occlusions," in *InformationTechnology Applications in Biomedicine*, 2007. ITAB 2007. 6th International Special Topic Conference on, 2007, pp. 49-52.
- [47] Watakabe M, Itoh Y, Mita K, Akataki K. Technical aspects of mechnomyography recording with piezoelectric contact sensor. *Med Biol Eng Comput.* 1998 Sep;36(5):557-61. doi: 10.1007/BF02524423. PMID: 10367437.

- [48] T. -h. Chen, S. -x. Xing, P. -y. Guo, H. -t. Tang and Z. Yu, "The Design of Digital Collecting System of Heart Sound Signals Based on DSP," 2010 International Conference on Biomedical Engineering and Computer Science, Wuhan, China, 2010, pp. 1-4, doi: 10.1109/ICBECS.2010.5462415.
- [49] ADXL103/ADXL203 Precision 61.7 g, 65 g, 618 g Single-/Dual-Axis iMEMS Accelerometer (2004) Analog Devices, p. 16.
- [50] Ayoob Khan TE, Vijayakumar P (2010) Separating heart sound from lung sound using LabView. International Journal of Computer and Electrical Engineering 3(2): 1793-8163.
- [51] B. H"ok, K. Nilsson, and H. Bjelkhagen, "Imaging of chest motion due to heart action by means of holographic interferometry," Med. & Biol. Eng. & Comput., vol.16, pp.353–368, July 1978.
- [52] H. Kajbaf , H. Ghassemian , Acoustic imaging of heart using microphone arrays, 13th International Conference on Biomedical Engineering, Springer, 2009.
- [53] S. Kraman, Speed of low-frequency sound through lungs of normal men, J. Appl. Physiol. 55 (6) (1983) 1862–1867.
- [54] K. Chihara, A. Kitajima, and Y. Sakurai, "Considerations on imaging method of diagnostic information of heart sounds," IECE trans.,vol.E63, no.9, pp.670–671, 1980.
- [55] M. Okada, "Chest wall maps of heart sounds and murmurs," Comput. Biomed. Res., vol.15, pp.281–294, 1982.
- [56] J. Verburg, "Transmission of vibrations of the heart to the chestwall,"Adv. Cardiovasc. Phys., vol.5(Part III), pp.84–103, 1983.
- [57] H. Vermarien, "Mapping and vector analysis of heart vibration data obtained by multisite phonocardiography," Adv. Cardiovasc. Phys., vol.6, pp.133–185, 1989.
- [58] M. Cozic, L.-G. Durand, and R. Guardo, "Development of a cardiac acoustic mapping system," Med. & Biol. Eng. & Comput., vol.36, pp.431–437, July 1998.
- [59] K. Ogata, A. Kandori, T. Miyashita, and K. Tsukada, "Visualization method of current distribution in cardiac muscle using a heart model," Japan Soc. Med. & Biol. Eng., vol. 41-1, pp.25–33, 2003.
- [60] J. Kusuno, T. Kiwa, K. Tsukada, K. Ogata, T. Miyashita, and A. Kandori, "Spatial analysis of cardiomagnetic field," Japan Soc. ME & BE, vol.42, p.23, Dogo Matsuyama, Nov. 2004.
- [61] M. Ranjkesh, R. Hasanzadeh, A fast and accurate sound source localization method using the optimal combination of SRP and TDOA methodologies, Inf.Syst. Telecommun. (2015) 100–109.
- [62] T.G. Dvorkind, S. Gannot, Time difference of arrival estimation of speech source in a noisy and reverberant environment, Signal Process. 85 (1) (2005)177–204.
- [63] J.M. Valin, F. Michaud, J. Rouat, Robust localization and tracking of simultaneous moving sound sources using beamforming and particle filtering, Rob. Auton. Syst. 55 (3) (2007) 216–228.
- [64] T. He, Q. Pan, Y. Liu, X. Liu, D. Hu, Near-field beamforming analysis for acoustic emission source localization, Ultrasonics 52 (5) (2012) 587–592.

- [65] Y. Wu, L. Ma, C. Hou, G. Zhang, J. Li, Subspace-based method for joint range and DOA estimation of multiple near-field sources, *Signal Process.* 86 (8)(2006) 2129–2133.
- [66] X. Zhang, E. Song, J. Huang, H. Liu, Y. Wang, B. Li, X. Yuan, Acoustic source localization via subspace-based method using small aperture MEMS arrays, *J.Sens.* 2014 (2014).
- [67] H. Nakashima, T. Mukai, 3D sound source localization system based on learning of binaural hearing, in 2005 IEEE International Conference on Systems, Man, and Cybernetics (Vol. 4), IEEE, 2005, pp. 3534–3539.
- [68] J. Weng, K.Y. Guentchev, Three-dimensional sound localization from a compact non-coplanar array of microphones using tree-based learning, *J.Acoust. Soc. Am.* 110 (1) (2001) 310–323.
- [69] Zhu N, Wu SF. Sound source localization in three-dimensional space in real time with redundancy checks. *J Comput Acoust.* 2012; 20 (01).
- [70] M. Azaria, D. Hertz, Time delay estimation by generalized cross correlation methods, *IEEE Trans Acoust. Speech Signal Process.* 32 (2) (1984) 280–285.
- [71] C. Knapp, G. Carter, The generalized correlation method for estimation of time delay, *IEEE Trans Acoust. Speech Signal Process.* 24 (4) (1976) 320–327.
- [72] M. Omologo, P. Svaizer, Acoustic source location in noisy and reverberant environment using CSP analysis, in: IEEE International Conference on Acoustics, Speech, and Signal Processing, 1996. ICASSP-96 (Vol. 2), IEEE, 1996, pp. 921–924.
- [73] H. Teutsch, *Modal Array Signal Processing: Principles and Applications of Acoustic Wavefield Decomposition*, vol. 348, Springer, 2007.
- [74] R.O. Schmidt, Multiple emitter location and signal parameter estimation, *IEEE Trans. Antennas Propag.* 34 (3) (1986) 276–280.
- [75] R. Roy, A. Paulraj, T. Kailath, ESPRIT—A subspace rotation approach to the estimation of parameters of cisoids in noise, *IEEE Trans. Acoust. Speech Signal Process.* 34 (5) (1986) 1340–1342.
- [76] A.J. Barabell, Improving the resolution performance of eigenstructure-based direction-finding algorithms, *IEEE International Conference on Acoustics, Speech, and Signal Processing, ICASSP-83 (Vol. 8), IEEE1983 (1983)* 336–339.
- [77] SCHMIDT, R.O. (1972). A new approach to the geometry of range difference location. *IEEE Transactions on Aerospace and Electronic Systems*, vol. 8, n. 6, pp. 821–835.
- [78] H. Schau and A. Robinson, "Passive source localization employing intersecting spherical surfaces from time-of-arrival differences," in *IEEE Transactions on Acoustics, Speech, and Signal Processing*, vol. 35, no. 8, pp. 1223-1225, August 1987, doi: 10.1109/TASSP.1987.1165266.
- [79] J. Smith and J. Abel, "Closed-form least-squares source location estimation from range-difference measurements," in *IEEE Transactions on Acoustics, Speech, and Signal Processing*, vol. 35, no. 12, pp. 1661-1669, December 1987, doi: 10.1109/TASSP.1987.1165089.

- [80] CHAN, Y.T. & HO, K.C. (1994). A simple and efficient estimator for hyperbolic location. *IEEE Transactions on Signal Processing*, vol. 43, n. 8, pp. 1905–1915.
- [81] BRANDSTEIN, M., ADCOCK, J.E. & SILVERMAN, H.F. (1997). A closed-form location estimator for use with room environment microphone arrays. *IEEE Transactions on Speech and Audio Processing*, vol. 5, n. 1, pp. 45–50.
- [82] GILLETTE, M.D. & SILVERMAN, H.F. (2008). A linear closed-form algorithm for source localization from time differences of arrival. *IEEE Signal Processing Letters*, vol. 5, pp. 1–4.
- [83] STOICA, P. & LI, J. (2006). Source localization from range-difference measurements. *IEEE Signal Processing Magazine*, vol. 23, n. 3, pp. 63–66.
- [84] HAHN, W. & TRETTER, S. (1973). Optimum processing for delay-vector estimation in passive signal arrays. *IEEE Transactions on Information Theory*, vol. 19, n. 5, pp. 608–614.
- [85] STOICA, P. & NEHORAI, A. (1990). MUSIC, maximum likelihood, and cramer-rao bound: further results and comparisons. *IEEE Transactions on Acoustics, Speech and Signal Processing*, vol. 38, n.12, pp. 2140–2150.
- [86] SEGAL, M., WEINSTEIN, E. & MUSICUS, B.R. (1991). Estimate-maximize algorithms for multichannel time delay and signal estimation. *IEEE Transactions on Signal Processing*, vol. 39, n. 1, pp. 1–16.
- [87] CHEN, J.C., HUDSON, R.E. & YAO, K. (2002). Maximum-likelihood source localization and unknown sensor location estimation for wideband signals in the near-field. *IEEE Transactions on Signal Processing*, vol. 50, n. 8, pp. 1843–1854.
- [88] GEORGIU, P.G. & KYRIAKAKIS, C. (2006). Robust maximum likelihood source localization: The case for sub-gaussian versus gaussian. *IEEE Transactions on Audio, Speech, and Language Processing*, vol. 14, n. 4, pp. 1470–1480.
- [89] DESTINO, G. & ABREU, G. (2011). On the maximum likelihood approach for source and network localization. *IEEE Transactions on Signal Processing*, vol. 59, n. 10, pp. 4954–4970.
- [90] Asir, Khadra, Abbasi, Mohammed. Time-Frequency Analysis of Heart Sounds *IEEE TENCON – DSP Applications 1996*; 2553-558.
- [91] Jiang, Z. , & Choi, S. (2006). A cardiac sound characteristic waveform method for in-home heart disorder monitoring with electric stethoscope. *Expert Systems with Applications*, 31 (2), 286–298.
- [92] Chetlur Adithya P, Hart S, Moreno VA, Sankar R. Trends in fetal monitoring through phonocardiography: Challenges and future directions. *Biomedical Signal Processing and Control* 2017;33:289-305.
- [93] Herzig, J. , Bickel, A. , Eitan, A. , & Intrator, N. (2015). Monitoring cardiac stress using features extracted from s1 heart sounds. *IEEE Transactions on Biomedical Engineering*, 62 (4), 1169–1178.
- [94] L.-G. Durand, M. Blanchard, G. Cloutier, H. N. Sabbah, and P. D. Stein, “Comparison of Pattern Recognition Methods for Computer-Assisted Classification of Spectra of Heart

- Sounds in Patients with a Porcine Bioprosthetic Valve Implanted in the Mitral Position,” IEEE Transactions on Biomedical Engineering, vol. 37, no. 12, pp. 1121–1129, 1990.
- [95] H. Liang, S. Lukkarinen, I. Hartimo, A heart Sound segmentation algorithm using wavelet decomposition and reconstruction, in: 19th Proc. Int. Conf. IEEE Engineering in Medicine and Biology Society, 1997, pp. 1630–1633.
- [96] X. Wang, Y. Li, C. Sun, C. Liu, Detection of the first and second heart sound using heart sound energy, Int. Conf. Biomed. Eng. Inform. (2009) 1–4.
- [97] H. Liang, S. Lukkarinen, I. Hartimo, Heart sound segmentation algorithm based on heart sound envelopogram, Comput. Cardiol. 24 (1997) 105–108.
- [98] J.M. Alajarin, R.R. Merino, Efficient method for events detection in phonocar-diographic signals, in Proc. SPIE Bioengineered and Bioinspired Systems II, vol.5839, no. 398, 2005.
- [99] H.L. Baranek, H.C. Lee, G. Cloutier, L.G. Durand, Automatic detection of sounds and murmurs in patients with Ionescu-Shiley aortic bioprostheses, Med. Biol. Eng. Comput. 27 (5) (1989) 449–455.
- [100] H. Liang, S. Lukkarinen, I. Hartimo, Heart sound segmentation algorithm based on heart sound envelopogram, Comput. Cardiol. 24 (1997) 105–108.
- [101] M.B. Malarvili, I. Kamarulafizam, S. Hussain, D. Helmi, Heart sound segmentation algorithm based on instantaneous energy of electrocardiogram, Comput. Cardiol. 30 (2003) 327–330.
- [102] D. Gill, N. Gavrieli, N. Intrator, Detection and identification of heart sounds using homomorphic envelopogram and self-organizing probabilistic model, Comput. Cardiol. 32 (2005) 957–960.
- [103] F. Beritelli, S. Serrano, Biometric identification based on frequency analysis of cardiac sounds, IEEE Trans. Inform. Forensics Security 2 (3) (2007) 596–604.
- [104] M. Sabarimalai Manikandan, K.P. Soman, Robust heart sound activity detection in noisy environments, Electron. Lett. 46 (16) (2010 August).
- [105] Z. Sharif, M.S. Zainal, A.Z. Sha’ameri, S.H.S. Salleh, Analysis and classification of heart sounds and murmurs based on the instantaneous energy and frequency estimations, in: TENCON 2000, Proc. IEEE 2 (2000) 130–134.
- [106] E. Comak, A. Arslan, I. Turkoglu, A decision support system based on support vector machines for diagnosis of the heart valve diseases, Comput. Biol. Med. 37 (2007) 21–27.
- [107] FitzHugh, R., Impulses and physiological states in theoretical models of nerve membrane. Biophys. J. 1(6):445–466, 1961.
- [108] S. Barma, B. W. Chen, W. Ji, S. Rho, C. H. Chou, and J. F. Wang, “Detection of the third heart sound based on nonlinear signal decomposition and time-frequency localization,” IEEE Trans. Biomed. Eng., vol. 63, no. 8, pp. 1718–1727, Aug. 2016.
- [109] P. Hult, T. Fjällbrant, K. Hildén, U. Dahlström, B. Wranne, and P. Ask, “Detection of the third heart sound using a tailored wavelet approach: Method verification,” Med. Biol. Eng. Comput., vol. 43, no. 2, pp. 212–217, 2005.

- [110]G. Andria, M. Savino, and A. Trotta, “Application of Wigner–Ville distribution to measurements on transient signals,” *IEEE Trans. Instrum.Meas.*, vol. 43, no. 2, pp. 187–193, Apr. 1994.
- [111]S. Barma, B.-W. Chen, K. L. Man, and J.-F. Wang, “Quantitative measurement of split of the second heart sound (S2),” *IEEE/ACM Trans. Comput. Biol. Bioinf.*, vol. 12, no. 4, pp. 851–860, Jul./Aug. 2015.
- [112]Patidar S, Pachori RB. Classification of cardiac sound signals using constrained tunable-Q wavelet transform. *Expert Syst Appl* 2014; 41: 7161-7170.
- [113]Uguz H. Adaptive neuro-fuzzy inference system for diagnosis of the heart valve diseases using wavelet transform with entropy. *Neural Comput Appl* 2012; 21: 1617-1628.
- [114]Saracoglu R. Hidden Markov model-based classification of heart valve disease with PCA for dimension reduction. *Eng Appl Artif Intel* 2012; 25: 1523-1528.
- [115]Dokur Z, Ölmez T. Heart sound classification using wavelet transform and incremental self-organizing map. *Digit Signal Process* 2008; 18: 951-959.
- [116]Safara F, Doraisamy S, Azman A, Jantan A, Ranga S. Wavelet packet entropy for heart murmurs classification. *Adv Bioinformatics* 2012; 1-6.
- [117]P. S. Wright, “Short-time Fourier transforms and Wigner–Ville distributions applied to the calibration of power frequency harmonic analyzers,” *IEEE Trans. Instrum. Meas.*, vol. 48, no. 2, pp. 475–478, Apr. 1999.
- [118]G. Livanos, N. Ranganathan, and J. Jiang, “Heart sound analysis using the S transform,” in *Proc. Comput. Cardiol.*, 2000, pp. 587–590.
- [119]E. Sejdic and J. Jiang, “Comparative study of three time-frequency representations with applications to a novel correlation method,” in *Proc. IEEE Int. Conf. Acoust., Speech, Signal Process.*, vol. 2. 2004, pp. 633–636.
- [120]A. Soualhi, K. Medjaher, and N. Zerhouni, “Bearing health monitoring based on Hilbert–Huang transform, support vector machine and regression,” *IEEE Trans. Instrum. Meas.*, vol. 64, no. 1, pp. 52–62, Jan. 2015.
- [121]E.D. Ubeyli, ECG beats classification using multiclass support vector machines with error correcting output codes, *Digital Signal Process.* 17 (3) (2007) 675–684.
- [122]Z. Dokur, T. Ölmez, Feature determination for heart sounds based on divergence analysis, *Digital Signal Process.* (2008), doi:10.1016/j.dsp.2007.11.003.
- [123]S. Poornachandra, Wavelet-based denoising using subband dependent threshold for ECG signals, *Digital Signal Process.* 18 (1) (2008) 49–55.
- [124]A. Al-Shrouf, M. Abo-Zahhad, Sabah M. Ahmed, A novel compression algorithm for electrocardiogram signals based on the linear prediction of the wavelet coefficients, *Digital Signal Process.* 13 (4) (2003) 604–622.
- [125]B.N. Singh, A.K. Tiwari, Optimal selection of wavelet basis function applied to ECG signal denoising, *Digital Signal Process.* 16 (3) (2006) 275–287.
- [126]D.W. Novey, M. Pencak, J.M. Stang, *The Guide to Heart Sounds: Normal and Abnormal*, CRC Press, Boca Raton, FL, 1988.

- [127]M. Anumukonda, P. R. Lakkamraju, and S. R. Chowdhury, "Classification of Abnormal and Normal Heart Sounds Using the MEMS-based High Performance PhonoCardioGraphy System," 2020 International Conference on Artificial Intelligence and Signal Processing (AISP), Amaravati, India, 2020, pp. 1-7, doi: 10.1109/AISP48273.2020.9073020.
- [128]H. Li, Y. Ren, G. Zhang, R. Wang, J. Cui, and W. Zhang, "Detection and Classification of Abnormalities of First Heart Sound Using Empirical Wavelet Transform," in IEEE Access, vol. 7, pp. 139643-139652, 2019, doi 10.1109/ACCESS.2019.2943705.
- [129]E. Messner, M. Zöhrer and F. Pernkopf, "Heart Sound Segmentation—An Event Detection Approach Using Deep Recurrent Neural Networks," in IEEE Transactions on Biomedical Engineering, vol. 65, no. 9, pp. 1964-1974, Sept. 2018, doi: 10.1109/TBME.2018.2843258.
- [130]Benjamin, Emelia & Muntner, Paul & Alonso, Alvaro & Bittencourt, Márcio & Callaway, Clifton & Carson, April & Chamberlain, Alanna & Chang, Alex & Cheng, Susan & Das, Sandeep & Dellinger, Francesca & Djoussé, Luc & Elkind, Mitchell & Ferguson, Jane & Fornage, Myriam & Jordan, Lori & Khan, Sadiya & Kissela, Brett & Knutson, Kristen & Virani, Salim. (2019). Heart Disease and Stroke Statistics—2019 Update: A Report From the American Heart Association. Circulation. 139. 10.1161/CIR.0000000000000659.
- [131]R.M. Rangayyan, R.J. Lehner, Phonocardiogram signal analysis: A review, Crit. Rev. Biomed. Eng. 15 (3) (1987) 211–236.
- [132]L. G. Durand and P. Pibarot, "Digital signal processing of the phonocardiogram: Review of the most recent advancements," CRC Crit. Rev. Biomed. Eng., vol. 23, pp. 163–219, 1995.
- [133]S.R.Messer, J.Agzarian, D.Abbott, Optimal wavelet denoising for phonocardiograms, Microelectron. J. 32 (2001) 931–941.
- [134]F.Liu, Y.Wang, Y.Wang, Research, and implementation of heart sound denoising, Phys. Procedia 25 (2012)777–785.
- [135]L.H.Charif, S.M.Debbal, F.Bereksi-Reguig, Choice of the wavelet analyzing in the phonocardiogram signal analysis using the discrete and the packet wavelet transform, Expert Syst. Appl. 37 (2010) 913–918.
- [136]V.S.Chourasia, A.K. Tiwari, Design methodology of a new wavelet basis function for fetal phonocardiographic signals, Sci. World J. 2013 (2013) 12.
- [137]Anderson JA. An introduction to neural networks. Boston: MIT Press; 1995
- [138]N. Andrisevic, K. Ejaz, F.R. Gutierrez, R.A. Flores, Detection of heart murmurs using wavelet analysis and artificial neural networks, J. Biomech. Eng. 127 (2005) 899–904.
- [139]Akay M. Noninvasive diagnosis of coronary artery disease using a neural network algorithm. Biol Cybern 1992;67:361–7.
- [140]Oskiper T, Watrous R. Detection of the first heart sound using time-delay neural network. Proc Comput Cardiol 2002;29:537–40.
- [141]H. Liang, I. Hartimo, "A heart sound feature extraction algorithm based on wavelet decomposition and reconstruction," in: Proceedings of the 20th Annual International Conference of the IEEE EMBS, vol. 3, 1998, pp. 1539–1542.

- [142]D. Barschdorff, S. Ester, E. Most, Phonocardiogram analysis of congenital and acquired heart diseases using artificial neural networks, in: *Advances in Fuzzy Systems-Applications and Theory*, vol. 3: Comparative Approaches to Medical Reasoning, World Scientific Publishing Co., 1995, pp. 271–288.
- [143]T.S. Leung, P.R. White, W.B. Collis, E. Brown, A.P. Salmon, Characterization of pediatric heart murmurs using self-organizing map, in: *Proceedings of 21st Annual International Conference of IEEE-EMBS*, vol. 2, October 1999, p. 926.
- [144]Chitra, R & Seenivasagam, V 2013, 'Review of Heart Disease Prediction System Using Data Mining and Hybrid Intelligent Techniques,' *ICTACT Journal on Soft Computing*, vol.3, no.4, pp. 605-609
- [145]Ölmez T, Dokur Z. Classification of heart sounds using an artificial neural network. *Pattern Recogn Lett* 2003; 24:617-629.
- [146]Uguz H, Arslan A, Turkoglu I. A biomedical system based on hidden Markov model for diagnosis of the heart valve diseases. *Pattern Recogn Lett* 2007; 28: 395-404.
- [147]V. Maknickas and A. Maknickas, "Recognition of normal–abnormal phonocardiographic signals using deep convolutional neural networks and mel-frequency spectral coefficients," *Physiological Measurement*, vol. 38, no. 8, pp. 1671-1684, 2017/07/31 2017.
- [148]P. Khunarsal, C. Lursinsap, and T. Raicharoen, "Very short time environmental sound classification based on spectrogram pattern matching," *Inf. Sci.*, vol. 243, pp. 57–74, Sep. 2013.
- [149]K. Z. Thwe and N. War, "Environmental sound classification based on time-frequency representation," in *2017 18th IEEE/ACIS International Conference on Software Engineering, Artificial Intelligence, Networking and Parallel/Distributed Computing (SNPD)*, 2017, pp. 251–255.
- [150]A. M. Badshah, J. Ahmad, N. Rahim, and S. W. Baik, "Speech Emotion Recognition from Spectrograms with Deep Convolutional Neural Network," in *2017 International Conference on Platform Technology and Service (PlatCon)*, 2017, pp. 1–5
- [151]Zhang, M., Vassiliadis, S., and Delgado-Frias, J. G., Sigmoid generators for neural computing using piecewise approximations. *IEEE Trans. Comput.* 45(9):1045–1049, 1996. ISSN: 0018–9340.
- [152]Yanai, H., and Sawada, Y., Associative memory network composed of neurons with hysteresis property. *Neural Netw.* 3:223–228, 1990.
- [153]O. Deperlioglu, "Classification of phonocardiograms with convolutional neural networks," *Broad Res. Artif. Intell. Neurosci.*, vol. 9, no. 2, pp. 22–33, 2018.
- [154]Chengyu L, Springer D, Qiao L, Benjamin M, Juan R, Chorro F, Castells F, Roig J, Silva I, Johnson A, Syed Z, Schmidt S, Papadaniil C, Hadjileontiadis L, Naseri H, Moukadem A, Dieterlen A, Brandt C, Hong T, Samieinasab M, Samieinasab M, Sameni R, Mark R, Clifford G D, An open access database for the evaluation of heart sound algorithms. *Physiological Measurement*, Volume 37 Number 9, September 2016
- [155]C.N. Gupta, R. Palaniappan, S. Swaminathan, S.M. Krishnan, "Neural network classification of homomorphic segmented heart sounds," *Appl. Soft Comput.* 7 (2007) 286–297.

- [156]Gabriel, A., 2017. Design and evaluation of safety instrumented systems: A simplified and enhanced approach. *IEEE Access*, 5, pp.3813-3823.
- [157]Joseph, A., Henriksen, K. and Malone, E., 2018. The architecture of safety: An emerging priority for improving patient safety. *Health Affairs*, 37(11), pp.1884-1891.
- [158]Vashist, S.K., 2017. Point-of-care diagnostics: Recent advances and trends. *Biosensors*, 7(4), p.62.
- [159]U. Afzaal and J. Lee, "A Self-Checking TMR Voter for Increased Reliability Consensus Voting in FPGAs," in *IEEE Transactions on Nuclear Science*, vol. 65, no. 5, pp. 1133-1139, May 2018.
- [160]Bland, J.M. and Altman, D.G., 2010. Statistical methods for assessing agreement between two methods of clinical measurement. *International Journal of nursing studies*, 47(8), pp.931-936.
- [161]Pan, W., He, A., Feng, K., Li, Y., Wu, D. and Liu, G., 2019. Multi-frequency components entropy as novel heart rate variability indices in congestive heart failure assessment. *IEEE Access*, 7, pp.37708-37717.
- [162]Elamaran, V., Arunkumar, N., Hussein, A.F., Solarte, M. and Ramirez-Gonzalez, G., 2018. Spectral fault recovery analysis revisited with Normal and abnormal heart sound signals. *IEEE Access*, 6, pp.62874-62879.
- [163]Avram, R., Tison, G.H., Aschbacher, K. et al. Real-world heart rate norms in the Health eHeart study. *npj Digit. Med.* 2, 58 (2019) doi:10.1038/s41746-019-0134-9.
- [164]Farbod Khoshnoud and Clarence W. de Silva Recent, "Advances in MEMS Sensor Technology-Biomedical Applications," *IEEE Instrumentation & Measurement Magazine*, February 2012.
- [165]N.Maluf, D.A.Gee, K.E.Petersen, G.T.A.Kovacs, "Medical Applications of MEMS," ISBN:0780326369, PP.300-306,2000.
- [166]User manual, UM1900 - Getting started with the digital MEMS microphone expansion board based on MP34DT01-M for STM32 Nucleo. *STMicroelectronics*
- [167]El-Segaier, M., Lilja, O., Lukkarinen, S., Sörnmo, L., Sepponen, R., & Pesonen, E. "Computer-based detection and analysis of heart sound and murmur." *Annals of biomedical engineering* 33.7 (2005): 937-942.
- [168]Duncan GW, Gruber JO, Dewey CF Jr, Myers GS, Lees RS. Evaluation of carotid stenosis by phonoangiography. *N Engl J Med.* 1975 Nov 27;293(22):1124-8. doi: 10.1056/NEJM197511272932205.
- [169]Jetley, R., Iyer, S.P. and Jones, P., 2006. A formal methods approach to medical device review. *Computer*, 39(4), pp.61-67.
- [170]Veytsenfeld A (2000) Microphones. *Zvukorezhisser* 1: 4-8.
- [171]Ken Gilleo, Ph.D. MEMS IN MEDICINE. <http://www.allflexinc.com/wp-content/uploads/2013/09/Medical-Electronics-MEMS.pdf>
- [172]CLAUDIO, E.D. & PARISI, R. (2001). *Microphone Arrays: Signal Processing Techniques and Applications*, chap. Multi-source localization strategies. Springer. 60

- [173]H. Teutsch, *Modal Array Signal Processing: Principles and Applications of Acoustic Wavefield Decomposition*, vol. 348, Springer, 2007.
- [174]Ibrahim, E. A., Al Awar, S., Balayah, Z. H., Hadjileontiadis, L. J., & Khandoker, A. H. (2017). A Comparative Study on Fetal Heart Rates Estimated from Fetal Phonography and Cardiocography. *Frontiers in Physiology*, 8, 764.
- [175]Fajkus, M., Nedoma, J., Martinek, R., Vasinek, V., Nazeran, H., & Siska, P. (2017). A non-invasive multichannel hybrid fiber-optic sensor system for vital sign monitoring. *Sensors*, 17(1), 111.
- [176]Varady, P., Wildt, L., Benyo, Z., & Hein, A. (2003). An advanced method in fetal phonocardiography. *Computer Methods and programs in Biomedicine*, 71(3), 283-296.
- [177]Luo, R.C. and Kay, M.G., 1989. Multisensor integration and fusion in intelligent systems. *IEEE Transactions on Systems, Man, and Cybernetics*, 19(5), pp.901-931.
- [178]Li, S., Li, F., Tang, S. and Xiong, W., 2020. A review of computer-aided heart sound detection techniques. *BioMed research international*, 2020.
- [179]Stoica, P.; Li, J. Lecture notes-source localization from range-difference measurements. *IEEE Signal Process.Mag.* 2006, 23, 63–66.
- [180]Syed Z, Leeds D, Curtis D, Nesta F, Levine R, et al. (2007) A Framework for the Analysis of Acoustical Cardiac Signals. *Biomedical Engineering*, *IEEE Transactions on* 54: 651–662.
- [181]Griffin, A.; Alexandridis, A.; Pavlidi, D.; Mastorakis, Y.; Mouchtaris, A. Localizing multiple audio sources in a wireless acoustic sensor network. *Signal. Process.* 2015, 107, 54–67.
- [182]J.C. Mosher, R.M. Leahy, Source localization using recursively applied and projected (RAP) MUSIC, *IEEE Trans. Signal Process.* 47 (2) (1999) 332–340.
- [183]X. Zhang, E. Song, J. Huang, H. Liu, Y. Wang, B. Li, X. Yuan, Acoustic source localization via subspace based method using small aperture MEMS arrays, *J.Sens.* 2014 (2014).
- [184]John L. Semmlow, “Improved Heart Sound Detection and Signal-to-Noise Estimation Using a Low-Mass Sensor,” *IEEE TRANSACTIONS ON BIOMEDICAL ENGINEERING*, MARCH 2016, Volume. 63, Number. 3, pp. 647-651
- [185]Ivan Jeleu Tashev, *Sound Capture and Processing: Practical Approaches*, Wiley, 2009.
- [186]Carsten Sydow, “Broadband beamforming for a microphone array,” *Journal of the Acoustical Society of America*, vol. 96, pp. 845–849, 1994.
- [187]I. Himawan, I. McCowan and S. Sridharan, “Clustered Blind Beamforming From Ad-Hoc Microphone Arrays,” *IEEE Transactions on Audio, Speech, and Language Processing*, 19(4), 661-676, May 2011, DOI: 10.1109/TASL.2010.2055560.
- [188]Jacob Benesty, Jingdong Chen, and Yiteng Huang, *Microphone Array Signal Processing*, Springer, 2008.
- [189]Knapp C, Carter GC. The generalized correlation method for estimation of time delay. *Acoustics, Speech, and Signal Processing*, *IEEE Transactions on*. 1976; 24(4):320-7.

- [190] Matthias Wolfel and John McDonough, Distant Speech Recognition, Wiley, New York, 2009.
- [191] DONOHUE, K.D., HANNEMANN, J. & DIETZ, H.G. (2007). Performance of phase transform for detecting sound sources with microphone arrays in reverberant and noisy environments. Signal Processing, vol. 87, n. 7, pp. 1677–1691. 33, 84, 88.
- [192] A. Zaeemzadeh, Z. Nafar, S.K. Setarehdan, Heart sound segmentation based on recurrence time statistics, in: 20th Iranian Conference on Biomedical Engineering (ICBME), IEEE, 2013, pp. 215–218.
- [193] Xilinx, “Zynq-7000 SoC Technical Reference Manual”, UG585 (v1.12.2) July 1, 2018.
- [194] Jerad Lewis, “Analog and Digital MEMS Microphone Design Considerations” MS-2472-Analog Devices Technical Article. <http://www.analog.com/media/en/technical-documentation/technical-articles/Analog-and-Digital-MEMS-Microphone-Design-Considerations-MS-2472.pdf>
- [195] Oppenheim A, Schafer R: Digital Signal Processing. Englewood Cliffs, NJ, 1975, Prentice Hall. p 87
- [196] L. Kumar, K. Singhal, R.M. Hegde, Near-field source localization using a spherical microphone array, in: 2014 4th Joint Workshop on Hands-Free Speech Communication and Microphone Arrays (HSCMA), IEEE, 2014, pp. 82–86.
- [197] H. Liu, P.H. Schimpf, Efficient localization of synchronous EEG source activities using a modified RAP-MUSIC algorithm, IEEE Trans. Biomed. Eng. 53 (4)(2006) 652–661.
- [198] M. Azaria, D. Hertz, Time delay estimation by generalized cross correlation methods, IEEE Trans Acoust. Speech Signal Process. 32 (2) (1984) 280–285.
- [199] Y. Bahadirlar, H. Gulcur, Time-frequency cardiac passive acoustic localization, in: Engineering in Medicine and Biology Society, 2001. Proceedings of the 23rd Annual International Conference of the IEEE, IEEE, 2001.
- [200] F.S. Avarvand, A. Ziehe, G. Nolte, Self-consistent MUSIC algorithm to localize multiple sources in acoustic imaging, 4th Berlin Beamforming Conference(2012).
- [201] T.G. Dvorkind, S. Gannot, Time difference of arrival estimation of speech source in a noisy and reverberant environment, Signal Process. 85 (1) (2005) 177–204.
- [202] M.W. Groch, J.R. Domnanovich, W.D. Erwin, A new heart-sounds gating device for medical imaging, IEEE Trans. Biomed. Eng. 39 (3) (1992) 307–310.
- [203] M. Omologo, P. Svaizer, Acoustic source location in noisy and reverberant environment using CSP analysis, in: IEEE International Conference on Acoustics, Speech, and Signal Processing, 1996. ICASSP-96 (Vol. 2), IEEE, 1996, pp. 921–924.
- [204] J. Dmochowski, J. Benesty, S. Affes, Linearly constrained minimum variance source localization and spectral estimation, IEEE Trans. Audio Speech Lang.Process. 16 (8) (2008) 1490–1502.
- [205] M. Kompis, H. Pasterkamp, G.R. Wodicka, Acoustic imaging of the human chest, Chest J. 120 (4) (2001) 1309–1321.

- [206]Jingdong Chen, Jacob Benesty, and Yiteng Huang, “Robust time delay estimation exploiting redundancy among multiple microphones,” IEEE Trans. Speech Audio Processing, vol. 11, pp. 549–557, 2003.
- [207]D. Ayllón, R. Gil-Pita, M. Rosa-Zurera, Design of microphone arrays for hearing aids optimized to unknown subjects, Signal Process. 93 (11) (2013) 3239–3250.
- [208]H. Chen, J. Zhao, Coherent signal-subspace processing of acoustic vector sensor array for DOA estimation of wideband sources, Signal Process. 85 (4) (2005) 837–847.
- [209]S.A. Salehin, T.D. Abhayapala, Lung sound localization using array of acoustic sensors, Signal Processing and Communication Systems, 2008. ICSPCS 2008. 2nd International Conference on, IEEE, 2008.
- [210]Saeed Gazor and Yves Grenier, “Criteria for positioning of sensors for a microphone array,” IEEE Trans. Speech Audio Processing, vol. 3, pp. 294–303, 1995.
- [211]C. Ahlström, Processing of the Phonocardiographic Signal: Methods for the Intelligent Stethoscope, Mater Thesis, Institutionen för medicinsk teknik, 2006, 2016.
- [212]R.J. Lehner, R.M. Rangayyan, A three-channel microcomputer system for segmentation and characterization of the phonocardiogram, IEEE Trans. Biomed. Eng. (6) (1987) 485–489.
- [213]IANNIELLO, J.P. (1982). Time delay estimation via cross-correlation in the presence of large estimation errors. IEEE Transactions on Acoustics, Speech and Signal Processing, vol. 30, n. 6, pp. 998–1003.33.
- [214]CHAMPAGNE, B., BERDARD, S. & STEPHENNE, A. (1996). Performance of time-delay estimation in the presence of room reverberation. IEEE Transactions on Speech and Audio Processing, vol. 4, n. 2, pp. 148–152. 33
- [215]M. Kitsunezuka, K.S. Pister, Cross-correlation-based, phase-domain spectrum sensing with low-cost software-defined radio receivers, Signal Process., IEEE Trans. 63 (8) (2015) 2033–2048.
- [216]BENESTY, J., CHEN, C.J. & HUANG, Y. (2004). Time-delay estimation via linear interpolation and cross correlation. IEEE Transactions on Speech and Audio Processing, vol. 12, n. 5, pp. 509–519. 3, 36.
- [217]D. Chen, “Time-frequency analysis of the first heart sound. Part 2: An appropriate time-frequency representation technique!” Med: Biol: Eng. Computation, 1997, 35, pp. 311–323
- [218]Madhubabu Anumukonda, Swathi Ramasahayam, L.V.R Prasada Raju, Dr. Shubhajit Roy Chowdhury, “Detection of Cardio Auscultation Using MEMS Microphone,” 9th International Conference on Sensing Technology (ICST), December 2015, pp.173-177.
- [219]A. Djebbari and F. Bereksi-Reguig, “Short-Time Fourier Transform Analysis of the Phonocardiogram Signal,” Proc. of IEEE conference, 2000, pp. 844–847.
- [220]A. Djebbari and F. Bereksi-Reguig, “Smoothed-pseudo Wigner–Ville distribution of normal and aortic stenosis heart sounds,” J. Mech. Med. Biol. , Sep. 2005, vol. 5, no. 3, pp. 415–428.
- [221]Mallat SG. A theory for multiresolution signal decomposition: The wavelet representation. IEEE Transactions on Pattern Analysis and Machine Intelligence 1989;11: 674–93.

- [222]D. Boutana, M. Benidir, and B. Barkat, “Segmentation and identification of some pathological phonocardiogram signals using time-frequency analysis,” *Signal Processing, IET Volume: 5, Issue: 6, 2011, Page(s): 527 -537.*
- [223]Ahlstrom, C., et al., “Feature extraction for systolic heart murmur classification.” *Ann Biomed Eng*, 2006. 34(11): p. 1666-77.
- [224]Michael Johnston, Sean P. Collins, Alan B. Storrow,” The third heart sound for diagnosis of acute heart failure,” *Current Heart Failure Reports*, 2007, Volume 4, Number 3, pp. 164-169.
- [225]L. D. Avendaño-Valencia, J. I. Godino-Llorente, M. Blanco-Velasco, G. Castellanos-Dominguez. “Feature extraction from parametric time-frequency representations for heart murmur detection.” *Annals of Biomedical Engineering*, Volume 38 Number 8, 2010, Page(s):2716–2732.
- [226]M. VishwanathShervegar, Ganesh V.Bhat, “Automatic segmentation of Phonocardiogram using the occurrence of the cardiac events,” *Informatics in Medicine Unlocked*, Volume 9,2017, Page(s):6-10.
- [227]I. Daubechies. *Ten Lectures on Wavelets*, Society for industrial and applied mathematics, 1992.
- [228]P.K. Sharma, S. Saha, S. Kumari, Study and design of a Shannon-energy-envelope based phonocardiogram peak spacing analysis for estimating arrhythmic heart-beat, *Int. J. Sci. Res. Publ.* (2014) 133.
- [229]J. A. Shaver, J. J. Leonard, and D. F. Leon, *Auscultation of the Heart: Part 4: Examination of the Heart*. American Heart Association, 1990.
- [230]Ari S, Saha G. “In search of an optimization technique for artificial neural network to classify abnormal heart sounds,” *Appl Soft Comput.* 2009;9:330–340.
- [231]Wu Mengze, Lu Yongdi, Yang Wenli, Wong Shen Yuong,” A Study on Arrhythmia via ECG Signal Classification Using the Convolutional Neural Network,” *Frontiers in Computational Neuroscience*, Volume 14, 2021.
- [232]Zeng, N., Li, H. & Peng, Y. A new deep belief network-based multi-task learning for diagnosis of Alzheimer’s disease. *Neural Comput & Applic* 35, 11599–11610 (2023). <https://doi.org/10.1007/s00521-021-06149-6>
- [233]Deep-reinforcement-learning-based images segmentation for quantitative analysis of gold immunochromatographic strip”, *Neurocomputing*, vol. 425, pp. 173-180, 2021.
- [234]Quantitative analysis of immunochromatographic strip based on convolutional neural network”, *IEEE Access*, vol. 7, no. 1, pp. 16257-16263, 2019.
- [235]Aydin Roland Can, Braeu Fabian Albert, Cyron Christian Johannes, “General Multi-Fidelity Framework for Training Artificial Neural Networks With Computational Models”, *Frontiers in Materials*, Volume 6, 2019.
- [236]Koutsiana Elisavet, Hadjileontiadis Leontios J., Chouvarda Ioanna, Khandoker Ahsan H.. “Fetal Heart Sounds Detection Using Wavelet Transform and Fractal Dimension,” *Frontiers in Bioengineering and Biotechnology*, Volume 5, 2017.

- [237] Hopfield J.J., Tank, D. W., "Neural computational of decisions in optimization problems," Biol. Cybern., vol.52, pp.141-152, 1985.
- [238] Hayakawa Y., Denda T., Nakajima K. (2004) Inverse Function Delayed Model for Optimization Problems. In: Negoita M.G., Howlett R.J., Jain L.C. (eds) Knowledge-Based Intelligent Information and Engineering Systems. KES 2004. Lecture Notes in Computer Science, vol 3213. Springer, Berlin, Heidelberg. https://doi.org/10.1007/978-3-540-30132-5_132
- [239] Y. Hayakawa, K. Nakajima, Design of the Inverse Function Delayed Neural Network for Solving Combinatorial Optimization Problems, IEEE Transactions on Neural Networks, 10.1109/TNN.2009.2035618, 21, 2, (224-237), (2010)
- [240] Nakajima, K., Hayakawa, Y.: Characteristics of Inverse Delayed Model for Neural Computation. In: Proceedings 2002 International Symposium on Nonlinear Theory and Its Applications, pp. 861–864 (2002).